State of Oregon
Oregon Department of Geology and Mineral Industries
Brad Avy, State Geologist

SPECIAL PAPER 51

COLUMBIA RIVER TSUNAMI MODELING: TOWARD IMPROVED MARITIME PLANNING RESPONSE

by Jonathan C. Allan[1], Joseph Zhang[2], Fletcher E. O'Brien[3], and Laura L. Gabel[1]

2018

[1]Oregon Department of Geology and Mineral Industries, Coastal Field Office, P.O. Box 1033, Newport, OR 97365
[2]Virginia Institute of Marine Science, College of William & Mary, Center for Coastal Resource Management, 1375 Greate Road, Gloucester Point, VA 23062
[3]Oregon Department of Geology and Mineral Industries, 800 NE Oregon Street, Suite 965, Portland, OR 97232

DISCLAIMER

This product is for informational purposes and may not have been prepared for or be suitable for legal, engineering, or surveying purposes. Users of this information should review or consult the primary data and information sources to ascertain the usability of the information. This publication cannot substitute for site-specific investigations by qualified practitioners. Site-specific data may give results that differ from the results shown in the publication.

Cover photo: (top left) U.S. Coast Guard performing search and rescue (SAR) drills at the mouth of Tillamook Bay; (top right) The New History *anchored in the lower Columbia River estuary offshore from Tongue Point, Astoria; (bottom left) a collection of fishing vessels docked at Tongue Point; and (bottom right) container ships docked at the Port of Longview, Washington. Photos taken by J. Allan, 2018*

Oregon Department of Geology and Mineral Industries Special Paper 51
Published in conformance with ORS 516.030

DOGAMI Administrative Offices
800 NE Oregon Street, Suite 965
Portland, OR 97232
Telephone (971) 673-1555
https://www.oregongeology.org/
https://www.oregon.gov/DOGAMI/

TABLE OF CONTENTS

LIST OF FIGURES

LIST OF TABLES

EXECUTIVE SUMMARY

Recent tsunamis affecting the West Coast of the United States have resulted in significant damage to ports and harbors, as well as to recreational and commercial vessels attempting to escape the tsunami. This study evaluates new tsunami modeling results completed for both distant and local tsunamis in the Columbia River system. The overall goal is to examine the interaction of tsunamis with dynamic tides (as opposed to modeling using a fixed tidal elevation such as mean higher high water), different riverine flow regimes, and friction to provide an improved understanding of tsunami effects on maritime traffic operating offshore the mouth of the Columbia River and within the estuary, as well as upriver toward the ports of Longview, Vancouver, and Portland. This was accomplished by evaluating a suite of tsunami simulations (35 in total) for the Columbia River focused on two distant earthquake scenarios: the 1964 Anchorage, Alaska (AK64) earthquake and a maximum considered eastern Aleutian Island (AKMax) earthquake, and two local Cascadia subduction zone (CSZ) scenarios: Large1 (L1) and Extra-extra-large1 (XXL1).

The Alaska 1964 scenario provides an excellent reference point for the potential maritime effects of the most extreme distant event to strike the Oregon coast in the past century. Our model simulations reveal the following:

- The simulation indicates that the tsunami arrived on the Oregon coast ~ 4 hours after the earthquake and occurred during a spring flood tide;
- Modeled maximum tsunami water levels reached 1 to 2 m (3–7 ft) along the open coast, while water levels at the mouth of the Columbia River (MCR), in Baker Bay, Warrenton, and Astoria ranged from 0.6 to 1.2 m (2–4 ft) high.
- Within the estuary, the simulated tsunami waves were found to rapidly decrease in height becoming negligible east of Tongue Point.
- Moderately strong currents of ~ 1.5–3 m/s (3–6 knots) are concentrated within the MCR, particularly the navigation channel, before dropping below 1.5 m/s (3 knots), the threshold below which damage within the ports and harbors is unlikely to occur.
- Damage for this event was minor and was limited to the community of Ilwaco, Washington, and included flooded streets and damage to pilings at a cannery.

For the maximum considered AKMax distant tsunami, our analyses indicate:

- The initial wave arrival at the MCR occurs ~3 hours 38 minutes after the start of the earthquake.
- The tsunami takes an additional 19 minutes to travel into Baker Bay, where it eventually inundates the lower areas of Ilwaco; the AKMax tsunami takes an additional 27 minutes to reach Warrenton, 39 minutes to reach Tongue Point, and arrives ~91 minutes later at Wauna; total time to Wauna is 5 hours 9 minutes.
- The tsunami is detectable as far up stream as St. Helens, although the amount of energy in the tsunami is effectively negligible such that the event can largely be ignored upriver of Longview.
- The simulations demonstrated significant along-coast and in-water variability in the maximum tsunami water levels and currents. The most dangerous conditions will occur at the MCR, within Baker Bay and Young's Bay, and by Tongue Point. Strong currents exceeding 4.5 m/s (9 knots) will dominate the estuary west of Chinook and Hammond, and some 8 km (5 mi) seaward of the MCR.

With respect to maritime evacuation for a maximum considered distant tsunami, we note the following:

- ***We recommend vessels seaward of the MCR evacuate to depths greater than 46 m (25 fathoms/150 ft). Dangerous currents (> 2.6 m/s [5 knots]) are expected to occur at depths shallower than 27 m (15 fathoms/90 ft) in this scenario***.
- Offshore maritime evacuation may be feasible for some vessels operating out of the ports of Ilwaco, Chinook, Hammond, and Warrenton.
- Vessels east of Warrenton may choose to evacuate upriver; seaward evacuation for vessels upriver of Warrenton is not advised because those vessels might be transiting the mouth at around the time at which the tsunami waves arrive.
- Large ships moored between Tongue Point and Rice Island, should probably consider deploying additional drag anchors to further safeguard their vessels; evacuation upriver is probably not warranted for these ships. No additional measures are required for vessels operating upstream of Fitzpatrick Island other than to ensure the presence of sufficient mooring lines.

Results from modeling a maximum considered locally generated CSZ tsunami revealed the following:

- The tsunami reaches the MCR in as little as 7 minutes. The tsunami takes an additional 18 minutes to travel northward up into Baker Bay, where tsunami waves inundate Ilwaco 25 minutes after the earthquake; the XXL1 local tsunami arrives at 31 minutes at Warrenton, 46 minutes at Tongue Point, and at ~99 minutes at Wauna. By the time the tsunami reaches Tongue Point, the tsunami is travelling at a speed of ~37.8 km/hr (23.5 mi/hr).
- The CSZ tsunami is detectable upriver as far as the confluence of the Columbia and Willamette Rivers and arrives 4 hours and 40 minutes after the start of earthquake shaking.
- The CSZ tsunami contains little energy upriver of St. Helens and can be effectively ignored. Accordingly, ***a maximum-considered CSZ tsunami will not impact the ports of Portland or Vancouver and no additional measures will be needed to safeguard vessels at these locations***, aside from having to deal with the earthquake shaking. The latter is likely to cause navigation hazards where water-saturated sediment liquefies and causes navigation channel sides, levees, and port foundations to fail.
- At the open coast, maximum water levels exceeding 18 m (60 ft) will be observed at Seaside, decreasing to 10–12 m (~33 to 40 ft) along the Clatsop Plains; water levels in the MCR will range from 6 to 12 m (20–40 ft) (relative to mean higher high water [MHHW]), decreasing to ~ 5 m (16 ft) by Sand Island.
- Extreme currents exceeding 6.1 m/s (12 knots) will be observed across much of the lower estuary, west of Astoria. These currents will be enhanced during ebb tide conditions, which could contribute to localized amplification of tsunami and wind waves at the MCR. In this scenario damage will probably be devastating for all ports and harbors in the lower estuary.
- Tsunami current velocities fall significantly upriver of ~Cathlamet and fall below the 1.5 m/s (3 knot) port damage threshold by the time the tsunami reaches Wauna. A transition area between Fitzpatrick Island and Cathlamet is characterized by current velocities in the 1.5 to 2 m/s range (3–4 knots).

With respect to maritime evacuation for a maximum considered CSZ tsunami, we note the following:

- There is insufficient time for mariners in ports to respond to this event other than to evacuate by foot to high ground.
- For vessels operating west of the MCR, the most effective strategy is to immediately evacuate toward deeper water and, accordingly, toward decreasing tsunami-generated currents. ***We recommend that vessels evacuate directly toward Astoria Canyon to depths greater than 146 m (80 fathoms).***

- Mariners should prepare to remain offshore for potentially days as the MCR is unlikely to be navigable following a CSZ earthquake and tsunami. As a result, plans to evacuate to potentially safe ports located south of Cape Mendocino on the California coast should be developed.
- Limited options are available for vessels caught out in the estuary west of Astoria.
- For vessels located east of Astoria, evacuation upriver toward Fitzpatrick Island may be an option. However, this is likely to be limited to smaller, faster boats.
- For vessels located upriver of Wauna, we recommend that ship operators attach additional mooring ropes to secure their boats or move vessels into the navigation channel.
- Because the tsunami is negligible by the time it reaches St Helens, no additional maritime safety requirements are needed upriver of this point.

Modeling undertaken using dynamic tides and varying river flows has yielded some useful insights, when compared with static models undertaken at MHHW and with no flows. These include:

- The predicted maximum velocities exhibit more local extrema along the coast and within the lower estuary, especially near the mouth where the interaction is found to be strongest due to powerful currents and shoaling of tsunami waves.
- The conventional wisdom is that tsunamis arriving with a flood spring tide are usually more damaging. This is largely true in the deep channel around Tongue Point. However, the situation becomes very complex in the shallow waters of the upper estuary, where tsunamis arriving at ebb and flood slack were found to be considerably more energetic.
- Tsunamis arriving at flood slack resulted in the greatest upriver penetration of the tsunami, with strong currents in the shallows east of Tongue Point and as far upriver as Wauna.
- The violent collision between tidal and tsunami currents at the MCR makes the ebb scenarios especially dangerous for ships of all sizes. Our modeling confirms that tsunamis arriving during an ebb phase produce considerably stronger currents when compared with the flood scenario.
- Model results that included varying the river discharge indicate generally little difference in the current velocities associated with low, average, or high flow scenarios in the Columbia River.
- Effects associated with low river flows are largely confined to areas offshore the MCR and along the open coast, where slightly stronger tsunami currents predominate. In this scenario, we find that the tsunami water levels in the estuary are generally reduced by ~ −0.25 m (−0.8 ft).
- The high river flow scenario yielded even stronger currents at the MCR and contributes ~0.2 m (0.7 ft) to the maximum tsunami water levels in the estuary.
- Changes caused by varying river flows on the modeled tsunami currents were found to be negligible in the lower estuary (< ±0.2 m/s [< ±0.4 knots]).
- The above observations apply to both the distant and local tsunamis.

1.0 INTRODUCTION

The objective of this study is to evaluate new modeling results completed for both distant and local tsunamis in the Columbia River system (**Figure 1**). The goal here is to provide an improved understanding of tsunamis and their effect on maritime traffic operating offshore the mouth of the Columbia River (MCR), within the estuary (**Figure 2**), and upriver toward the ports of Longview, Vancouver, and Portland (**Figure 1**). An ancillary objective is to provide needed tsunami inundation information based on the Large (L1) scenario to staff in the Washington Geological Survey and the Washington Military Department.

Figure 1. Location map of the Columbia River system showing key place names, model domain (dashed line), and tide gauge stations.

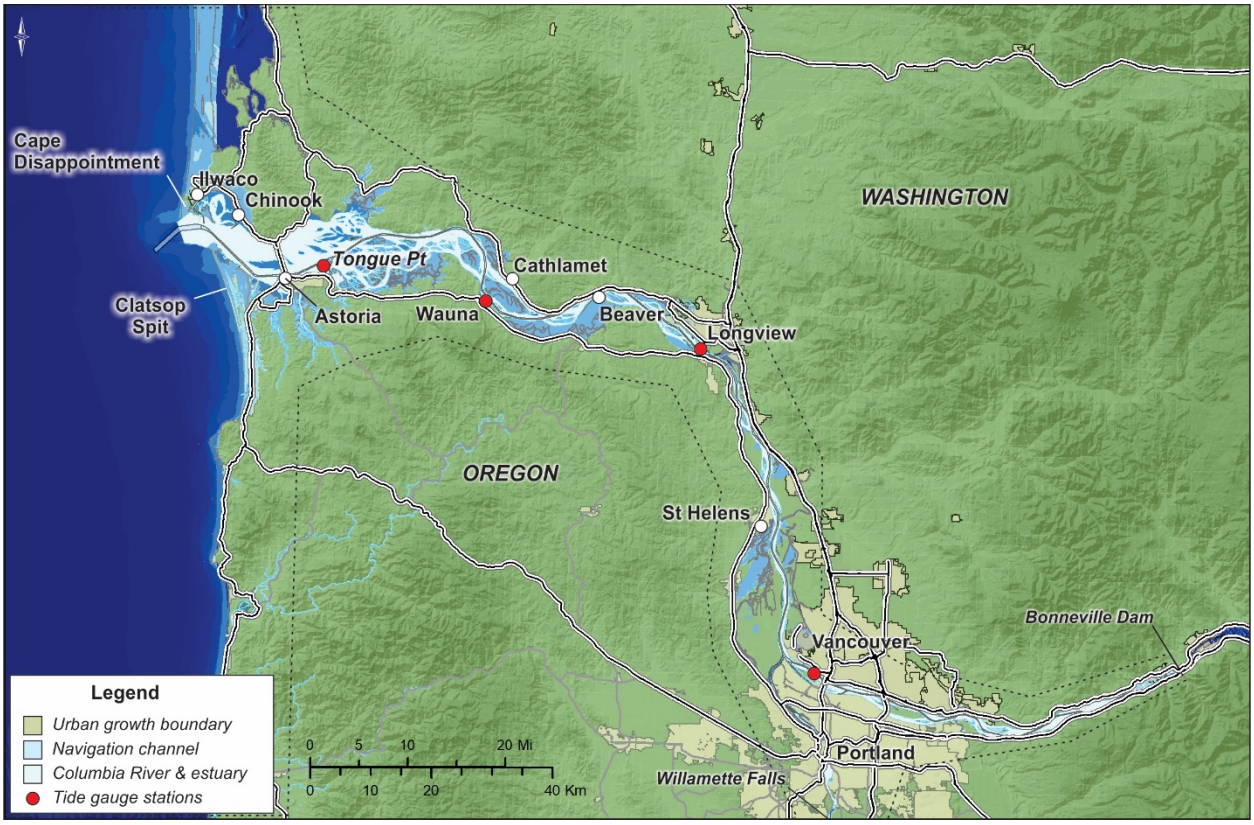

The coast of Oregon and its many estuaries are exposed to significant risk from tsunamis generated locally due to great (~ Mw 8-9) earthquakes on the Cascadia subduction zone (CSZ) (Atwater and others, 1995; Satake and others, 2003; Witter and others, 2003; Atwater and others, 2005; Nelson and others, 2006; Priest and others, 2009; Witter and others, 2012), as well as from distant tsunamis generated elsewhere in the Pacific basin (Allan and others, 2018). Local tsunamis generated on the CSZ are estimated to occur on the order of 220 to 350 years (Goldfinger and others, 2017). Conversely, similar magnitude events from distant sources have historically had only a modest impact on the Oregon coast but occur much more frequently than local tsunamis (Lander and others, 1993; Priest and others, 2009). Although local tsunamis will strike the coast within minutes after the start of earthquake shaking, providing little response time to evacuate, distant tsunamis are expected to arrive some 4 to 12 hours after the event,

providing more time to respond. These differences are important not just for land-based tsunami evacuation but also for maritime evacuation for vessels operating offshore the coast and potentially within ports and harbors.

The Columbia River is the fourth largest river in North America and the largest river on the U.S. West Coast. From its mouth, the river extends some 234 km (145 mi) upriver to Bonneville Dam. The slope of the channel bed is negligible, with the river bed remaining below mean sea level all the way to Bonneville Dam (Yeh and others, 2012). The largest tributary is the Willamette River, which enters the Columbia River at Portland, ~160 km (99 mi) from the coast. The entire system to Bonneville Dam and the Willamette Falls is tidally influenced (Jay and others, 2015). Jay and others (2016) identified several system zones along the Columbia River, including:

- A wave- and current-dominated entrance, which extends from the mouth to an area located approximately between Clatsop Spit tip and Sand Island (**Figure 2**);
- The estuary, which extends upriver to near Beaver (located just west of Longview, **Figure 1**). This region is further subdivided into
    - a lower reach (between Clatsop Spit and Rice Island, **Figure 2**) characterized by extensive salinity intrusion; and
    - an upper estuary reach without salinity (Rice Island to near Beaver). This reach is approximately 13 km wide at its lower end, narrows landward, and exhibits complex shallow-water bathymetry with braided channels (**Figure 2**);
- The tidal river, with lower, middle, and upper reaches in which river flow becomes increasingly dominant over tides in determining water levels. This area extends from near Beaver upriver to a few miles below the Bonneville Dam (**Figure 1**).

The river experiences considerable maritime traffic to and from the Pacific Ocean, and upriver to major ports at Astoria, Longview, Portland, and Vancouver (**Figure 1**). This traffic includes commercial and recreational fishing boats, survey boats, coast guard vessels, oil tankers, and large transoceanic cargo vessels. The economic value of this system is large. For example, approximately 62 million tons of goods worth over $16 billion were shipped down the river in 2015 (Flores and others, 2017). Furthermore, forecasts suggest that the number of vessels traversing the Columbia River could increase substantially in the next decade. Coincident with an increase in maritime traffic would be an accompanying increase in supporting infrastructure needed to service these vessels, along with enhancements and expansion to moorage facilities. Due to the proximity of such facilities to the river and their location relative to the tsunami inundation zone, such facilities are potentially at risk from damage and destruction by both local and distant tsunamis. Importantly, while there is time for maritime operators to respond to a distant tsunami event, the current state of knowledge is less clear for a local event. For example, due to the vastness of the Columbia River is there sufficient time for ships in some localities to potentially reach safer areas upstream. Determining where safety may be found in the Columbia River is a major objective of this study. Thus, detailed guidance may be needed for multiple ports in Oregon and Washington for both distant and local tsunamis.

To facilitate this work, new tsunami modeling has been completed for the Columbia River, extending from offshore the coast upriver to Bonneville Dam (Columbia River) and Willamette Falls (Willamette River) (**Figure 1**). The specific tasks included the following:

1) Quality assessment (QA) modeling of the 1964 Alaska tsunami to compare model results with dynamic (varying) tides versus a fixed (e.g., mean higher high water) tidal elevation;
2) New tsunami modeling based around three specific scenarios drawn from Priest and others (2013):

a. AKMax (maximum-considered distant tsunami event);
b. Large1 (L1), which has an estimated recurrence rate of ~2,500–3,333 years (used by the state of Washington to model its tsunami inundation extent); and
c. Extra-extra-large1 (XXL1), which has an estimated recurrence rate of >10,000 years (used by the state of Oregon to model its tsunami evacuation zone).

Each of these scenarios was used to evaluate the sensitivity of peak tsunami currents, maximum water levels, vorticity, and minimum water depths to various tidal and riverine flow effects in different parts of the estuary. These data provide important insights into the role of dynamic tides and riverine flows in modifying tsunami waves. In addition, these data have been used to refine our understanding of timing of tsunamis at various points in the estuary system; and

3) Produce this technical report documenting the overall modeling approach and results, as well as key information that can be incorporated into needed maritime guidance information.

Figure 2. Map of the Columbia River estuary, including the entire lower estuary and part of the upper estuary. Note: MCR = mouth of the Columbia River, blue to yellow shading defines the offshore bathymetry and subaerial topography inundated by an XXL1 tsunami (Run11a).

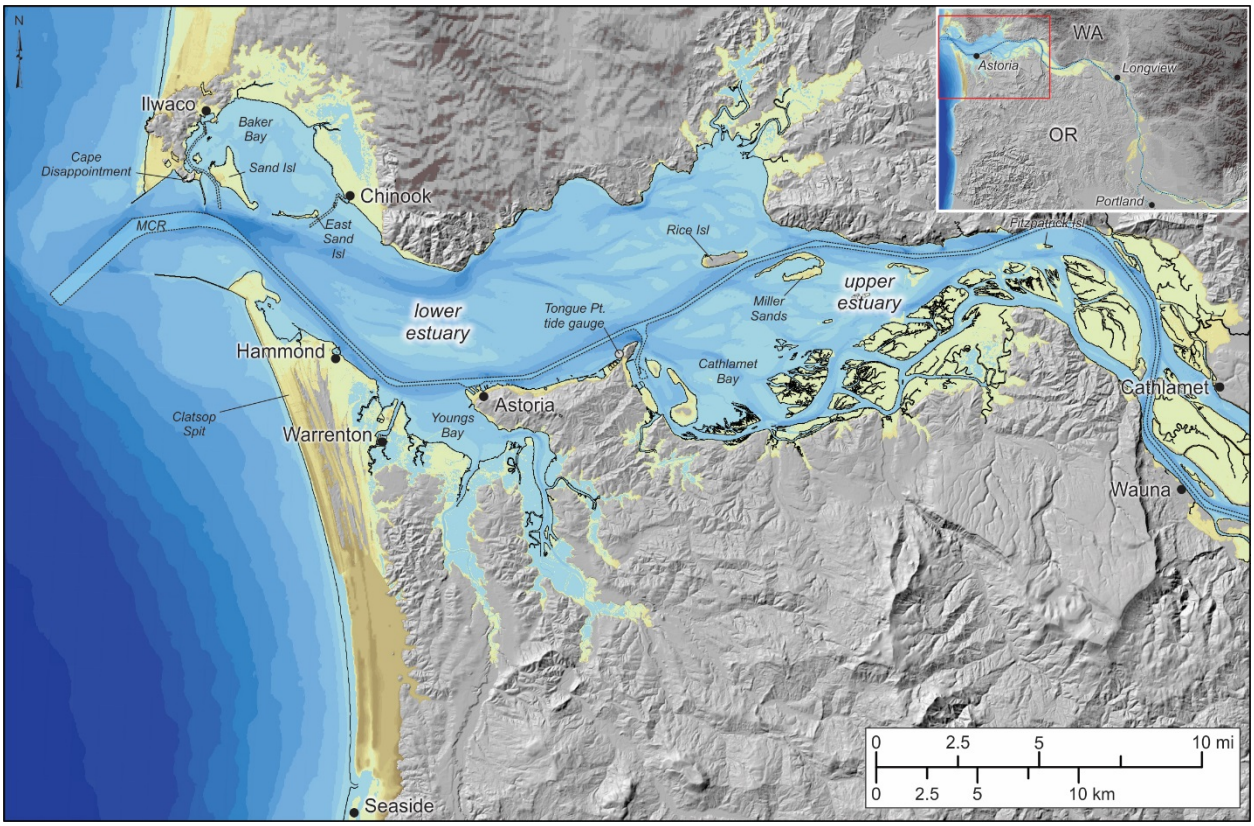

2.0 METHODS

2.1 Background

Between 2009 and 2013, the Oregon Department of Geology and Mineral Industries (DOGAMI) initiated a comprehensive effort to model and map tsunami inundation zones for the entire Oregon coast (Priest and others, 2010; Witter and others, 2011; Priest and others, 2013; Witter and others, 2013). Modeling of possible earthquake scenarios settled on two Gulf of Alaska distant source scenarios and five locally generated earthquake scenarios occurring on the CSZ. The local earthquake source parameters were guided by data that describe the geometry and tectonic behavior of the CSZ (Mitchell and others, 1994; Hyndman and Wang, 1995; McCrory and others, 2004; McCaffrey and others, 2007) and by knowledge of the size and frequency of earthquakes identified from offshore turbidite records that are inferred to record the occurrence of 42 tsunamigenic CSZ earthquakes over the last 10,000 years (Goldfinger and others, 2012). Here we briefly define the characteristics of the various earthquake source parameters before describing the hydrodynamic model used to simulate tsunami inundation.

2.1.1 Distant earthquake sources

Over the past 160 years, 29 distant (far-field) earthquake events have produced transoceanic tsunamis that struck the Oregon coast (Allan and others, 2018). The majority (19) of the tsunamis were small (maximum water level heights of < 0.2 m (0.7 ft)), which resulted in little to no impact to ports and harbors along the Oregon coast. Five events produced water level heights in the range of 0.2 to 0.6 m (0.7 to 2 ft), and the remaining five generated maximum water level heights exceeding 0.6 m (2 ft) (NGDC, 2017). The latter five occurred in:

- 1873, from northern California;
- 1946, from Unimak, Alaska;
- 1960, from Chile;
- 1964, from the Gulf of Alaska; and
- 2011, from Tōhoku, Japan.

Of these, the 1964 Alaska tsunami produced the largest observed water levels, with estuarine water levels between ~2.5 and 3.7 m (8 and 12 ft)) (Schatz and others, 1964; Zhang and others, 2011) but higher wave heights at the open coast based on only a few observations proximal to the beaches: ~5 m (16 ft) in northern Oregon at Cannon Beach (Witter, 2008) and Seaside (Tsunami Pilot Study Working Group (TPSWG), 2006, Appendix C) and > 3.7 m (12 ft) at Sunset Beach in southern Oregon (Zhang and others, 2011). The Alaska tsunami caused significant damage to infrastructure in the coastal communities of Seaside and Cannon Beach, Oregon (Witter, 2008) and killed four people camping along Beverly Beach near Newport on the central Oregon coast; no damage was reported for the Columbia River system. Other notable water levels produced by distant tsunamis include 3.05 m (10 ft) in 1873 at Port Orford, 1.8 m (6 ft) in 1946 at Clatsop Spit, and 1.5 m (5 ft) in 1960 at Seaside. Each of these previous events exceeded the effects of the March 11, 2011, Japan tsunami and, by inference, had greater potential to cause damage to ports and harbors along the Oregon coast.

The March 11, 2011, Japan earthquake provided scientists with the most comprehensive set of modern observations of a major distant tsunami. The magnitude (Mw) 9.0 earthquake took place 129 km offshore from the coast of Sendai, northeast Honshu, Japan (Mori and Takahashi, 2012), triggering a catastrophic tsunami that within minutes inundated the northeast coast of Japan, sweeping far inland and killing ~18,000 people (Mori and others, 2011; Suppasri and others, 2013). In addition to loss of life, over 28,000

boats (including 26 ships) and 319 ports (Suppasri and others, 2013) were damaged or destroyed. Economic losses due to port closures were estimated at $3.4 billion per day (Wiśniewski and Wolski, 2012).

The 2011 tsunami propagated eastward across the Pacific Ocean, impacting coastal communities in Hawaii and along the west coast of the continental United States, including Oregon where the tsunami was relatively small, reaching heights ~0.7–3.4 m (2.3–11.2 ft) at tide gauges near the open coast (Allan and others, 2012); at Astoria, the maximum wave reached 0.25 m (0.8 ft). Damage in Oregon was entirely confined to harbors, including the ports of Depoe Bay, Coos Bay, and at Brookings; the majority of ports were unaffected. Fortunately for Oregon, the tsunami impact was moderated as the highest waves arrived during a low tide (Allan and others, 2012)—had the tsunami arrived at high tide, the local impact could have been much worse. At Brookings on the southern Oregon coast, 12 fishing vessels put to sea at about 6 am, prior to the arrival of the tsunami waves. However, the *Hilda*, a 220-ton fishing boat and the largest in the harbor, broke loose under the forces of the wave-induced currents and sank several other boats as it washed around the harbor. The tsunami destroyed much of the commercial part of the harbor and about one third of the sports basin; the total damage was estimated at about $10 million. At Crescent City in California where offshore bathymetry amplifies all tsunamis relative to the Oregon coast, the tsunami was 4.2 m high in the local harbor (Allan and others, 2012). The tsunami damaged the entire open-coast breakwater, destroyed all of the docks in the Inner Boat Basin, and sank or damaged numerous vessels. The estimated damage associated with the event for Crescent City harbor was ~$20 million (Wilson and others, 2013). Accordingly, even modest distant tsunamis like the one in 2011 pose a significant risk to Oregon ports and harbors and to the safety of commercial and recreational fishermen who operate offshore of the coast.

For the purposes of our simulations for a distant tsunami affecting the Columbia River, Priest and others (2013) and Witter and others (2011) defined two far-field earthquake sources (Mw ~9.2) for maximum-considered tsunamis originating on the eastern part of the Alaska-Aleutian subduction zone. The first scenario, termed AK64, reflects the historical 1964 Prince William Sound earthquake, which produced the largest distant tsunami to reach the Oregon coast in the written historical record. Simulations of this event were used to provide quality control against known observations of water levels and tsunami wave runup identified along the Oregon coast, enabling validation of the hydrodynamic model, Semi-implicit Eulerian-Lagrangian Finite Element model (SELFE), used to simulate tsunami inundation (Priest and others, 2010).

A hypothetical maximum-considered event originating in the Gulf of Alaska was also simulated. This second scenario, termed AKMax, is identified as "Source 3" in Table 1 of González and others (2009); more detailed information describing the earthquake parameters is provided by TPSWG (2006). The AKMax fault model reflects a distributed slip source on 12 subfaults, with each subfault assigned an individual slip value of 15, 20, 25, and 30 m (49, 66, 82, and 98 ft). These extreme parameters result in maximum seafloor uplift that is nearly twice as large as the uplift produced by the 1964 Prince William Sound earthquake estimated by Johnson and others (1996). Examination of the simulated tsunami amplitudes for this source indicates beams of high energy directed more efficiently toward the Oregon coast (González and others, 2009; Allan and others, 2018), when compared with other Alaska-Aleutian subduction zone sources. Accordingly, the hypothetical Gulf of Alaska scenario was used by the State of Oregon as the maximum-considered distant tsunami source for modeling a far-field tsunami for the Oregon coast. Priest and others (2013) noted that testing the geological plausibility of the AKMax scenario and the possibility of other potential sources with better directivity toward the Oregon coast was beyond the scope of the Witter and others (2011) and Priest and others (2009, 2010) studies.

2.1.2 Local earthquake sources

Guided by CSZ geometry and tectonic behavior (Mitchell and others, 1994; Hyndman and Wang, 1995; McCrory and others, 2004; McCaffrey and others, 2007), Priest and others (2010) and Witter and others (2013) described the range of plausible CSZ earthquake sources for the Oregon coast. These data were calibrated against coastal paleoseismic records that document the impacts of as many as 13 major subduction zone earthquakes and associated tsunamis over the past ~7,000 years (Witter and others, 2003; Kelsey and others, 2005; Witter and others, 2010), while recent studies of turbidite records within sediment cores collected in deep water at the heads of Cascadia submarine canyons provide evidence for at least 19 full-margin ruptures and accompanying tsunamis over the past ~10,200 years (Goldfinger and others, 2003; Goldfinger and others, 2012; Goldfinger and others, 2017). Peak fault slip was assumed to be approximately equal to the plate convergence rate (i.e., coupling ratio = 1.0), while the variation in the time intervals between offshore turbidites were determined to be representative of variations in coseismic slip (Priest and others, 2010).

The earthquake scenarios that were ultimately used to model tsunami inundation for the Oregon coast reflect a full-length rupture of the Cascadia megathrust and the corresponding surface deformation used for tsunami simulations (Witter and others, 2013). This was necessary because the primary purpose of that effort was to develop regional tsunami inundation maps. For the purposes of that effort, representative slip models were defined and tested, including slip partitioned to a hypothetical splay fault in the accretionary wedge and models that varied the updip limit of slip on the megathrust. Each tsunami scenario was then weighted using a logic tree, and the results summarized on maps depicting the percent confidence that the local CSZ tsunami will reach no farther inland than each inundation line. Inter-event time intervals inferred to separate the 19 sandy turbidites range from as little as ~110 yr to as long as ~1,150 yr (Table 1 from Witter and others, 2011). From these data, four time intervals (mean values rounded to the nearest quarter century) were defined as representative of four general earthquake size classes: small (S), medium (M), large (L), and extra-large (XL). Respectively, these events have a mean inter-event time of 300 years (range=~110 to 480 years, 5 events), 525 years (range=~310 to 660 years, 10 events), 800 years (range=~680 to 1,000 years, 3 events), and 1,150 years (1 event), rounded to 1,200 years. The mean inter-event time interval multiplied by the CSZ plate convergence rate at each latitude equals the peak slip deficit released in each scenario earthquake. Slip was tapered to zero up and down dip from the peak value (Priest and others, 2010). Slip was also reduced progressively from north to south on the CSZ to account for evidence in the paleoseismic record of increasing numbers of partial CSZ ruptures from north to south (Goldfinger and others, 2012; Witter and others, 2013). A fifth scenario, termed extra-extra-large (XXL), simulated a maximum-considered tsunami, which would be used to guide evacuation planning (Witter and others, 2013). This last hypothetical scenario assumes 1,200 years of slip deficit release but without any reduction of slip from north to south. According to Witter and others (2013), these size classes correspond to approximate recurrence rates as follows: S, 1/2,000 yr; M, 1/1,000 yr; L, 1/3,333 yr; and XL, <1/10,000 yr. Recurrence for the maximum-considered XXL event is not known.

2.2 Tsunami Simulation

Vertical components of seabed deformation from the earthquake rupture were used to set up the initial water surface for tsunami simulations as well as the initial velocity, assuming a short (10 s) initial constant acceleration of the seafloor. Simulations of tsunami propagation and inundation used the hydrodynamic finite element model SCHISM (Semi-implicit Cross-scale Hydroscience Integrated System Model, schism.wiki)

(Zhang and others, 2016a), which is derived from the model SELFE (Semi-implicit Eulerian-Lagrangian Finite Element model) (Zhang and Baptista, 2008; Priest and others, 2009; Zhang and others, 2011; Witter and others, 2012). Algorithms used to solve the Navier-Stokes equations in these models are computationally efficient and stable. SELFE passed all standard tsunami benchmark tests (Zhang and Baptista, 2008; Zhang and others, 2011) and closely reproduced observed inundation and flow depths of the 1964 Alaska tsunami in a trial at Cannon Beach (Priest and others, 2009). More recently, SCHISM successfully passed a suite of standardized tsunami current benchmark tests (Zhang and others, 2016b; Lynett and others, 2017), indicating that the original SELFE model results are acceptable for simulating tsunami currents used in maritime evacuation planning.

The unstructured finite element mesh used in our Columbia River modeling was constructed by first compiling digital elevation models (DEMs) covering the model domain and then retrieving from the DEM elevations at a series of points defining a triangular irregular network (TIN). The DEM for the tsunami simulations was derived from a combined 2-m (6 ft) bathymetric/topographic seamless digital surface model created by the Portland District of the U.S. Army Corps of Engineers (USACE, 2010). These data were originally compiled to support hydraulic modeling efforts related to the Columbia River treaty negotiation of 2014. The DEM comprises a variety of data sources, including USACE single-beam surveys, multibeam data collected by David Evans and Associates for NOAA and the USACE, single-beam surveys conducted by David Evans and Associates on personal watercraft for the Lower Columbia Estuary Partnership (LCREP), NOAA historic smooth sheet data, and U.S. Bureau of Reclamation acoustic doppler current profiler (ADCP) data collected on the Sandy River (USACE, 2010). The most comprehensive data set reflects high-resolution multibeam data collected by David Evans and Associates for NOAA to update nautical charts of the Columbia from river mile 110 to 30. These data consist of a 0.5-m (1.6 ft) grid of multibeam bathymetric data with some single-beam bathymetric data in shallow water (USACE, 2010). In areas of dry land, the data were supplemented with 2009 lidar data collected by DOGAMI. Due to an absence of lidar data in a small area in southwest Washington (primarily around the Chinook River valley), we resorted to using U.S. Geological Survey (USGS) 10-m (33 ft) topographic maps to generate elevation data to fill gaps in the Chinook DEM.

The completed tsunami model domain (**Figure 1**) developed for the Columbia River extended from Bonneville Dam at river mile (RM) 146.5, downstream to RM 0 at the river mouth; similarly, we include the region from Willamette Falls to the confluence of the Columbia River/Willamette Falls. The offshore extent of the model domain extends a farther ~70 km (44 mi) west of the mouth of the Columbia River, 77 km (48 mi) south along the Oregon coast, and 39 km (24 mi) north along the Washington coast. The size of the unstructured grid is large, with ~5.14 million nodes and ~10.2 million triangular elements in the horizontal dimension. The nominal resolution is ~30–40 m (98–131 ft) in the river channel, and ~5–10 m (15–33 ft) in areas adjacent to the estuary and river channel. The DEM was further refined by adding finer-resolution detail in areas adjacent to the north Columbia River jetty, and the breakwaters at the ports of Ilwaco and Chinook (**Figure 2**). A sensitivity run with 15- to 20-m (45–66 ft) resolution in the navigational channel of the lower estuary was also undertaken (Run04a), and comparisons with the slightly coarser grid (Run03d) yielded similar results for the simulated water levels and current velocity.

We use only one layer in the vertical, so the model is effectively 2D depth averaged. This is consistent with the majority of existing tsunami inundation maritime modeling efforts presently being implemented; incorporation of fully 3D modeling is left for future study. Ideally, SCHISM 3D would provide better results, especially in terms of resolving the density-driven currents that are important for this system (Burla and others, 2010). However, the effects of the density flow (on the order of 1 m/s [1.9 knot]) are arguably minor compared to those from the tsunami event (on the order of 5 m/s [9.7 knot]). Furthermore, a fully 3D model with the required very fine resolution needed for tsunami simulations is still too expensive at present. Each simulation was run for 24 hours, providing sufficient time for the tsunami to run its course;

the simulation time step is 1 second for distance and 2 seconds for local sources; the data output was established at 40 second intervals. The model is fully parallelized with hybrid openMP[1] and MPI[2] and runs ~7 times faster[3] than real time on 500 Intel® Xeon® cores using this higher-resolution grid.

The tsunami simulations were run using both static (i.e., fixed tidal elevation) and dynamic tides (tide elevation varies over time), as well as different river discharge levels. The complete suite of simulations is summarized in **Table 1**. For static tidal runs, we used mean higher high water (MHHW) and mean high water (MHW) determined at the Tongue Point, Astoria tide gauge station (**Figure 3**), respectively 2.63 m (8.6 ft) and 2.42 m (7.9 ft). For dynamic tide runs, the tsunami was timed to arrive at Tongue Point at the following tide stages: flood, ebb, flood slack, and ebb slack (**Table 1, Figure 3**). Tidal forcing at the ocean boundary is calculated from the WEBTIDE package (http://www.bio.gc.ca/science/research-recherche/ocean/webtide/index-en.php).

Figure 3. Tidal stages defined for the Tongue Point, Astoria tide gauge.

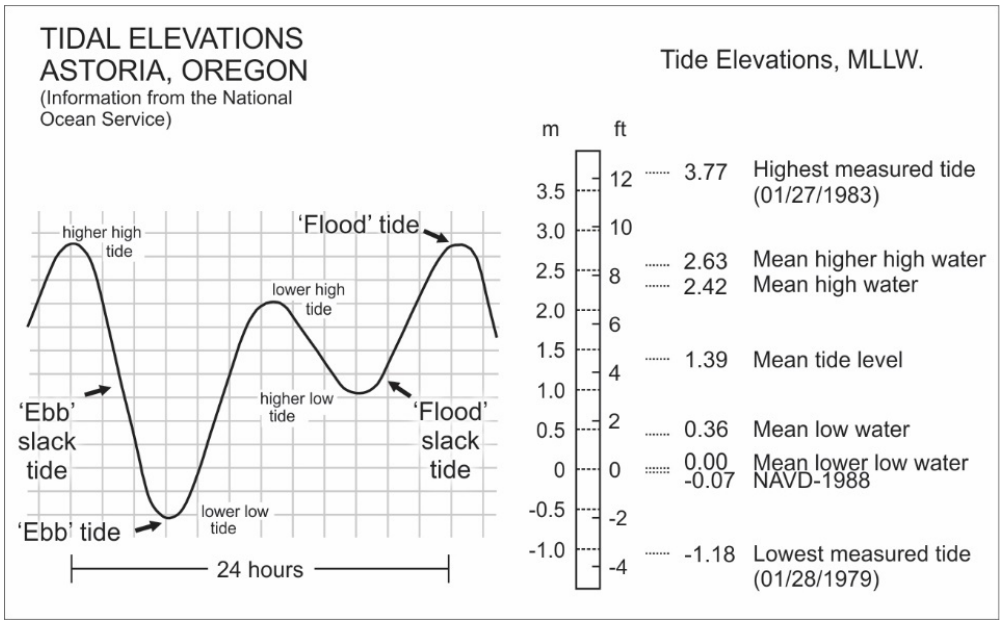

Columbia River discharge information at Bonneville Dam was obtained from the Bonneville Power Administration (BPA), while discharge on the Willamette River is taken from the USGS river gauge at Morrison Bridge, Portland. We focused on three river flow regimes (**Figure 4**, **Table 1**): average, low, and high flow scenarios.

The bottom drag coefficient (*Cd*) or friction used in tsunami modeling is specified from Manning-*n*, which is known to be a function of land cover type (USACE, 2008). The Columbia River study area is characterized by a wide range of land cover types, including open water, developed space, pastures, shrubs, wetlands, evergreen forest, and woodland, which are captured in the USGS 2011 National Land Cover Data (Homer and others, 2015). Values of Manning-*n* are estimated for each land cover type based on published values provided by Bunya and others (2010) and provided in **Table 2.** This process is

1 openMP: share memory parallelism (MP=multi-processing)

2 MPI: message passing protocol (for distributed parallelism)

3 24/7=3.4 hours to finish one simulation day

accomplished using a look-up table script that assigns the Manning-n value based on the local land cover data. The spatial dataset of friction is then used in the model simulations. The friction generally increases landward, thus helping to dissipate the tsunami wave energy. For the subaqueous portion of the DEM, we used Manning-*n* = 0.02.

Table 1. Columbia River simulated tsunami scenarios. See text for scenario definitions.

Group Number	Scenario	Tidal Phase	Spring/ Neap	River Flow (m^3/sec) (Q)*	Bottom Friction**	Run Name
1	AK64	event	event	estimated	landscape	RUN02e
2	AKMax/L1/XXL1	static (MHHW)	N/A	0	0	XXL1 = Run05a L1 = Run05a-L1 AKMax = Run05a-pmel01
3	XXL1	static (MHHW)	N/A	7,000	0	Run3d (coarse grid) vs. Run04a (fine grid)
4	L1	static (MHHW and MHW)	N/A	0	WA = 0.025 and 0.03	L1 = Run05b-L1 L1 = Run05c-L1
5	AKMax/L1/XXL1	dynamic, flood	spring	average	landscape	XXL1 = Run06a L1 = Run06a-L1 AKMax = Run06a-pmel01
6	AKMax/L1/XXL1	dynamic, ebb	spring	average	landscape	XXL1 = Run07a L1 = Run07a-L1 AKMax = Run07a-pmel01
7	AKMax/L1/XXL1	dynamic, flood slack	spring	average	landscape	XXL1 = Run08a L1 = Run08a-L1 AKMax = Run08a-pmel01
8	AKMax/L1/XXL1	dynamic, ebb slack	spring	average	landscape	XXL1 = Run09a L1 = Run09a-L1 AKMax = Run09a-pmel01
9	AKMax/L1/XXL1	dynamic, flood	neap	average	landscape	XXL1 = Run12a L1 = Run12a-L1 AKMax = Run12a-pmel01
10	AKMax/L1/XXL1	dynamic, flood	spring	low	landscape	XXL1 = Run10a L1 = Run10a-L1 AKMax = Run10a-pmel01
11	AKMax/L1/XXL1	dynamic, flood	spring	high	landscape	XXL1 = Run11a L1 = Run10a-L1 AKMax = Run10a-pmel01
12	Tide+flow	dynamic, flood		average	landscape	RUN01m
13	Tide+flow	dynamic, flood		low	landscape	RUN01j
14	Tide+flow	dynamic, flood		high	landscape	RUN01k

Notes: WA is Washington state.

Static means a fixed tidal elevation, and dynamic means the tide varies over time.

*Average spring "freshet" (spring thaw resulting from snowmelt) flows = June 2002 conditions.

*High flow = June 1997 event.

*Low flow = September 15, 2001, event.

Nodal Manning-*n* coefficients are spatially assigned using land-cover definitions from the USGS National Land Cover Data (NLCD) for Oregon and Washington (see **Table 2). For the ocean bottom we used Manning-*n* = 0.02.

Table 2. Manning-*n* values for various landform types (from Bunya and others, 2010, Tables 4 and 5).

Description	Manning-*n* Value
Open water	0.020
Sand beach, bare ground, recreational grass	0.030
Fallow, transportation	0.032
Pasture	0.033
Grassland, farmed wetlands, urban grassy pasture, herbaceous wetland	0.035
Agriculture, bare rock	0.040
Low-density urban/commercial	0.050
Shrub land	0.070
Transitional, orchard, vineyard	0.100
Medium-density urban	0.120
Woody wetland	0.140
High-density urban	0.150
Deciduous forest	0.160
Mixed forest	0.170
Evergreen forest	0.180

Multiple model runs were undertaken to independently simulate the effects of tides, river flow, and tsunamis before these were combined in the final "dynamic-tide" runs. **Table 1** shows the information for all important model runs completed for this study. In this report we will focus initially on comparisons between static- and dynamic-tide run results to illustrate the importance of incorporating tides in tsunami simulations for this high-energy system. For dynamic-tide simulations, the effects of spring[4]/neap[5] tides, tidal phases, and river flow conditions are examined. Most of the simulations are done for 1 day under an average spring freshet[6] condition as observed in 2002 (**Figure 4**). Longer simulations (12 to 24 days) are done for tidal runs.

Finally, **Figure 5** presents a map identifying the locations where time series information has been extracted from the simulations in order to generate plots of tsunami currents and water levels. These data are useful for better understanding the complex responses of the tsunamis as they interact with tides and riverine flows.

4 Spring tides occur twice each lunar month when the Earth, sun and moon are nearly in alignment, producing high tides that are a little higher than normal.

5 Neap tides occur seven days after the spring tide occurring when the sun and moon are at right angles to each other. This results in high tides that are slightly lower than normal.

6 A term used to describe a spring thaw resulting from snowmelt.

Figure 4. Variations in Columbia River flows from 1996 to 2015. For simulation purposes, average flow is based on June 1, 2002 data, low flow reflects September 15, 2001 data, and high flow is based on June 1997 data. Discharge unit is one cubic meter of water per second or one cubic feet per second.

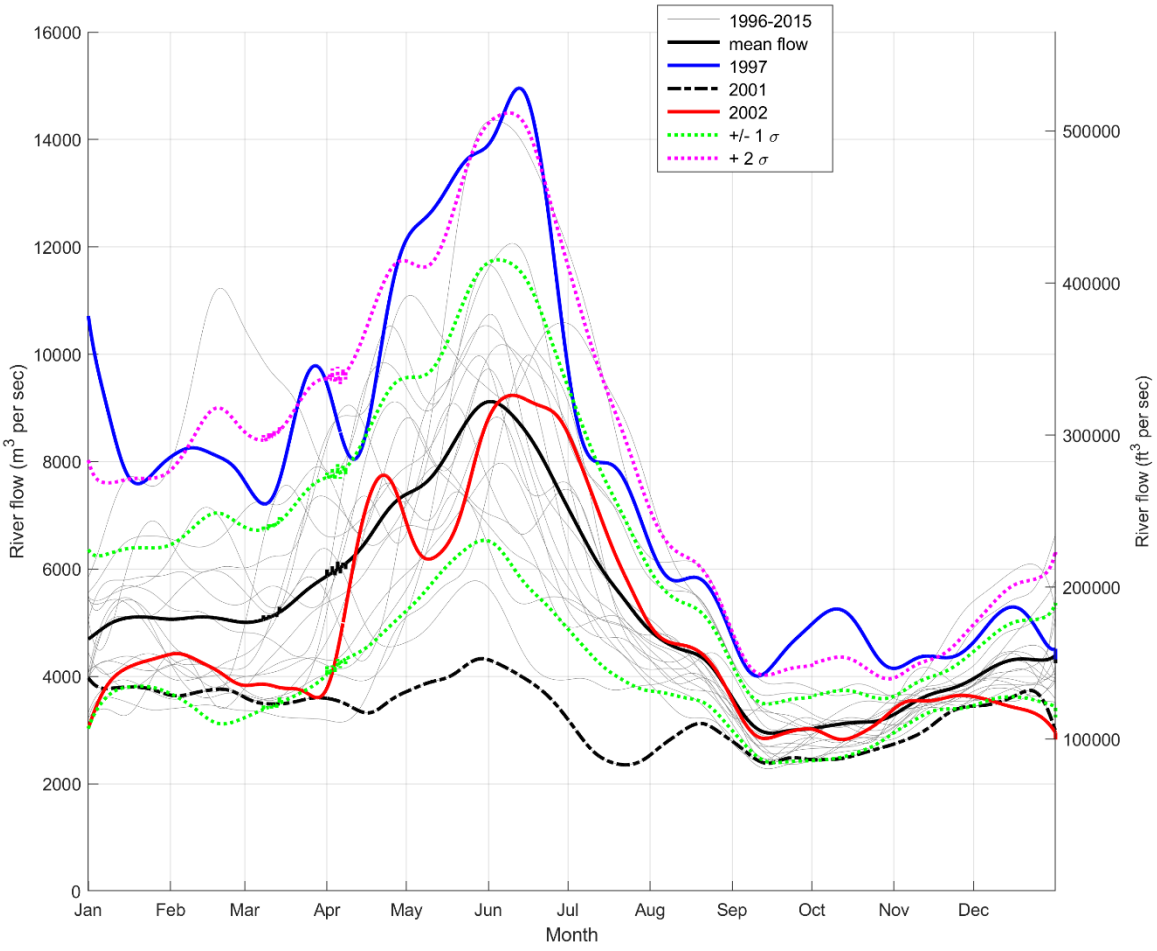

Figure 5. Map showing the locations of virtual water level stations in the Columbia River estuary and along the tidal river (inset map) used to observe tsunami currents and water level time series information. Inset example shows the simulated water levels for Run06a (flood tide) and Run07a (ebb tide) at station 3 located at the mouth of the Columbia River (MCR). Dashed line denotes the navigation channel. Blue to yellow shading defines the offshore bathymetry and subaerial topography inundated by an XXL1 tsunami (Run11a).

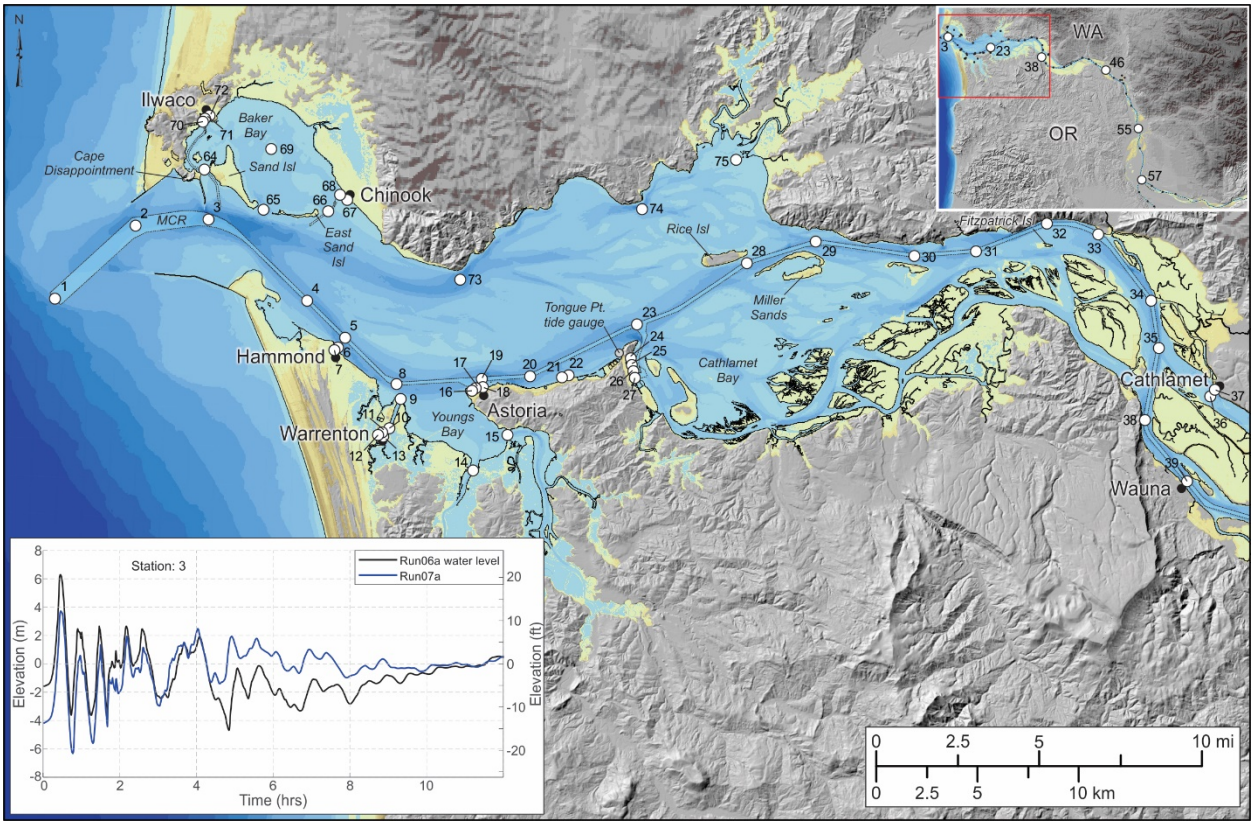

3.0 MODEL VALIDATIONS

3.1 Tides

We first validate the model for tidal elevations under the average spring freshet condition defined for June 2002. Columbia River tides undergo dramatic transformation from the Pacific Ocean to the estuary and upstream toward Portland/Vancouver, where the tides are mostly non-stationary (Kukulka and Jay, 2003). Therefore, it is challenging to capture this transformation, especially in 2D mode. **Figure 6** provides a comparison between the measured tides at four tide gauges (their locations are included in **Figure 1**) with the model results determined by SCHISM. As can be seen in **Figure 6**, our 2D model replicates the measured data well. Of note, the results obtained in the lower (Tongue Point) and upper (Wauna) estuary stations (**Figure 2**) are satisfactory. With progress upriver, the tides become increasingly distorted as they propagate upstream under the influence of river flow and shallow bathymetry. By the time the tide reaches the upstream river stations at Longview and Vancouver, the tidal amplitudes are greatly attenuated; this response is captured by the model simulations at the Longview tide gauge (**Figure 6**), while slightly larger anomalies are evident at Vancouver. Previous studies with the 3D version of the model demonstrated that better accuracy can be achieved using the 3D baroclinc SCHISM (Burla and others, 2010).

Figure 6. Comparison of modeled and observed tidal elevations at four National Ocean Service (NOS) tide gauge stations on the Columbia River. Note that the vertical datum at Vancouver is uncertain, so we have adjusted it to roughly match the mean level of the model there.

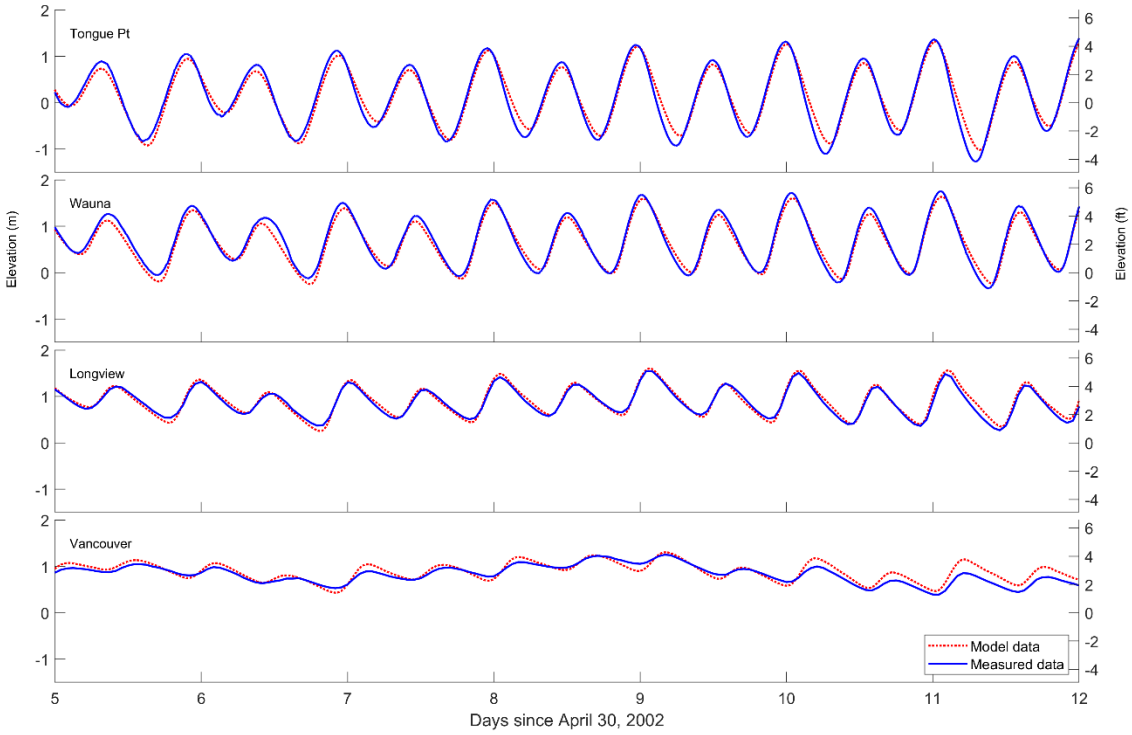

3.2 1964 Great Alaska Tsunami

The great Alaska 1964 earthquake and tsunami were previously validated using SELFE and a grid that covers a large region from Alaska to the U.S. west coast, while the modeling accounted for both tsunami waves and the dynamic tides (Zhang and others, 2011). Damage from this event was largely confined to the community of Ilwaco, Washington, where a couple of streets were flooded and pilings at the Moore cannery were damaged (Stewart, 2006; Whitmore and others, 2008). Here we re-validate the model using higher-resolution DEM data developed for the Columbia River.

All dynamic-tide runs discussed in this report consist of three separate runs:

- A tidal run (with river flow) that starts before the tsunami event and ends after the event;
- A static-tide run with tsunami only (with no river flow or tides); and
- A final dynamic-tide run that is initiated from the tidal run at the start of the earthquake event and uses the information at the ocean boundary from the other two runs.

The static-tide run uses MHHW as the vertical datum (2.63 m [8.6 ft] based on the Tongue Point tide gauge) while the other two runs (tidal and dynamic-tide runs) use mean sea level (MSL) datum (2.42 m [7.9 ft] at the Astoria gauge). For the 1964 event, the dynamic-tide run is initiated at 03:36 GMT on March 28, 1964, when the earthquake occurred. The first waves of tsunami arrived at the U.S. west coast approximately 4 hours later. The Tongue Point tide gauge located at approximately mid estuary provides a complete record of the 1964 tsunami, allowing us to compare our model simulation with the actual measured data (**Figure 7**). The tsunami waves coincided with a spring flood tide, which further exacerbated local impacts (Zhang and others, 2011). The tsunami waves are visible during the subsequent ebb and flood and persisted more than one day after the earthquake.

Figure 7. Comparison of measured and simulated water level elevations at the Astoria tide gauge during the 1964 event.

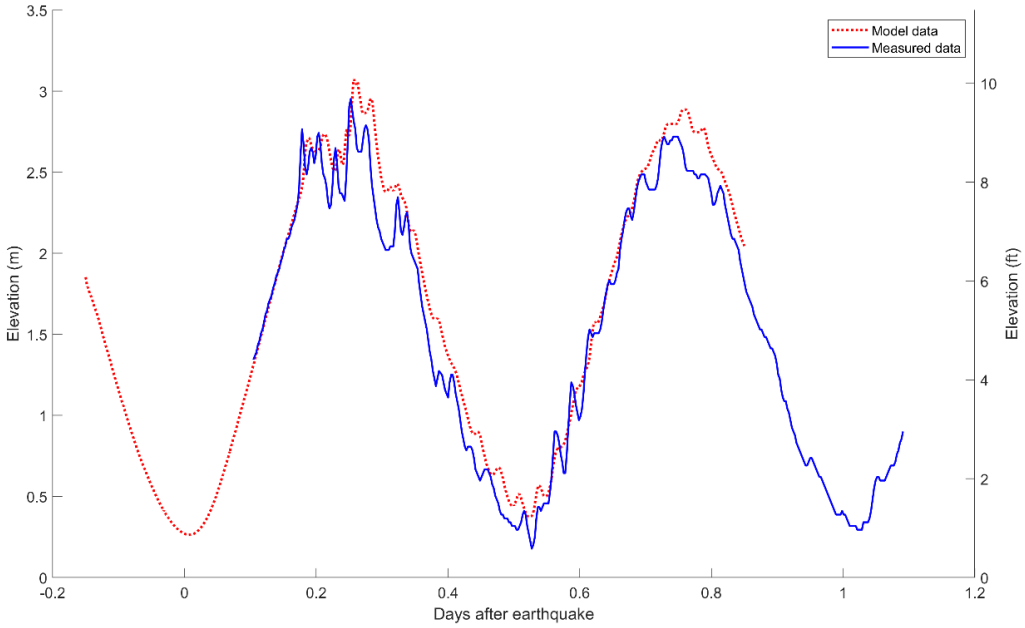

Overall, SCHISM did a reasonable job in capturing this complex interaction between tsunami waves and tides (**Figure 7**). Moreover, the model also captured the wave runup processes inside the estuary. There are field estimates of the tsunami runup at two sites: near Cape Disappointment (124.05°W 46.28°N) and Ilwaco (124.03°W 46.3°N) (**Figure 2**), where the maximum wave runups were estimated to be 1.74 m and 1.4 m, respectively (Wilson and Tørum, 1972). These compare well with the model results of 1.79 m and 1.44 m, estimated along a transect from each observation point, perpendicular to the nearest maximum inundation line (**Figure 8**). These comparisons suggest that the model is sufficiently accurate to be used in the study of tsunami-tide interaction.

Figure 8. Method used to calculate the maximum runup near Cape Disappointment. The black line in (b) is the maximum inundation line calculated from the model, and the red dashed line is the transect from the observation point to the nearest inundation point (shown by the x).

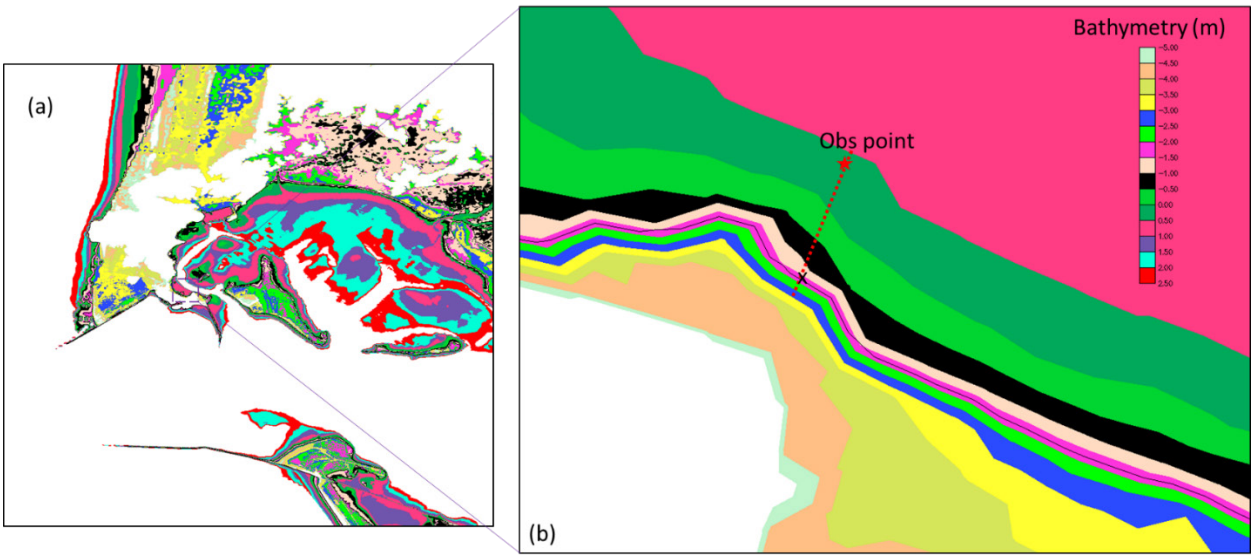

Lynett and others (2014) examined the impact of the 2011 Tōhoku tsunami on ports and harbors on the California coast and found a strong relationship between the velocity of tsunami currents and damage potential (**Table 3**). In general, they observed that for velocities ranging from 1.5 to 3 m/s (3 to 6 knots), moderate tsunami damage tended to occur to port facilities and moored vessels. When the current velocities increased to ~3–4.5 m/s (6-9 knots), ports and docks were subject to major damage. Extreme damage occurred when current velocities exceeded 4.5 m/s (9 knots) (Lynett and others, 2014). We use the same binning approach in figures throughout this report when examining and discussing tsunami current velocities.

Table 3. Damage index and corresponding damage type (after Lynett and others, 2014).

Damage Index	Associated Current Velocity	Damage Type
0		no damage/impacts
1	< 1.5 m/s (< 3 knots)	small buoys moved
2	1.5–3 m/s (3–6 knots)	1-2 docks/small boast damaged and/or large buoys moved
3		moderate dock/boat damage (<25% of docks/vessels damaged and/or midsized vessels off moorings)
4	3–4.5 m/s (6–9 knots)	major dock/boat damage (<50% of docks/vessels damaged and/or midsized vessels off moorings)
5	> 4.5 m/s (> 9 knots)	extreme/complete damage (>50% of docks/vessels damaged)

Figure 9 and **Figure 10** present the simulated maximum water levels and current velocities generated for the Alaska 1964 tsunami. This event remains the most significant far-field tsunami to strike the Oregon coast in the last century, and hence these data are useful for assisting with the development of maritime tsunami guidance for the Columbia River.

As can be seen in **Figure 9**, maximum water levels range from 0.6 to 1.2 m (2 to 4 ft) at the MCR, within Baker Bay (near Sand Island), and near the communities of Warrenton and Hammond in the lower estuary. However, for much of the Columbia River estuary, including ship-mooring sites near Tongue Point, the simulated water levels are found to be <0.3 m (<1 ft). On the open coast, water levels are highest at Seaside, where they reach 2.9 m (9.5 ft). As can be seen in **Figure 10**, the modeled currents are generally low throughout the lower Columbia River estuary. Strongest currents are observed at the MCR, in the narrow channels between Sand Island and Cape Disappointment, and between Sand Island and East Sand Island (**Figure 10**). Damage from the Alaska 1964 event was confined to the community of Ilwaco, Washington (NGDC, 2017); no additional damage was reported for communities elsewhere in the Columbia River estuary.

Figure 9. Simulated maximum water levels for the Alaska 1964 tsunami.

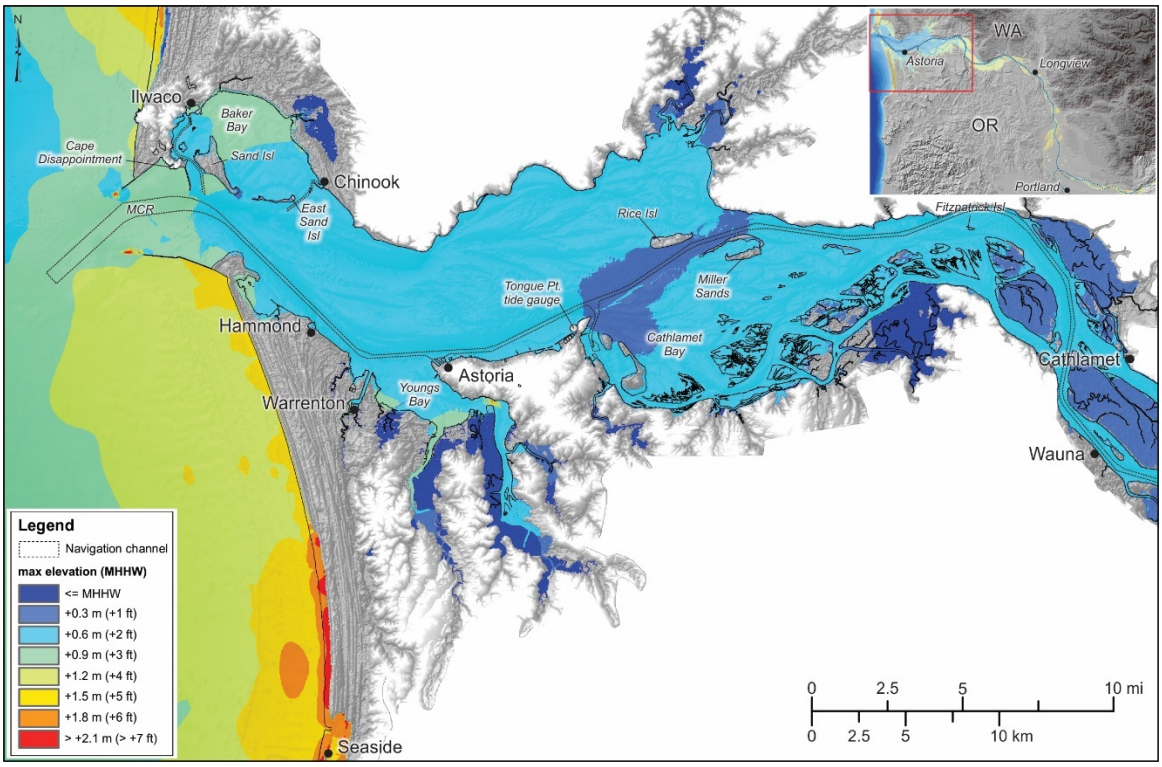

Figure 10. Simulated maximum currents for the Alaska 1964 tsunami.

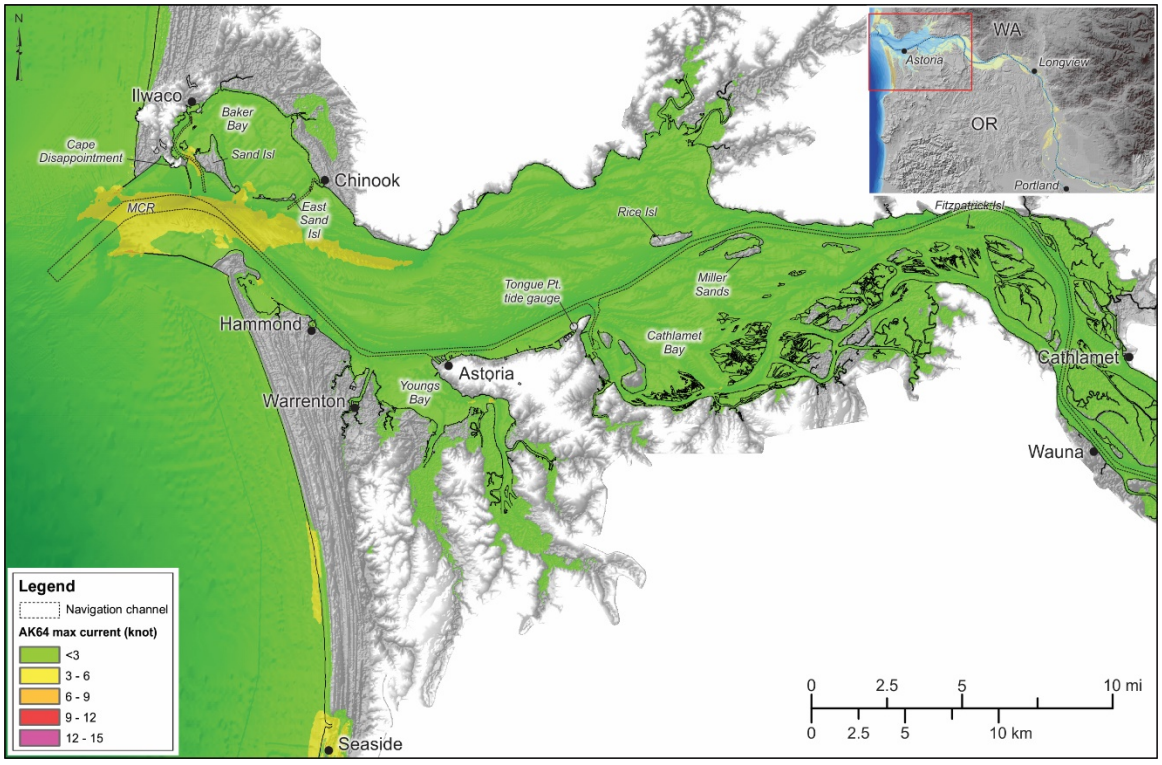

4.0 STATIC AND DYNAMIC TSUNAMI SIMULATIONS

4.1 Static-Tide Results

Simulations involving static-tide modeling were implemented for AKMax (distant) and the two local CSZ scenarios (L1 and XXL1). Recall that these runs do not include river flow and use a frictionless bottom (**Table 1**, group 2), making them consistent with previous modeling efforts undertaken for the Oregon Coast from 2009 to 2013 (Priest and others, 2009; Witter and others, 2011; Priest and others, 2013). The major difference between these newer runs and previous efforts is the adoption of a much higher resolution DEM. The vertical datum used is MHHW at the Tongue Point tide gauge (**Figure 11**). Comparisons of the inundation extents produced from our current simulations versus modeling undertaken in 2013 (Priest and others, 2013) indicate that for most areas within the lower and upper estuary, differences between the two simulations are relatively minor, with the newest run resulting in slightly greater inundation. By far the biggest difference between the simulations occurs along the central Clatsop Plains (between Sunset Beach and Surf Pines to the north of Gearhart), where a sequence of old dunes mapped as safe in 2013 are now inundated by tsunami waves. The cause of this difference can be attributed to an error in the 2013 grid, which artificially raises the seabed west of the Clatsop Plains. As a result of the shallower bathymetry, there is greater energy dissipation across the nearshore shelf, which produces lower runup and inundation. This suggests that tsunami evacuation maps for this area may need updating.

Because the estuary geometry serves as an effective dissipater of short-wavelength tsunami waves, the impact of tsunamis is mostly confined in the estuary downstream of Cathlamet Bay. Not surprisingly, the maximum considered XXL1 scenario generated the largest impact in terms of inundation extent (**Figure 11**, yellow zone) and tsunami velocities (**Figure 12**), followed by L1 (red zone); the distant event AKMax (orange zone) caused only minor inundation inside the estuary (**Figure 11**). When considering the degree of inundation shown in **Figure 11**, it is important to appreciate that while the inundation defined for XXL1 may appear small, it actually includes the areas inundated by L1 (red) and AKMax (orange). Hence, the inundation extent for XXL1 includes all colored areas in the figure.

Figure 11. Comparison of maximum tsunami inundation from static-tide runs modeled using MHHW, no river flow, and a frictionless landscape. Runs are in increasing order of inundation: AKMax (Run05a) in orange, L1 (Run05a) in red, and XXL1 (Run05a) in yellow. Note: the inundation extent for XXL1 includes all colored areas in the figure.

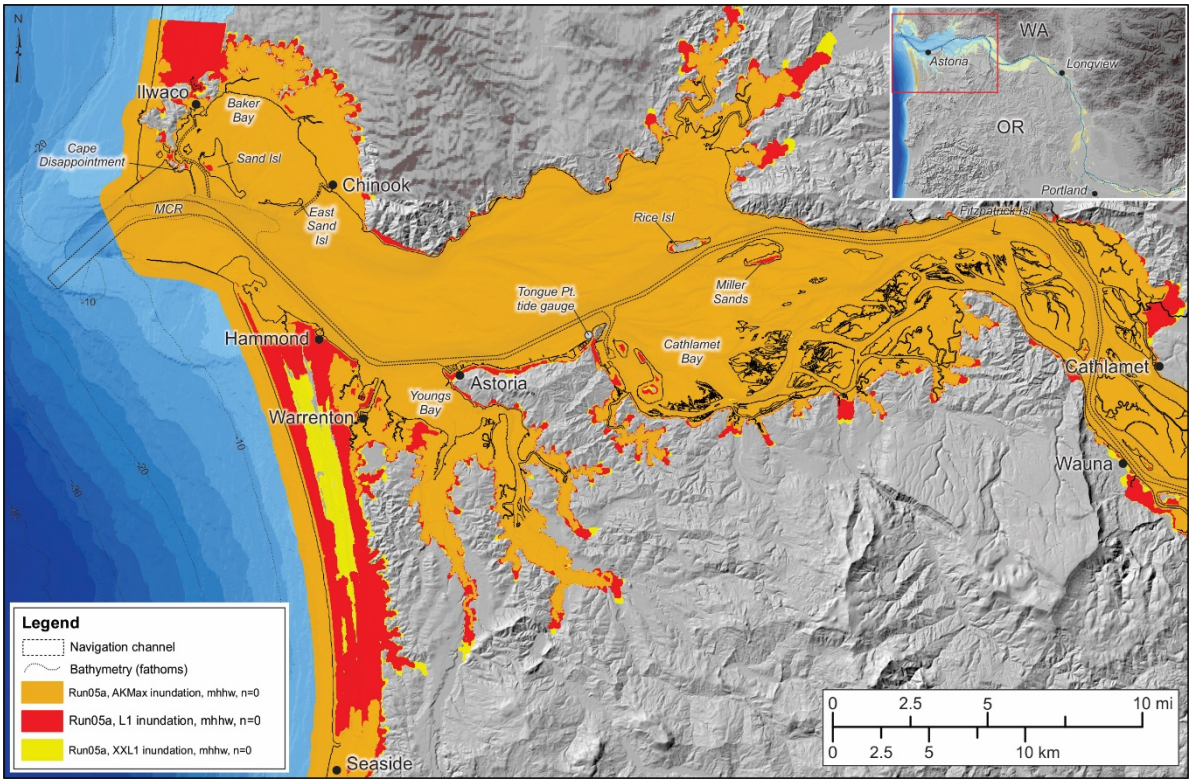

Figure 12. Maximum tsunami velocities (in knots) generated for the maximum considered XXL1 (Run05a) simulation, modeled using MHHW, no river flow, and a frictionless landscape.

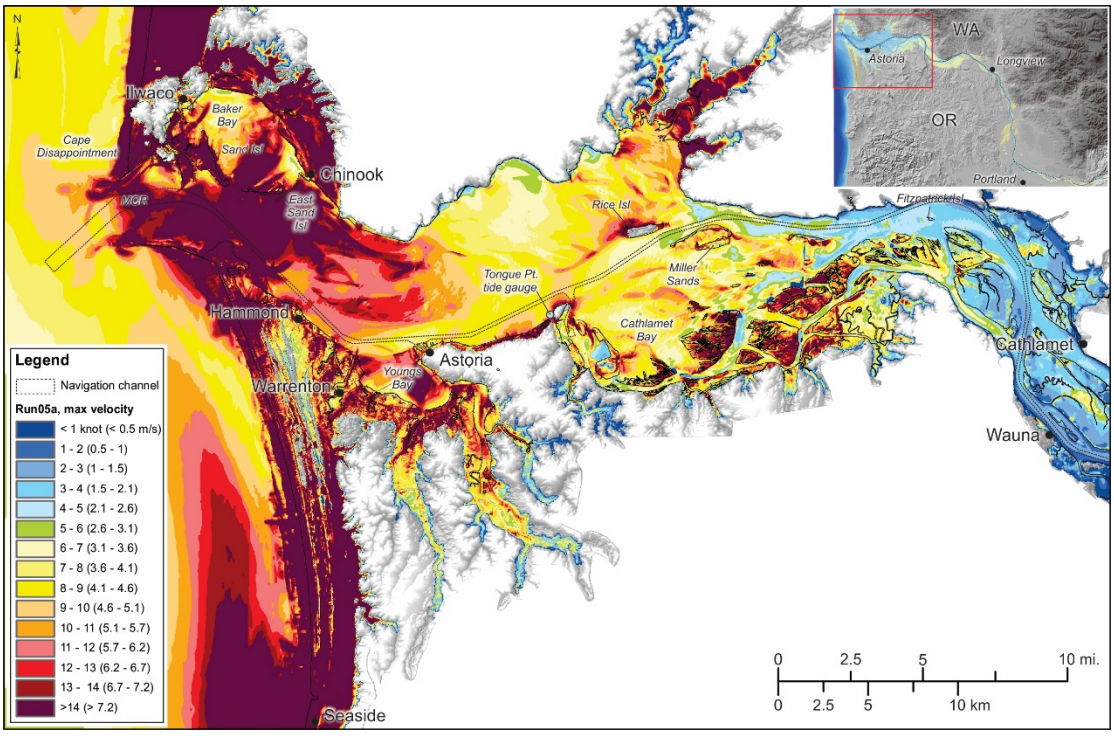

Comparisons between the two local events (XXL1 and L1) indicate large differences in the tsunami velocities along the Clatsop Plains, adjacent to the MCR, and in some isolated remote locations near the distal ends of the inundation zone (**Figure 13**). Upstream of Tongue Point, these differences drop to ~ 3 knots or less.

Figure 13. Maximum tsunami velocities (in knots) expressed as the difference between the L1 (Run05a-L1) and XXL1 (Run05a) simulations. Velocities less than 0 indicate XXL1 currents dominate, while velocities great than 0 indicate that L1 dominates.

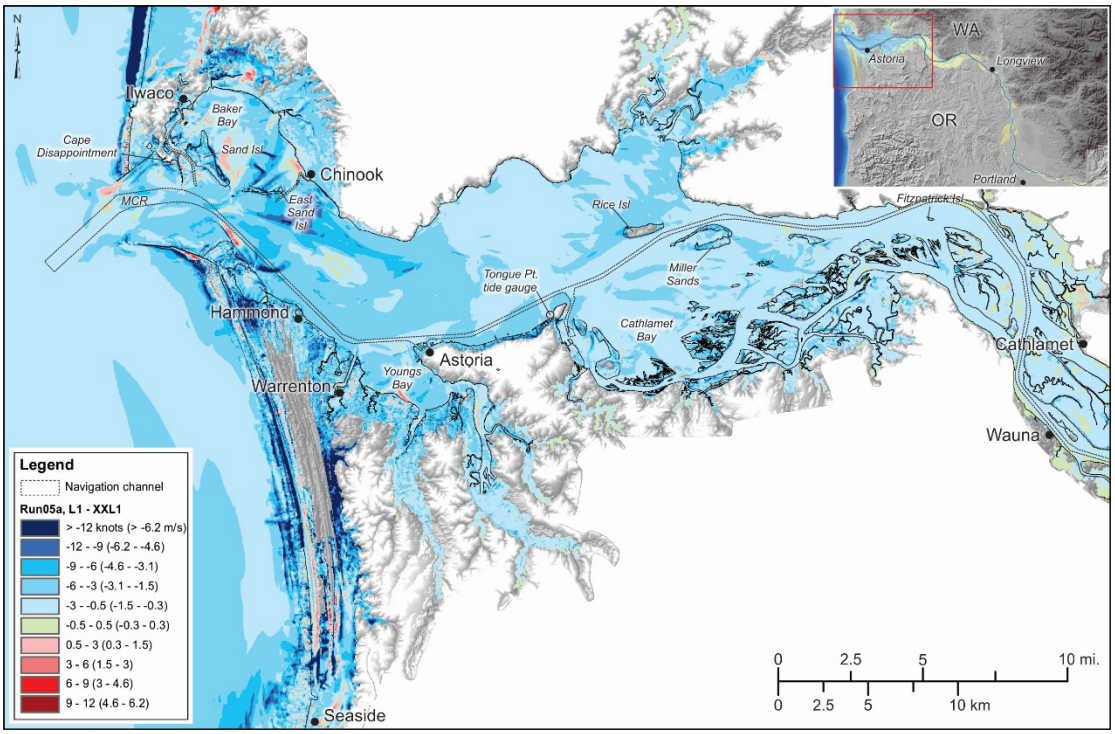

Figure 14 presents a comparison of the L1 scenario using a frictionless landscape (Run05a-L1, red zone), with the same scenario but with Manning-*n* = 0.025 and with the tide now fixed at MHW (Run05c-L1, green zone); Manning-*n* = 0.025 is akin to a sand beach, and values in the range of 0.02 to 0.03 are commonly used in tsunami modeling (e.g., Bricker and others, 2015). Hence, it introduces some nominal roughness into the simulations (see **Table 2**). The latter inundation zone was requested by the Washington Geological Survey for the development of tsunami inundation zones on the Washington side of the estuary. Overall, the incorporation of friction produces a measurable reduction in the inundation extent (and flow velocities). This is most apparent in areas that are generally low lying, with the largest changes apparent in Oregon, along the Clatsop Plains and near Astoria, and to a lesser degree northeast of Ilwaco on the Washington coast (**Figure 14**). Near Ilwaco, the addition of friction effectively blocks the tsunami from crossing the Long Beach barrier spit as it inundates from the west. Because the terrain in this area increases from ~3 to 12 m, the difference in inundation can largely be attributed to the effects of friction as opposed to the 0.2-m height difference in tidal datums used. Elsewhere, the effect of friction produces less inundation in areas to the north of Cathlamet, southeast of Wauna, and at the distal extents of the model domain.

Figure 14. Comparison of maximum tsunami inundation lines from static-tide runs modeled using MHHW (Run05a-L1) and a frictionless landscape, and Run05c-L1 modeled using MHW and *n* = 0.025.

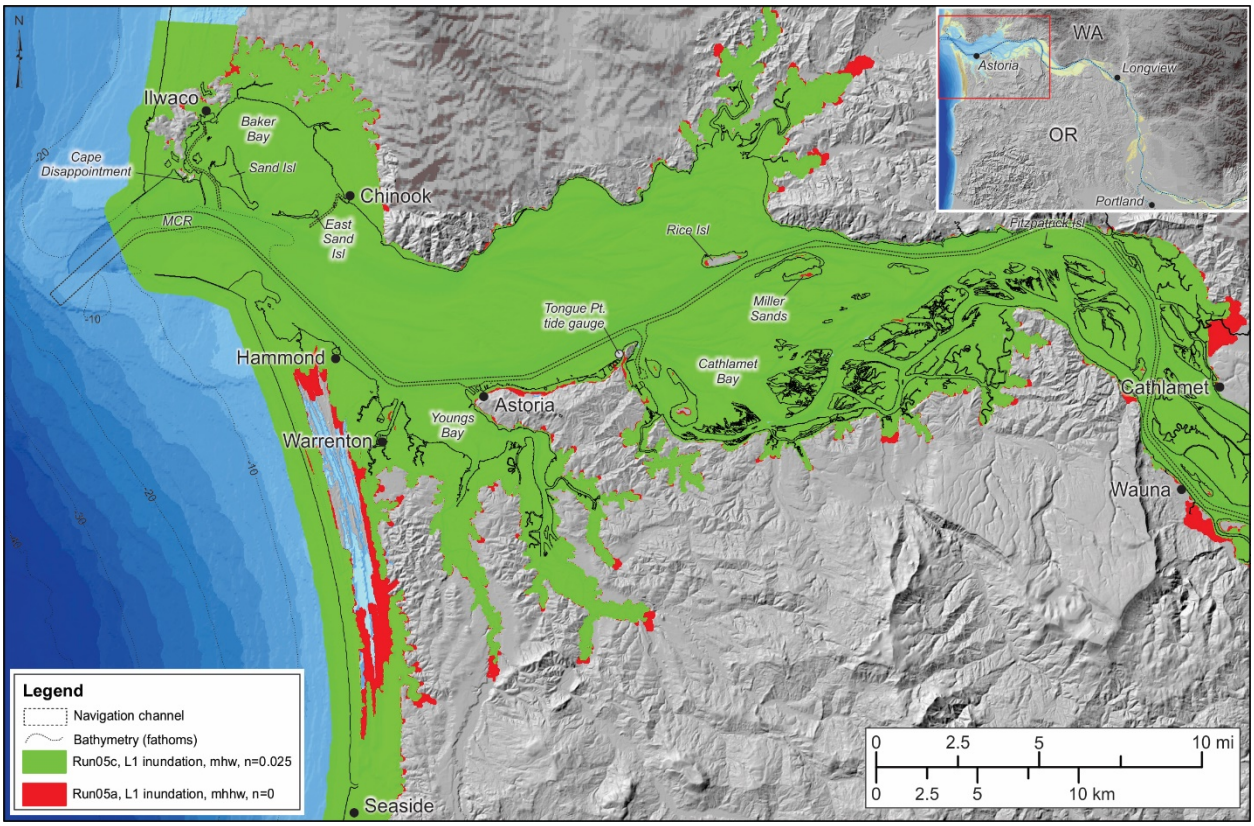

To highlight the upriver extent of the tsunami incursion associated with the maximum considered local event (Run05a), we define the maximum tsunami water level along the length of the navigation channel, which extends from offshore the mouth of the Columbia River (MCR) to Bonneville Dam (**Figure 15**). The maximum water level is defined as:

$$\max \text{wl} = FD - d \tag{2}$$

where *FD* is the flow depth and *d* is the elevation of the ground or bathymetric surface after subsidence.

As can be seen in **Figure 15**, the largest tsunami waves are concentrated at the MCR within the first 13 km (8 miles) of the channel. Upon entering the estuary, dispersive effects cause the tsunami waves to decrease in height. Due to the proximity of the navigation channel at Astoria, the tsunami water levels increase in height again as the tsunami is focused toward the shore, where the tsunami runs up and inundates Astoria (**Figure 15**). Water levels remain high until just east of Tongue Point, where the estuary opens up and the waves are dispersed over a broad, shallow area that makes up the upper estuary. The tsunami waves continue their progress upriver, with the most landward tsunami incursion near the I-205 bridge adjacent to the Portland airport.

Included in **Figure 15** is the combined result of our simulation of the tsunami, but with the effects of an average river flow incorporated; the three flow regimes used in our simulations are included in the bottom plot in **Figure 15** in order to highlight the range of possible river flows. In this scenario, the incorporation of river flow essentially elevates the tsunami water levels between Kelso and Miller Sands by approximately 0.25 m (0.8 ft), while outgoing riverine currents depress the incoming tsunami waves (by ~0.5 m [1.6 ft]) near the MCR.

The nearly linear increase in water levels upriver of Kelso reflects the increasing effect of riverine effects in controlling water levels along the channel. Jay and others (2015) noted that although water levels at Beaver are superficially similar to those at Tongue Point, but with smaller amplitudes, spring freshets raise the mean water level at Beaver by about 0.5–1 m (1.6–3.3 ft). At St. Helens and Vancouver, the mean water levels increase to ~1.5–3.2 m (4.9–10.5 ft) during the spring freshet (Jay and others, 2015).

Figure 15. ***(top)*** **Maximum tsunami water levels interpolated along the Columbia River navigation channel for XXL1 (Run05a), and with the incorporation of average river flows (Run04a);** ***(bottom)*** **Simulations of Columbia River flows based on three river flow regimes (no tsunami). Note: 0Q denotes no river flow, while aveQ denotes an average river flow.**

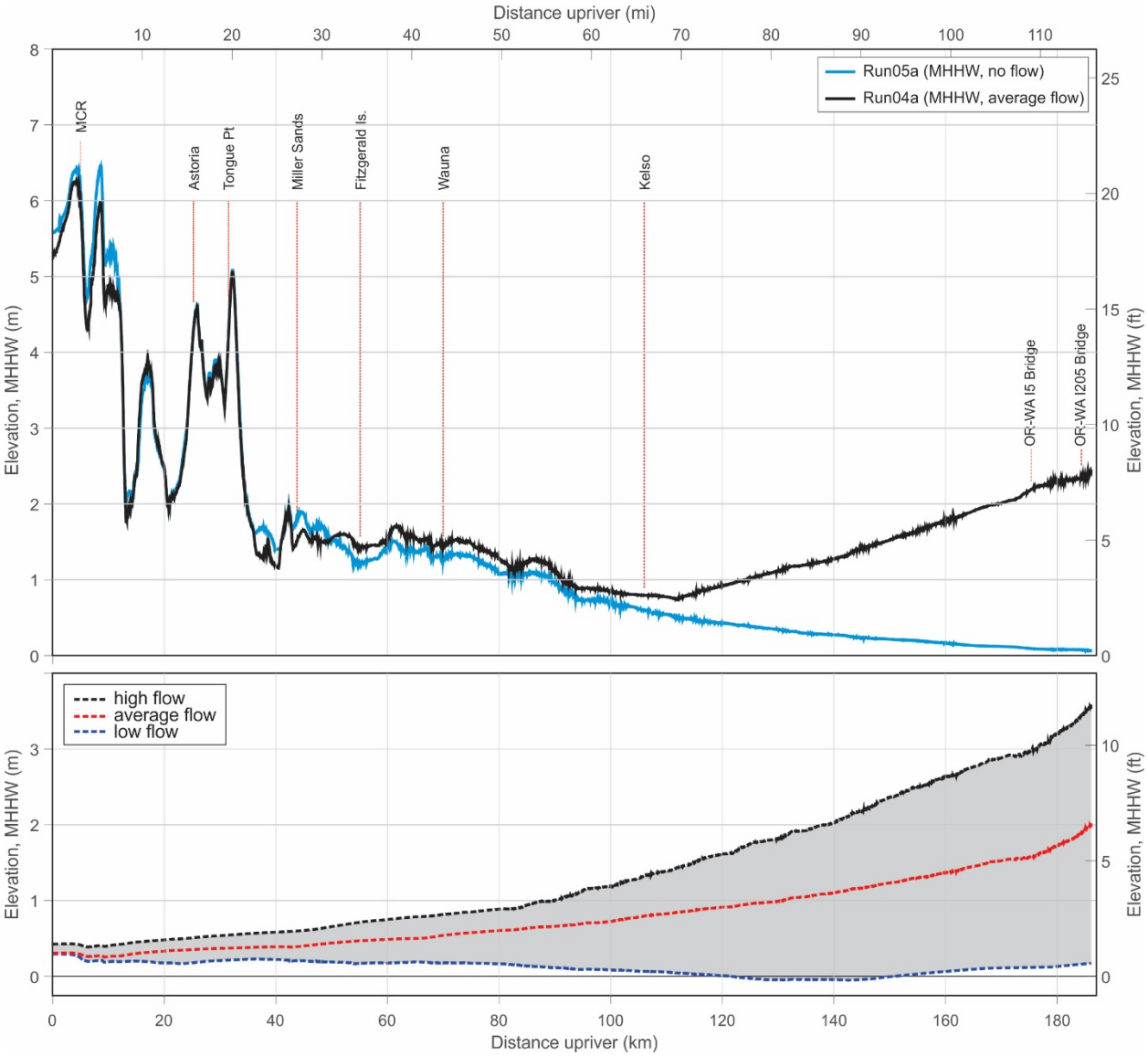

4.2 Dynamic-Tide Results

4.2.1 Tidal effects: flood versus ebb conditions

The addition of dynamic tides introduces a great deal of complexity into the results, due to the nonlinear interaction between tides and tsunamis in this high-energy system. The predicted maximum velocity exhibits more local extrema along the coast and within the lower estuary, especially near the mouth where the interaction is found to be strongest due to powerful currents and shoaling of tsunami waves (compare **Figure 16** with **Figure 12**). Not surprisingly, the wave patterns are highly dependent on the tidal phase at which the tsunamis arrive. The conventional wisdom is that tsunamis arriving with a flood spring tide are usually more damaging. This is generally true in the deep channel around Tongue Point evident in **Figure 17**, which shows differences in current velocities between the flood (Run06a) and ebb (Run07a) tide conditions. Velocities less than −0.5 knots indicate that the flood (Run06a) currents dominate, while currents greater than 0.5 knots indicate that ebb (Run07a) conditions dominate. The region between ±0.5 knots denote little difference between the simulations. Not surprisingly, flood conditions lead to greater inundation evident by the abundant blue on Clatsop Spit (including Hammond and Warrenton), and on the Washington coast around Chinook and Ilwaco. This difference is almost entirely due to the tidal elevation difference.

Figure 16. Maximum tsunami velocities (in knots) generated for the XXL1 (Run06a) simulation, modeled using dynamic tides, average river flow and friction. Note: timing of the wave arrival coincides with a flood tide at Tongue Point.

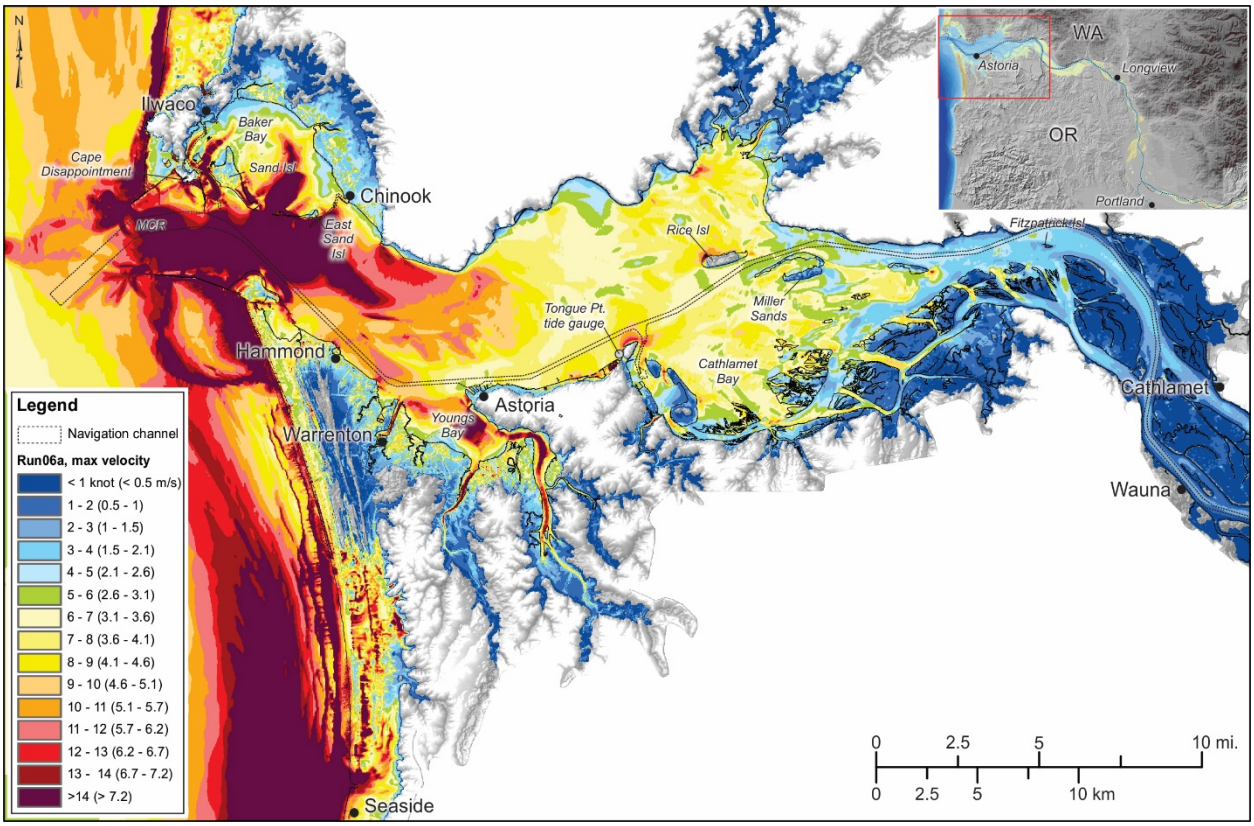

The situation becomes very complex in the shallow waters of the lower estuary, where tsunamis arriving at ebb and flood slack are usually more energetic (compare **Figure 17**, **Figure 18**, and **Figure 19**). As can be seen in **Figure 17**, strong currents dominate the ebb phase (Run07a) at the MCR, in Baker, Youngs, and Cathlamet Bay, and around Rice Island and Miller Sands. The presence of a ring of strong currents offshore Clatsop Spit (west of Hammond), probably reflects the formation of a gyre that develops in the hook of the jetty and spit. Tsunamis arriving at flood slack reveal generally minor differences in the current velocities relative to the flood stage (**Figure 18**), particularly when compared with the generally larger differences (and stronger currents) that characterize flood/ebb tide conditions (**Figure 17**); see **Figure 3** for a cartoon of these different tidal stages. Nevertheless, tsunamis arriving at flood slack produce greater upriver penetration of the tsunami, with currents that are stronger in the shallows east of Tongue Point, when compared to a typical flood tide situation. Strong current velocities are further apparent even during an ebb slack (**Figure 19**), with our simulation indicating even stronger current velocities offshore of the MCR, extending some 5 to 10 miles to the north and south of the mouth, as well as in the smaller harbors such as at Hammond, Chinook and Ilwaco, and within Baker Bay as a whole. Ebb slack also contributes to generally stronger currents immediately north of Astoria, due to shoaling around various sand banks.

Figure 17. Maximum tsunami velocities (in knots) expressed as the difference between ebb (Run07a) and flood (Run06a) simulations assuming average river flow and friction. Velocities less than 0 indicate Run06a currents dominate, while velocities greater than 0 indicate that Run07a currents dominate.

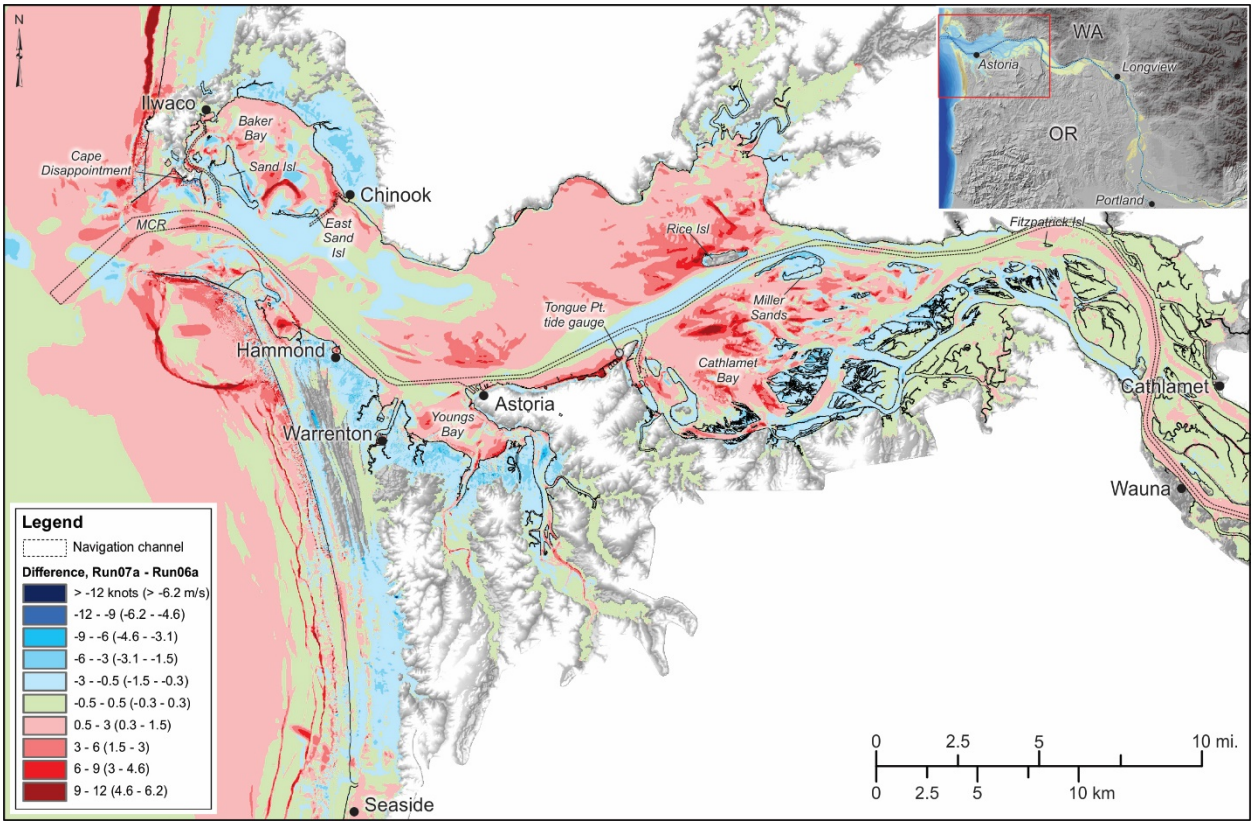

Figure 18. Maximum tsunami velocities (in knots) expressed as the difference between flood slack (Run08a) and flood (Run06a) simulations, average river flow and friction. Velocities less than 0 indicate Run06a currents dominate, while velocities greater than 0 indicate that Run08a currents dominate.

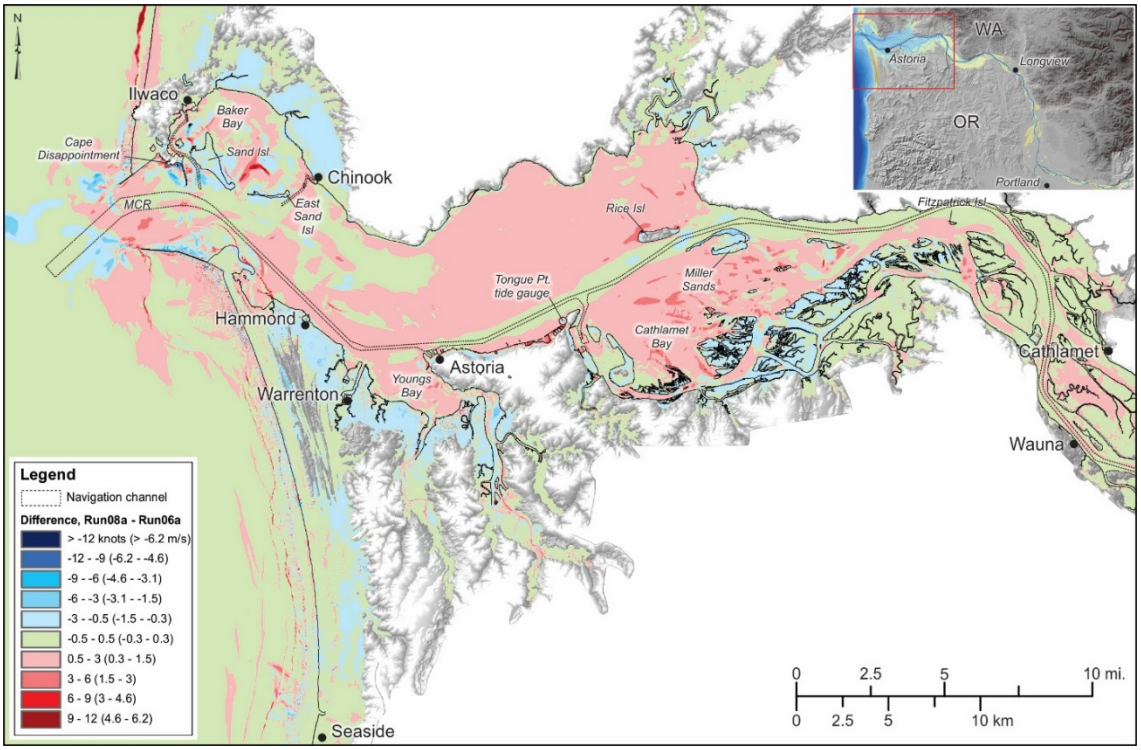

Figure 19. Maximum tsunami velocities (in knots) expressed as the difference between ebb slack (Run09a) and flood (Run06a) simulations, average river flow and friction. Velocities less than 0 indicate Run06a currents dominate, while velocities greater than 0 indicate that Run09a currents dominate.

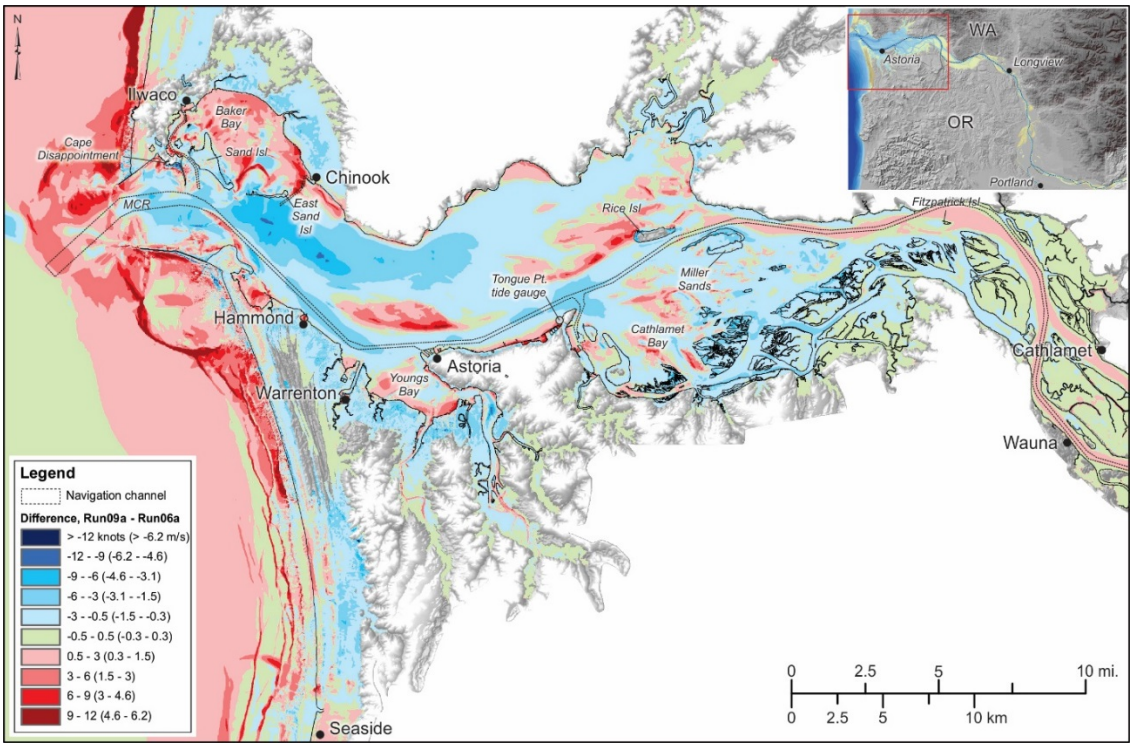

The violent collision between the tidal and tsunami currents at the MCR makes the ebb scenarios especially dangerous for ships of all sizes. **Figure 20** and **Figure 21** presents time series information of tsunami currents and water levels for two sites: MCR (3) and near Tongue Point (23) in the lower estuary (station locations are identified in **Figure 5**). The plots confirm the important fact that the tsunami wave arrival during an ebb phase produces considerably stronger currents when compared with the flood scenario (**Figure 20** and **Figure 21**). These effects extend well into the estuary (**Figure 17**). Not surprisingly, the water level time series reveals the opposite response, with the flood scenario exceeding the ebb. As noted previously, this response is entirely due to the different tidal stages on which the tsunamis are arriving. At Tongue Point, the response is a little more complicated due to the outgoing tide coupled with an initial drawdown caused by the approaching tsunami (**Figure 21**). The first peak current during the ebb is slightly lower initially compared with the flood, but subsequent incoming waves see the ebb currents exceeding the flood as water piles up in the estuary. Even at the MCR site, the velocity from the ebb scenario (**Figure 20**, *top*) is actually comparable to the flood case despite the maximum wave heights being noticeably lower (**Figure 20**, *bottom*). This finding can be attributed to the collision of the tsunami waves against opposing currents. Of importance, these collisions appear to prolong the period of strong currents for almost 4 hours. We find similar patterns characterizing the other two earthquake scenarios (L1 and AKMax) modeled in this study.

The simulations illustrate that there is generally little difference in the current velocities between average flow and the low (**Figure 22**) or high (**Figure 23**) flow scenarios in the Columbia River. For the low flow scenario, the largest differences are confined to offshore the MCR and along the open coast, where the low flow scenario enables slightly stronger tsunami currents to develop. This is essentially because the river is not as efficient at counteracting the incoming tsunamis. An offshore directed jet of strong current that typically exists west of the MCR (not shown), normally present in the other simulations, is weakest in the low flow condition. Strong currents in the hook of Clatsop Spit and the south jetty again reflect the formation of a large gyre, the product of the incoming tsunami waves reflecting off Clatsop Spit and the south jetty that causes rotation and the formation of strong vortices (**Figure 22**). Within the lower estuary, differences between low and average flow conditions are essentially negligible and are entirely due to the scale of the physical system and its ability to disperse the effect of the tsunamis over a broad area.

Figure 20. Time series for Run06a (flood) and Run07a (ebb) showing the modeled *(top) u* and *v* tsunami currents and *(bottom)* water levels at water level station 3 located at the mouth of the Columbia River simulated on an average river flow. Note: positive *u* indicates eastward directed currents, while negative *u* denotes westward directed currents; positive *v* indicates northward directed currents, while negative *v* denotes southward directed currents. Note also how rapidly currents reverse direction and water levels change in the first few hours.

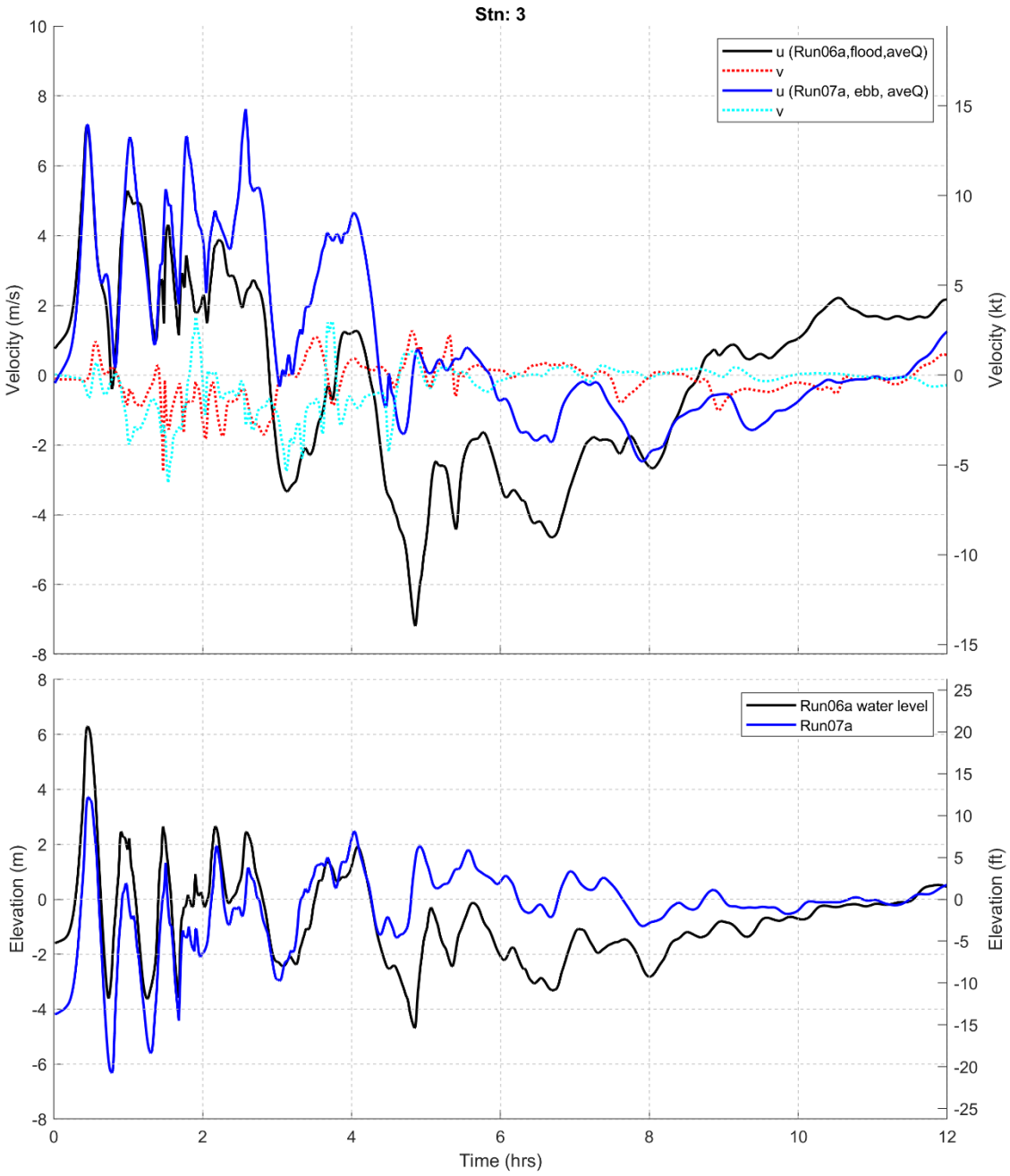

Figure 21. Time series for Run06a (flood) and Run07a (ebb) showing the modeled *(top) u* and *v* tsunami currents and *(bottom)* water levels at water level station 23 located adjacent to Tongue Point simulated on an average river flow. Note: positive *u* indicates eastward directed currents, while negative *u* denotes westward directed currents; positive *v* indicates northward directed currents, while negative *v* denotes southward directed currents. Note also how rapidly currents reverse direction and water levels change in the first few hours.

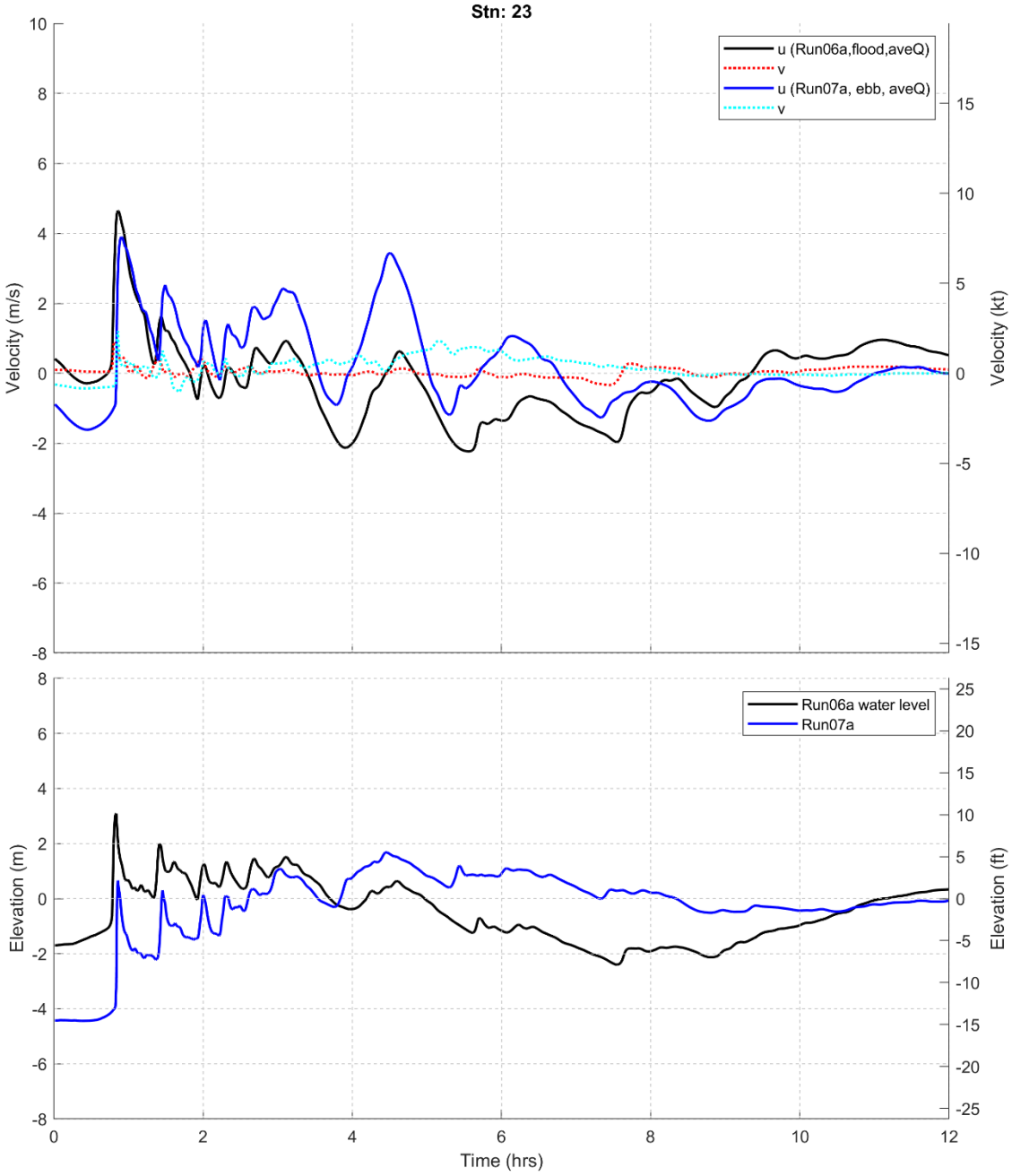

4.2.2 Effects from riverine flows: average, low, and high flow conditions

Figure 22 and **Figure 23** compare the modeled tsunamis arriving during the low (Run10a) and high (Run11a) river flow scenarios with conditions modeled using the average flow (Run06a); dynamic tides are used in all three examples with the tsunami arriving at flood stage.

Figure 22. Maximum tsunami velocities (in knots) expressed as the difference between flood and low river flow (Run10a) and flood (Run06a) simulations. Velocities less than 0 indicate Run06a currents dominate, while velocities greater than 0 indicate that Run10a currents dominate.

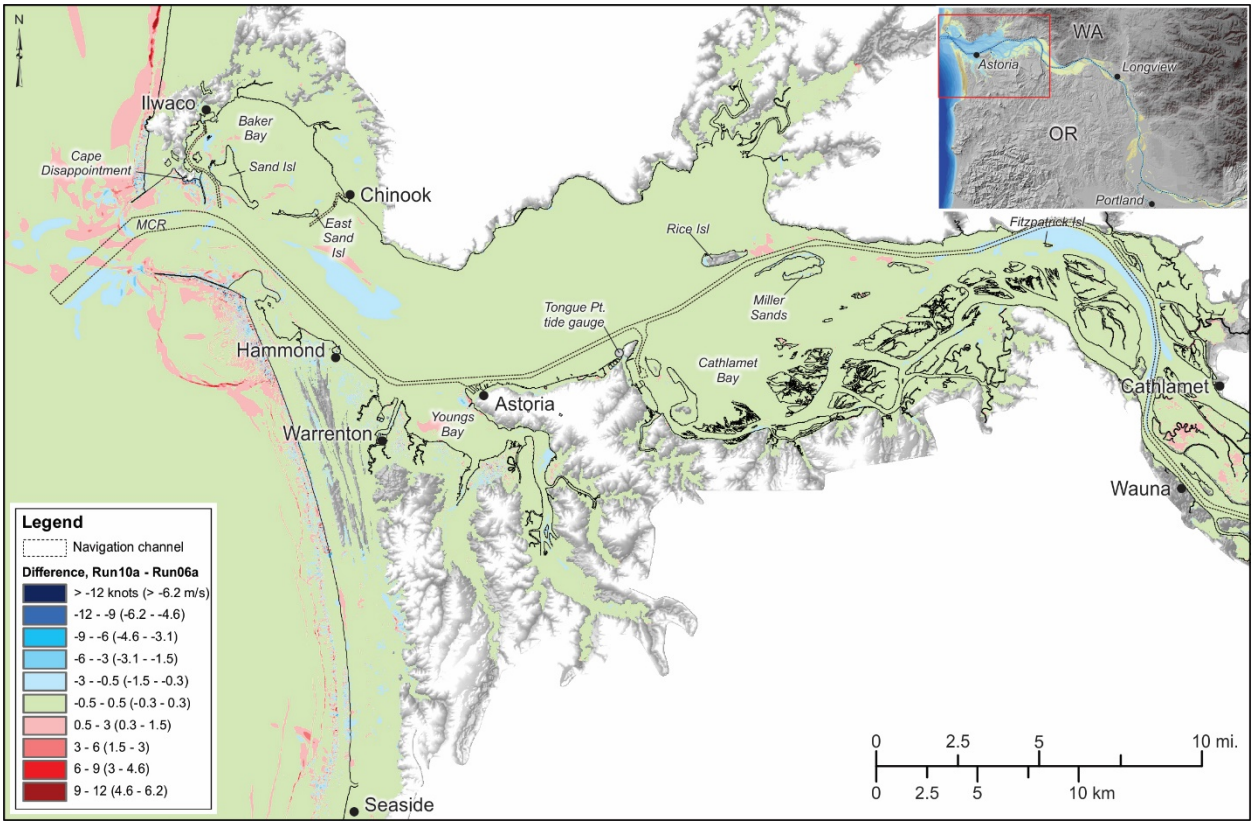

Differences between the high (Run11a) and average (Run06a) flow scenarios are essentially the inverse of the low flow conditions. In general, the most important differences are concentrated at the mouth (especially seaward of the MCR), with much less of an influence along the open coast to the north and south of the MCR. This can be attributed to stronger outflows associated with a flood, which contributes to the formation of strong offshore directed currents, particularly around the MCR. Not surprisingly, with progress upriver stronger currents emerge, which are associated with the higher river flow regime (pink region upriver of Rice Island). However, what is telling under both low and high flow conditions is the fact that there is very little difference between the scenarios in the lower estuary; this is entirely a function of the size of this system and its capacity to absorb the tsunami wave effects. This lack of difference is especially highlighted in **Figure 24**, which compares the differences in the modeled water levels and current velocities along the length of the navigation channel relative to average flow condition (Run06a). Under the high flow situation, high flow contributes only about 0.2 m (0.7 ft) to the maximum water levels within the lower Columbia River estuary (downstream of Fitzpatrick Island) (**Figure 24**, *top*);

for low flow, the difference is only about −0.25 m (−0.8 ft). Larger (lower) differences upstream of Fitzpatrick Island are dominated by Columbia River flows.

Effects on the current velocities are greatest adjacent to the MCR. For the high flow regime the currents initially decrease with progress up the estuary (**Figure 24**, *bottom*); upstream of Miller Sands the current velocities begin to increase. Conversely, for the low flow scenario stronger currents occur between Astoria and Miller Sands. However, beyond Miller Sands, the currents decrease significantly until just east of Kelso.

Overall, we find that varying the river flows has generally a negligible effect on the tsunami, especially within the lower estuary. This contrasts with the tidal component, which has a significantly greater influence on the modeled tsunami currents and water levels produced.

Figure 23. Maximum tsunami velocities (in knots) expressed as the difference between flood and high river flows (Run11a) and flood (Run06a) simulations. Velocities less than 0 indicate Run06a currents dominate, while velocities greater than 0 indicate that Run11a currents dominate.

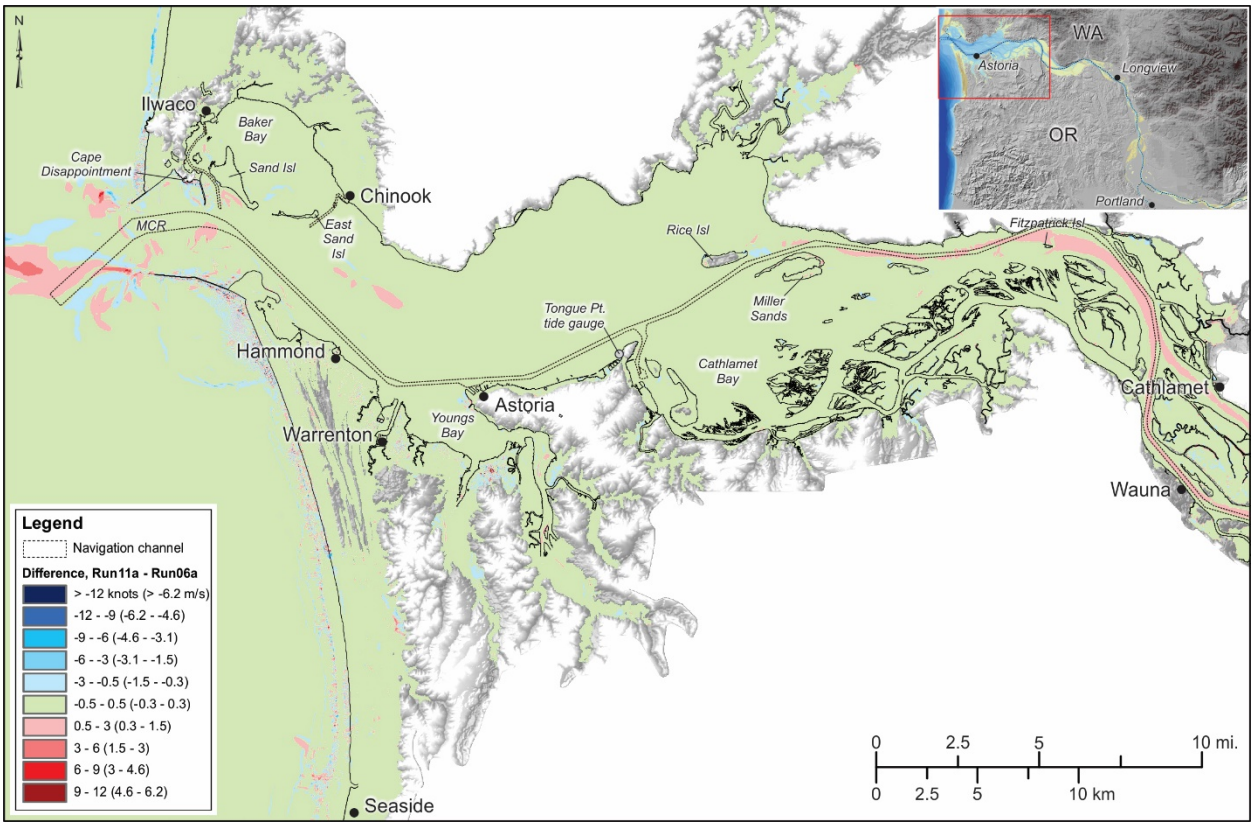

Figure 24. Plot showing differences in the simulated maximum tsunami water levels and current velocities occurring under high/low river flows and relative to the average flow scenario modeled on a flood tide.

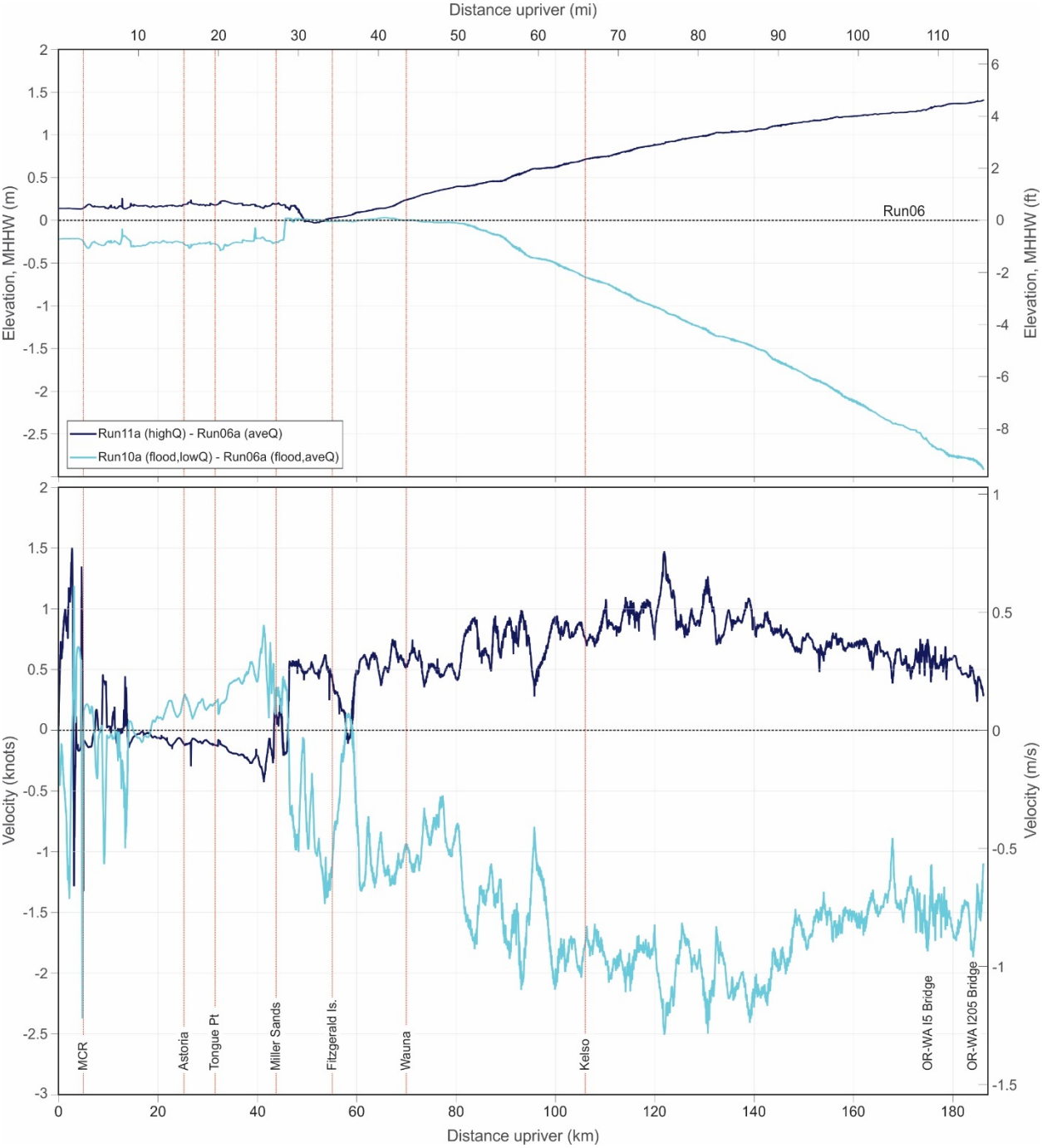

4.3 Wave Arrival Times

Knowledge of tsunami wave arrival times is vital to both terrestrial and maritime evacuation planning, because arrival times determine how much time the public will have to respond. In defining the tsunami arrival times along the Columbia River, we examined the water level time series determined for a number of key stations within the system, the locations of which are presented in **Figure 5**. Tsunami wave arrivals were defined on the basis of three criteria:

1. An initial wave arrival time, which reflects the moment at which the water level begins to depart from the normal background tidal signal;
2. The time at which the maximum water level is reached for the first wave; and
3. The time associated with the peak water level.

The reason for the latter is that although the first wave generally produced the highest water level, multiple upriver sites were identified where the maximum water level occurred some hours later. These data are summarized in the following sections for the maximum-considered local (XXL1) and distant (AKMax) tsunamis.

Figure 25 presents the XXL1 wave arrival times for select sites along the Columbia River, while **Figure 26** shows the maximum tsunami water levels for the various simulations along the length of the navigation channel. Included in the latter figure are the expected wave arrival times at various locations along the river channel. As can be seen in **Figure 25** and **Figure 26**, the largest tsunami waves are concentrated at the MCR within the first 13 km (8 mi) of the channel. Water levels remain high for most scenarios until approximately Miller Sands (**Figure 26**), before falling appreciably. This response is likely due to a variety of factors including the meandering shape of the estuary channel, which helps dissipate the tsunami energy, as well as in response to the presence of numerous bars and islands and the general shallowing in the upper estuary east of Tongue Point. The exception to this pattern is Run08 (flood slack), which shows greater upriver penetration of the tsunami beyond Wauna.

The local tsunami arrives at the MCR ~7 minutes after the start of earthquake shaking, while the peak wave arrives some 17 minutes later. Thus, the tsunami maxima at the mouth occurs about 24 minutes following the onset of shaking (**Figure 25**).

Initial wave arrivals at Hammond, Ilwaco, and Chinook are 23, 25, and 22 minutes, respectively. Having entered the estuary, the tsunami takes an additional 8–12 minutes to reach its maximum. Notable exceptions occur at the MCR and in the harbor at Ilwaco, where it takes longer (~16–20 minutes) for the peak of the wave to be reached. The former is due to the time it takes for the mass of water to funnel its way through the MCR, while the latter is a function of refraction processes that drive the wave north between Cape Disappointment and Sand Island (initial wave arrival), as well as from reflection of the tsunami waves within Baker Bay as the waves are redirected after striking the community of Chinook and are driven back westward toward Ilwaco (these changes effectively extend the duration of the peak wave). The tsunami reaches Astoria 34 minutes after the onset of earthquake shaking (**Figure 25** and **Figure 27**) and ~12 minutes later at Tongue Point.

Figure 25. Tsunami wave arrival times defined for XXL1 (local) for discrete locations along the Columbia River. Times reported are in minutes. Background image reflects the integration of the maximum water levels determined from all XXL1 model simulations to form an "ensemble" result of maximum water levels. Example water level time history plot is for station 3 at the mouth of the Columbia River (MCR). Red numbers correspond to the initial wave arrival (the point at which the water level begins to depart from normal), while black numbers reflect the time at which the maximum wave arrives.

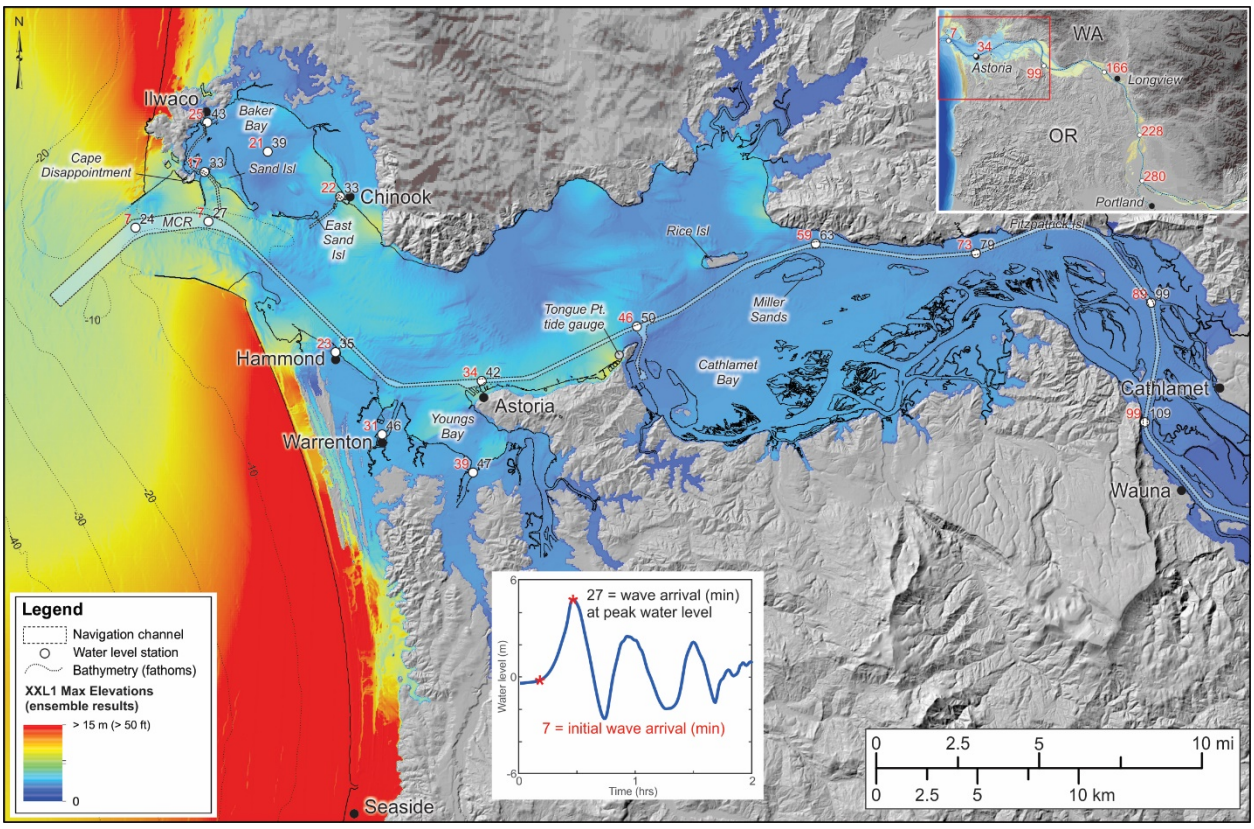

Figure 26. Maximum tsunami water levels interpolated along the Columbia River navigation channel for various XXL1 simulations. Included in the plot are the expected wave arrival times. Blue shading denotes the range covered by high/low river flows, while gray shading covers the spectrum of responses associated with various tidal stages modeled using an average river flow.

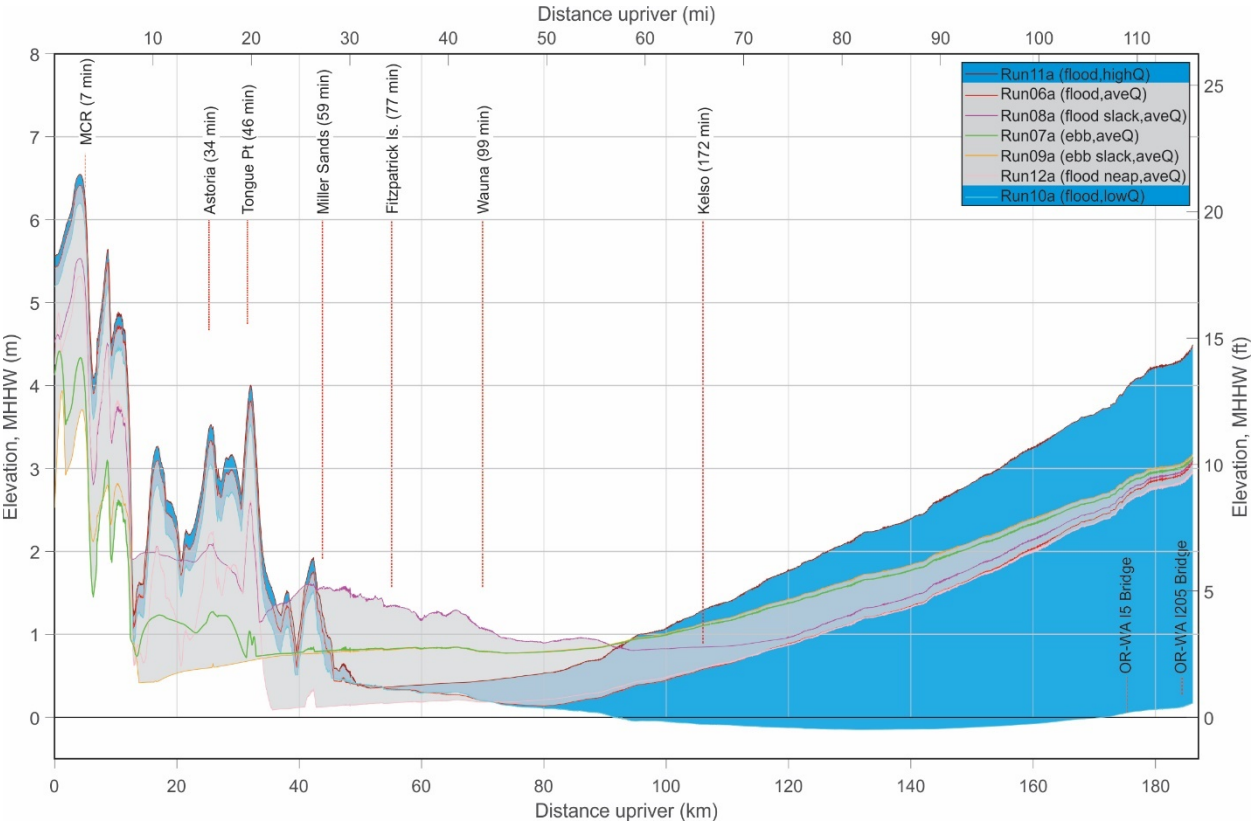

To better understand the timing of the tsunami wave sequence travel and arrival at sites upriver from Astoria, we performed a wavelet analysis[7] (e.g., Torrence and Compo, 1998) of the tsunami frequency bands for selected sites along the Columbia River. This approach allows for a more rigorous assessment of differences in the power within the tsunami time series (essentially the time-varying frequency content of the tsunami signal), allowing us to more definitively track the tsunami progress as it travels. As noted by Torrence and Compo (1998), converting a time series of water levels into time-frequency space allows one to determine the dominant modes of energy variability, and further how those modes change over time. Essentially, the approach allows one to track the dominant energy signal of the tsunami as it propagates upriver.

Figure 27 presents the results of the wavelet analysis for two sites along the Columbia River channel: Tongue Point (station 23) and the confluence of the Columbia and Willamette Rivers (station 57). The plots indicate that most of the power in the tsunami signal is concentrated in the tsunami band for periods ~2 hours (the left y-axis), with some energy also present at both higher and lower frequencies. The change in the tsunami power over time is captured on the x-axis (time in hours), which shows the signal over 24 hours (the length of the model simulation). The shaded regions on either end (shaped like the keel of a boat) indicate the "cone of influence (COI)," where edge effects become important and errors are

7 http://noc.ac.uk/marine-data-products/cross-wavelet-wavelet-coherence-toolbox-matlab

introduced from the analyses. The latter occurs because the approach assumes the time series is cyclic. As a result, below the COI line, the results are not considered to be significant.

The initial peak signal in the time domain occurs at ~46 minutes and is consistent with the peak wave arrival time for Tongue Point presented in **Figure 25**, with additional peaks occurring at 1.4, 2, and 5.6 hours (**Figure 27**) as additional tsunami waves arrive at the site. Of importance, the dominant energy signal at Tongue Point is strongest during the first 5–7 hours after the earthquake, with the bulk of the energy expended by hour 10, and negligible by hour 15.

At ~90 minutes, the tsunami begins to wrap around the bend toward Cathlamet and Wauna and reaches Longview some 2 hours and 46 minutes after the start of earthquake shaking (**Figure 25** and **Figure 26**). The tsunami is detectable as far upriver as the confluence of the Columbia and Willamette Rivers (**Figure 27**), arriving 4 hours and 40 minutes after the start of earthquake shaking (**Figure 25**). However, the tsunami contains very little energy (**Figure 27**) by this stage such that the waves and currents can be effectively ignored. Similar wavelet analyses were undertaken for other stations along the Columbia River. From these data and the generated currents, we find that the tsunami will have little impact to shipping upriver of St. Helens. Furthermore, *we conclude that effects of a maximum-considered XXL1 local tsunami will not impact the ports of Portland or Vancouver and no additional measures will be needed to safeguard vessels at these locations*, aside from having to deal with the earthquake shaking. With respect to the latter, estimates of horizontal ground acceleration at various distances inland from a CSZ earthquake are given by Gregor and others (2002) and more recently by Madin and Burns (2013). These ground accelerations could possibly cause navigation hazards where water-saturated sediment liquefies and causes navigation channel sides, levees, and port foundations to fail.

Figure 27. Wavelet analysis of the XXL1 (local) tsunami water level time series at Tongue Point and at the Columbia/Willamette River confluence. Note: hot colors indicate significant energy; shaded regions on either end indicate the "cone of influence," where edge effects become important; solid contour is the 95% confidence level. Time (x axis) in hours is after the earthquake.

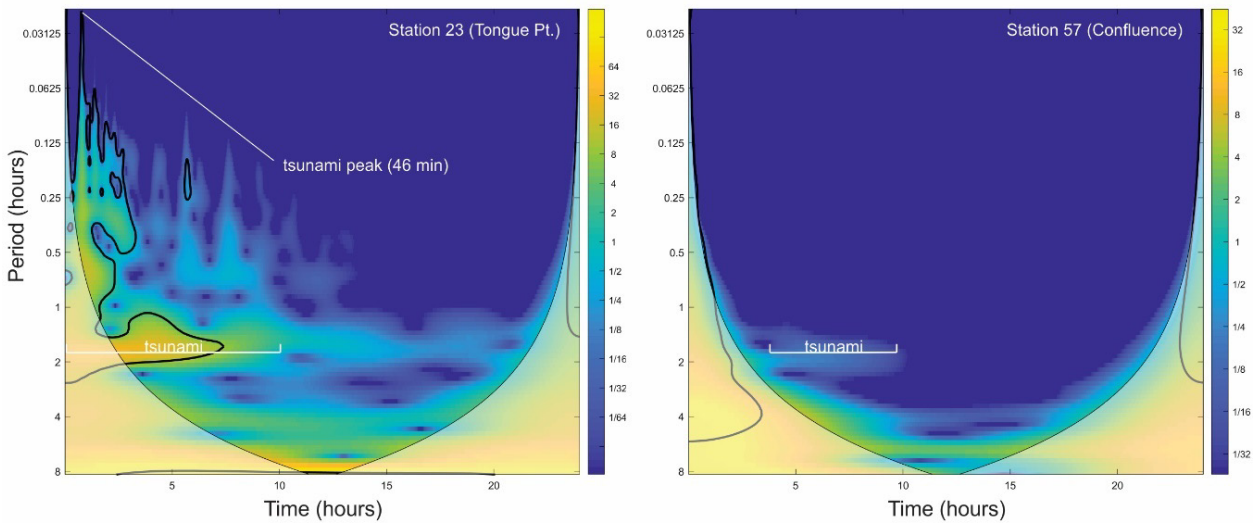

4.3.1 Distant (AKMax) tsunami wave arrival times

The AKMax distant tsunami reaches the MCR ~3 hours 38 minutes after the earthquake, with the wave maximum occurring ~12 minutes after the water levels begin to increase (**Figure 28**). Within the lower Columbia River estuary, the initial peak tsunami wave is reached ~6–8 minutes after the wave begins to arrive. Longer times for the maximum wave arrival are evident for Ilwaco and within Baker Bay (e.g., 5 hours 45 minutes after the earthquake) that are caused by a much larger later arriving tsunami wave.

The tsunami reaches Astoria in 4 hours and 8 minutes (**Figure 28** and **Figure 29**) and ~ 9 minutes later arrives at Tongue Point. This is evident in **Figure 30** by the initial peak, followed by several other ensuing peaks thereafter. At Tongue Point, the distant tsunami event is effectively over ~ hour 7, with some residual activity until ~ hour 11.

Once the tsunami has entered the estuary, it takes ~ 90 minutes for the wave to travel upriver to Wauna, arriving there ~ 5 hours 9 minutes after the Aleutian earthquake. From Wauna, it takes an additional 62 minutes for the wave to reach Longview. The distant tsunami scenario can be detected as far upriver as St. Helens (**Figure 30**). However, as with the XXL1 local event, there is effectively little energy left and the distant tsunami can be effectively ignored upriver of Longview.

Figure 28. Tsunami arrival times defined for AKMax (distant) for discrete locations along the Columbia River. Times reported are in minutes and are relative to the initial (3 hr 38 min) wave arrival at the mouth of the Columbia River (MCR). Background image reflects the integration of the maximum water levels determined from all AKMax model simulations to form an "ensemble" result of maximum water levels. Example water level time history plot is for station 3 at the MCR. Red numbers correspond to the initial wave arrival (the point at which the water level begins to depart from normal), while black numbers reflect the time at which the maximum wave arrives.

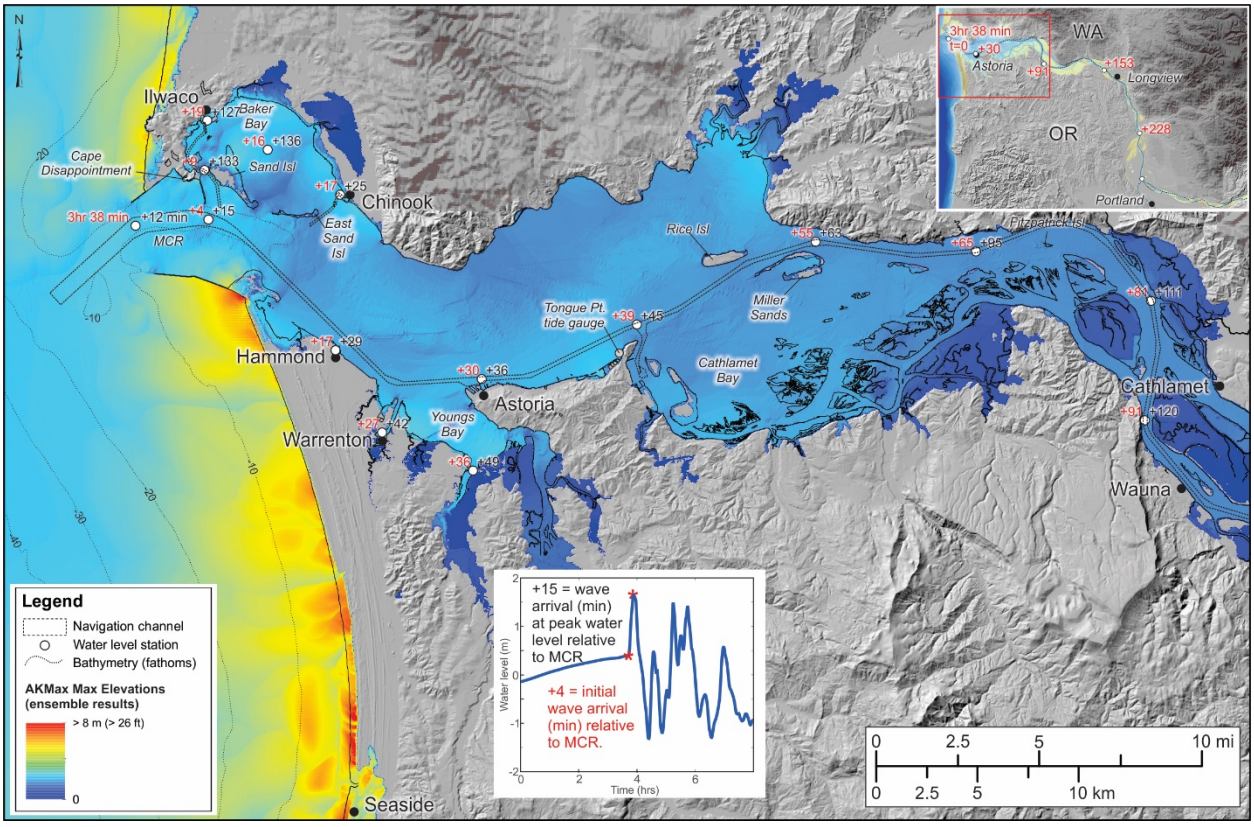

Figure 29. Maximum tsunami water levels interpolated along the Columbia River navigation channel for various AKMax simulations. Included in the plot are the expected wave arrival times. Blue shading denotes the range covered by high/low river flows, while gray shading covers the spectrum of responses associated with various tidal stages modeled using an average river flow.

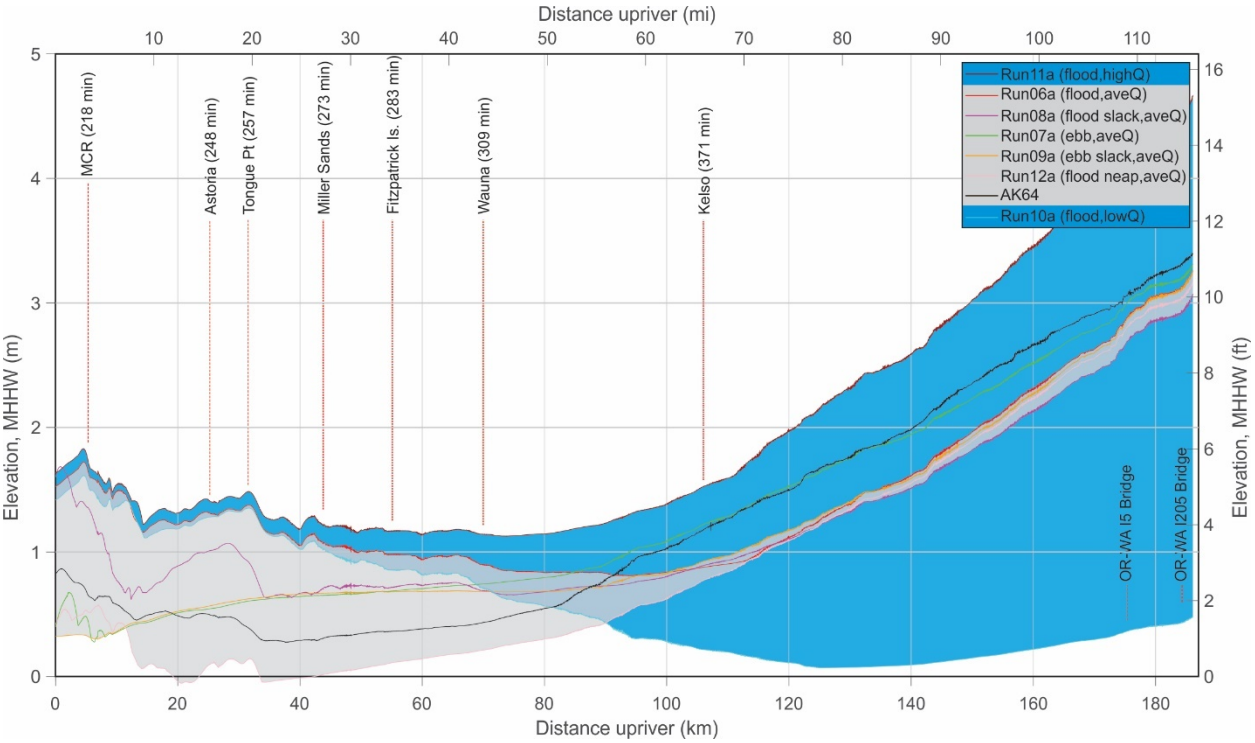

Figure 30. Wavelet analysis of the AKMax (distant) tsunami water levels time series at Tongue Point and at St. Helens. Note: hot colors indicate significant energy; shaded regions on either end indicate the "cone of influence," where edge effects become important; solid contour is the 95% confidence level. Time (x axis) in hours is after the earthquake.

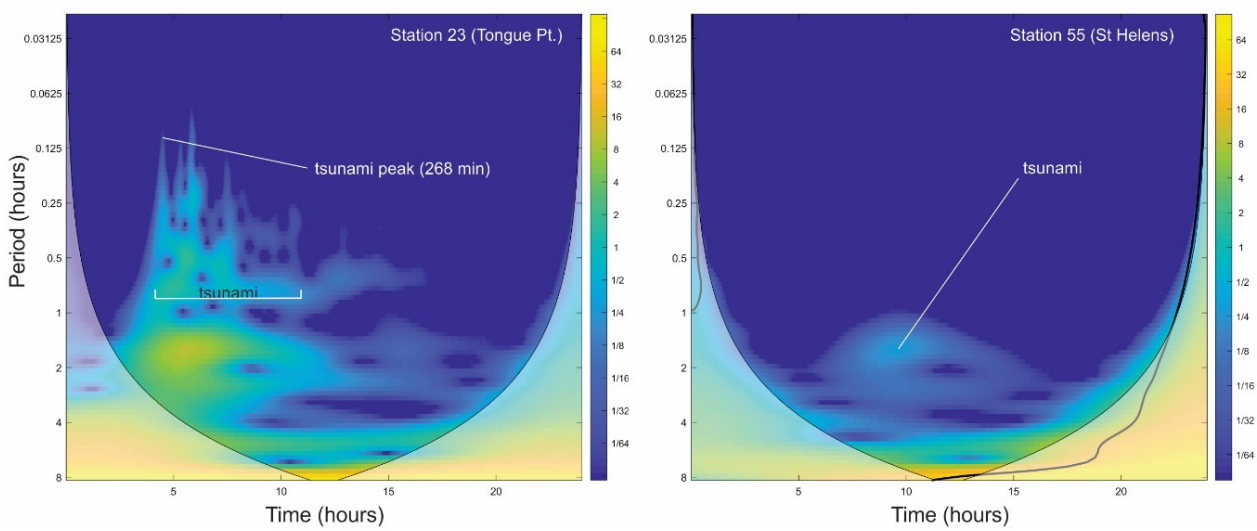

5.0 ENSEMBLE MODEL RESULTS

Due to uncertainties in the timing of a local or distant tsunami event, coincident with different tidal stages and Columbia River flow regimes, we derive "ensemble" modeling results for each earthquake source. The approach effectively combines maximum water levels, currents, vortices, and minimum water levels for each scenario into a single merged raster for each of these parameters. This allows us to incorporate the uncertainty characterized by the range of tsunami/tide/flow combinations, providing a more conservative model estimate of the tsunami effect for incorporation into appropriate response guidance. To generate the ensemble product, we produced individual rasters for each model simulation in ArcGIS and for each of the previously mentioned parameters. We then created the ensemble raster by using the ArcGIS "mosaic to new raster" tool with the maximum value defined for each grid cell; for the minimum flow depth, we used the minimum value assigned to the grid cell.

5.1.1 Local (XXL1 and L1) tsunami ensemble results

5.1.1.1 XXL1 and L1 water levels

Figure 31 presents the merged water levels for both an XXL1 and an L1 local event. The plots demonstrate two contrasting responses: the extreme water levels that will be experienced along the open coast (warm colors), and the generally much lower water levels (cool colors) upstream of Wauna. Between these two areas is a large region in which the water levels are expected to range from 1 to 4 m (3.3–13 ft), relative to MHHW for an XXL1 size event, decreasing to about 1–3 m (3.3–9.8 ft) for the L1 scenario (**Figure 31**). Furthermore, both figures highlight several sites at the shore where tsunami flooding (and hence damage) is likely to be extreme (red colors), including Chinook in Washington, and between Astoria and Tongue Point in Oregon. Catastrophic conditions will characterize both scenarios, especially adjacent to the MCR (west of Hammond), while damaging waves and strong currents will affect much of the area within the estuary, especially between Hammond and Tongue Point (**Figure 31**).

Time series information for select stations along the river is presented in **Figure 32** (XXL1) and **Figure 33** (L1). These data have been truncated to span the first 12 hours of the simulations, providing improved insight into the variability and range of modeled water levels. The gray shading in each plot defines the envelope (range) of variability from the combined suite of simulations. Both time series highlight the extreme nature of the tsunami waves at the MCR (Station 3), which decreases rapidly by the time the tsunami reaches Tongue Point (Station 23). At Wauna, the wave reflects a large bore (~ 2.5 m [8 ft] high) with a steep front with water levels remaining high for at least 3 hours before subsiding. As can be seen in both figures, the tsunami continues to lose energy as it travels upriver; at Longview the XXL1 bore is about 0.6 m (2 ft) in height, and it takes ~47 minutes for the water levels to rise (**Figure 32**); the response there would be akin to a fast rising tide.

Figure 31. Ensemble model results of the maximum tsunami water levels (flow depth–depth) generated by a *(top)* XXL1 and (*bottom)* L1 CSZ earthquake. Cartoon showing water level time history and attributes is of station 3 at the mouth of the Columbia River (MCR).

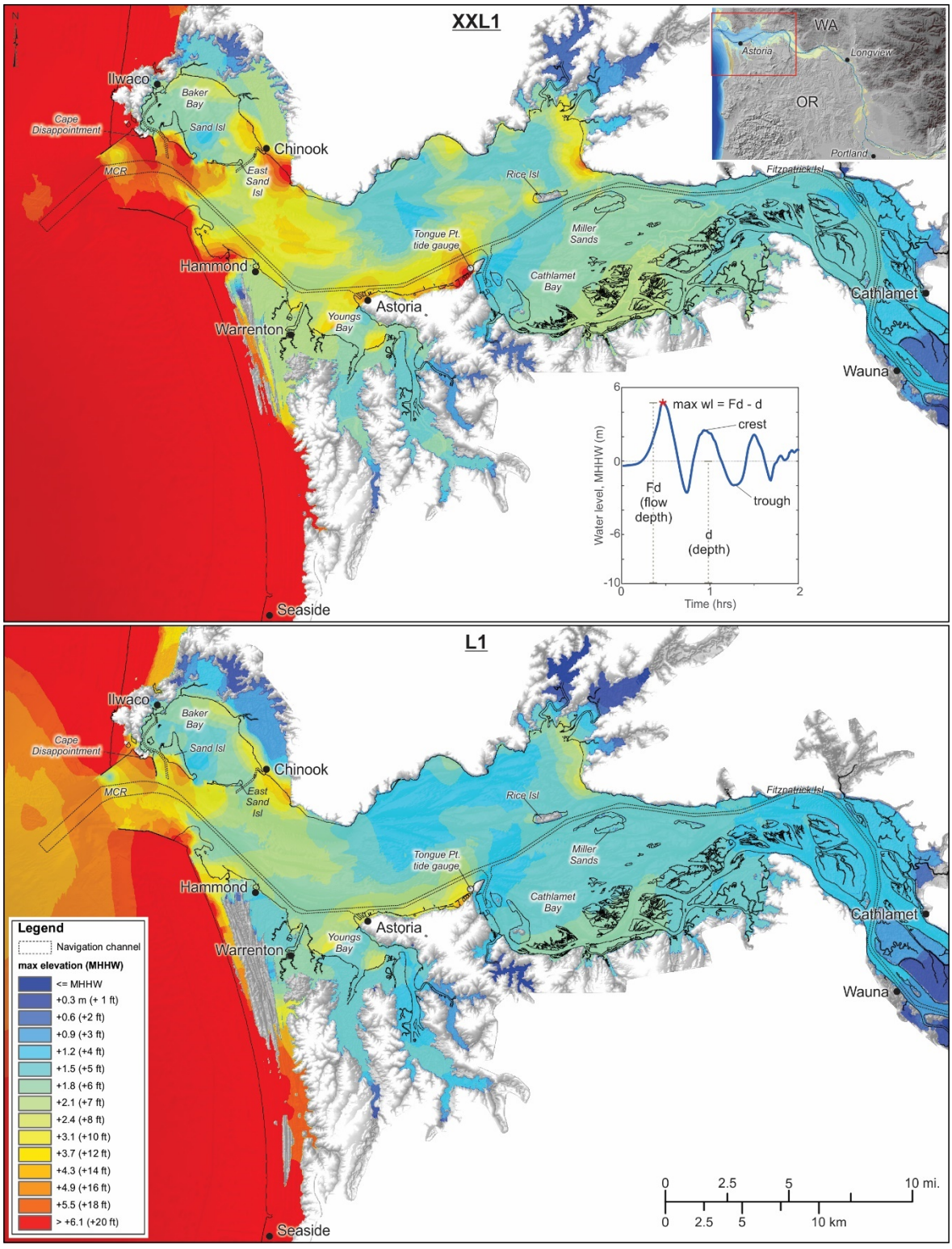

Figure 32. Time series showing the modeled water levels (flow depth–depth) for two simulations of a CSZ tsunami (XXL1) travelling along the navigation channel from the MCR to Longview. Gray shading denotes the envelope of variability in the water levels from all simulations. Station 3 is at the mouth of the Columbia River, station 23 is at Tongue Point, station 38 is at Wauna, and station 46 is at Longview.

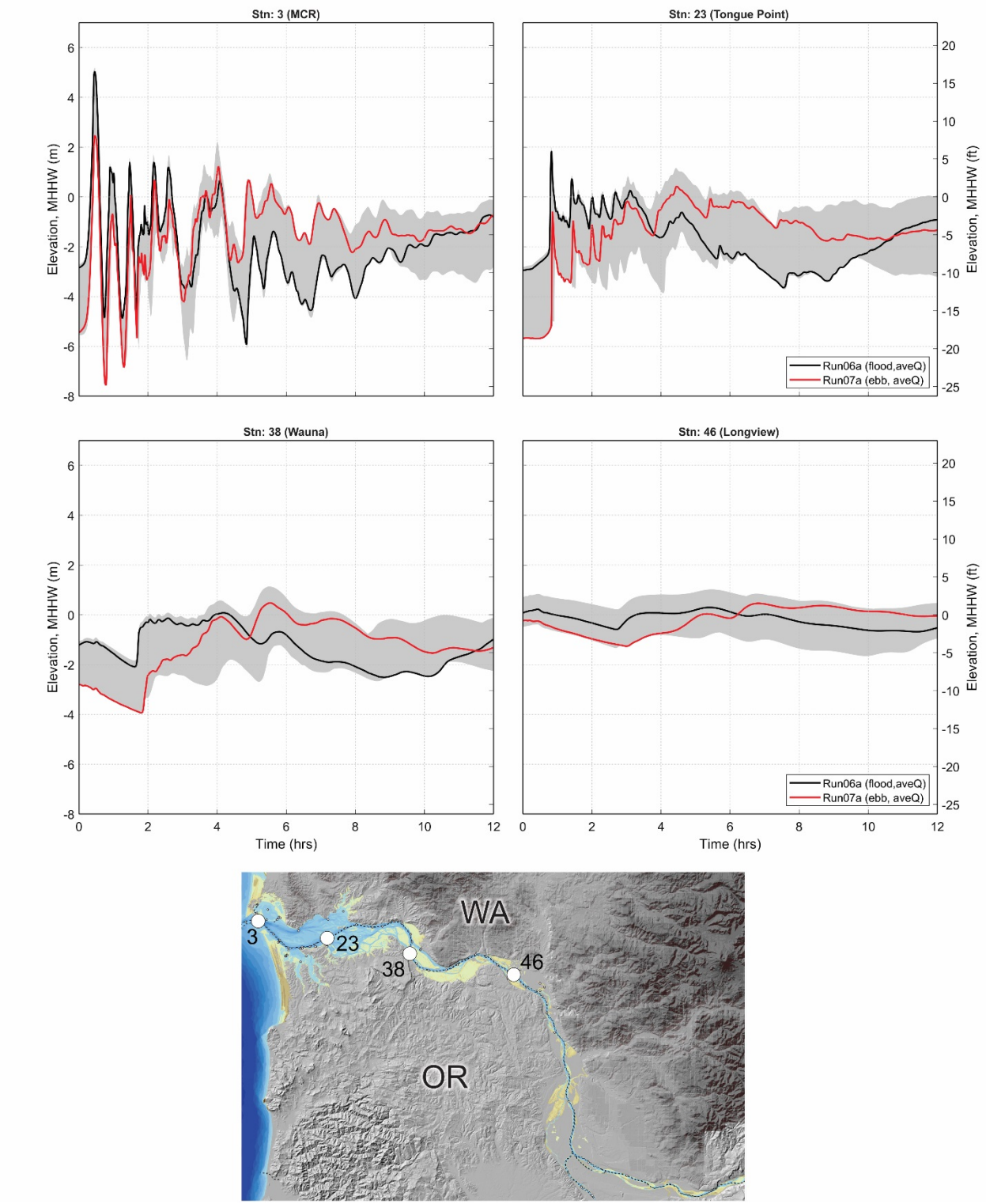

Figure 33. Time series showing the modeled water levels (flow depth–depth) for two simulations of a CSZ tsunami (L1) travelling along the navigation channel from the MCR to Longview. Gray shading denotes the envelope of variability in the water levels from all simulations. Station 3 is at the mouth of the Columbia River, station 23 is at Tongue Point, station 38 is at Wauna, and station 46 is at Longview.

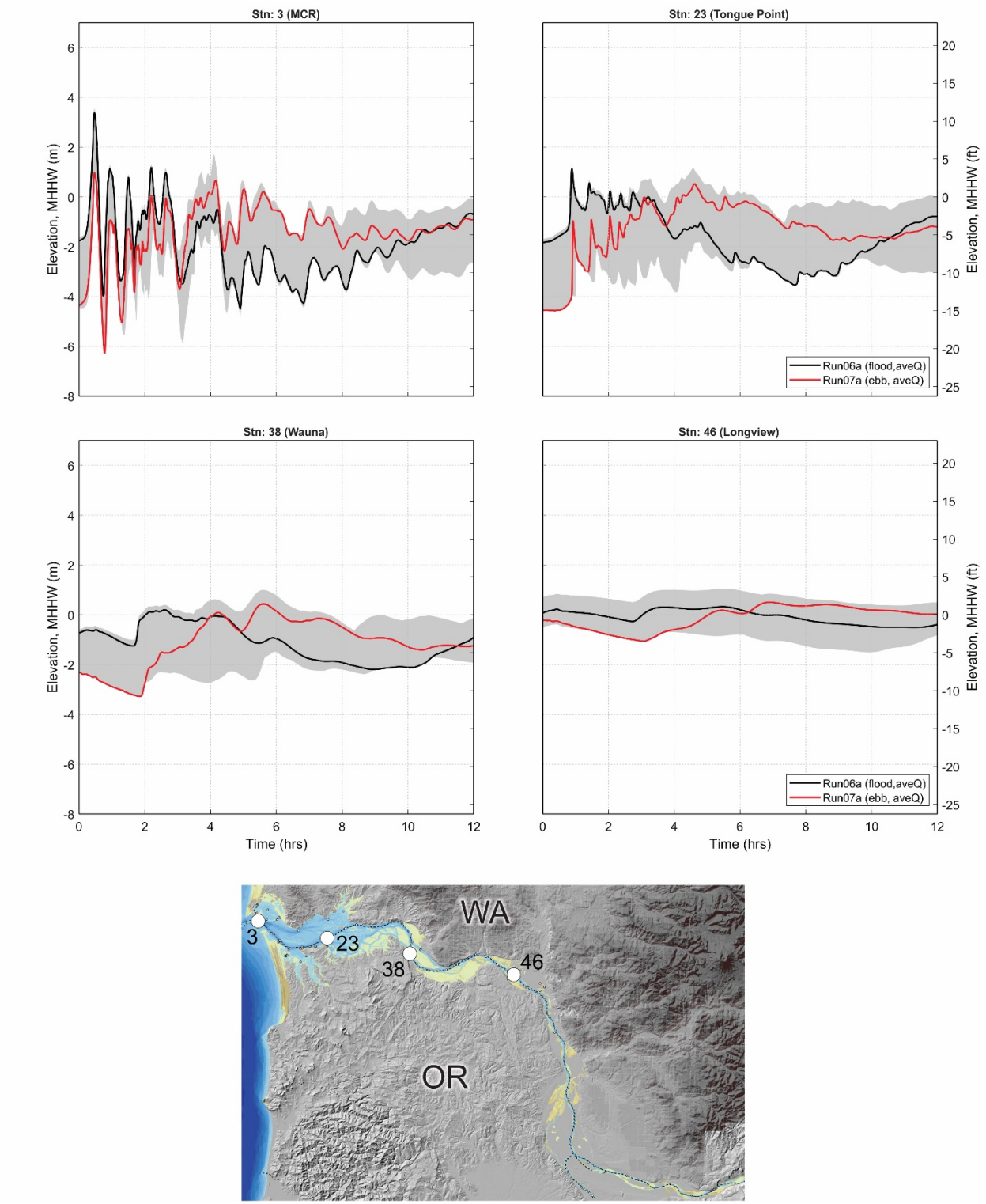

5.1.1.2 XXL1 and L1 tsunami currents

Figure 34 presents the modeled currents for the lower Columbia River estuary. For the purposes of assisting with maritime guidance, we have binned the current velocities into five categories consistent with the work of Lynett and others (2014). In general, current velocities exceeding 4.5 m/s (>9 knots) were found to result in extreme damage to ports and harbors, while little to no damage was found to occur at velocities < 1.5 m/s (<3 knots).

Modeling of the tsunami currents for an XXL1 event indicates catastrophic conditions will predominate across much of the lower Columbia River estuary (**Figure 34**, *top*). In this scenario, extreme currents (>4.5 m/s (>9 knots)) will affect all major ports in the lower estuary and damage is expected to be catastrophic. Damaging currents generated by the L1 scenario are not as severe as with the maximum considered XXL1 event. For the L1 scenario we find that extreme currents (>4.5 m/s (>9 knots)) will be largely confined to the immediate area around the MCR. Although damaging currents are expected to be observed in the vicinity of Tongue Point, our analyses suggest that under the L1 scenario the tsunami currents are likely to be mainly in the range of 1.5 to 4.5 m/s (3 to 9 knots) (**Figure 34**, *bottom*). These differences are most apparent when one compares the time series of modeled currents for both XXL1 (**Figure 35**) and L1 (**Figure 36**) at the MCR and Tongue Point. Strong currents decrease rapidly upriver of Tongue Point due to the meandering shape of the estuary channel, which helps to dissipate the tsunami energy, as well as in response to the presence of numerous bars and islands and the general shallowing in the upper estuary. In particular, there is a significant decrease in the current velocities in both scenarios upriver of Fitzpatrick Island, where the currents drop to ~ 1.5–2 m/s (3–4 knots). As a result, in-water conditions upriver of Fitzpatrick Island are likely to be navigable by any vessels operating in this area. Farther upriver, conditions improve significantly. For example, at Wauna the modeled XXL1 currents are largely below the critical 1.5 m/s (3 knot) threshold (**Figure 35**) and are almost entirely below that threshold in the L1 scenario (**Figure 36**); current conditions are generally benign by the time the tsunami reaches Longview.

Knowing how long strong currents can be expected to persist following a CSZ earthquake is also important to mariners and emergency officials. Because performing such analyses is computationally demanding, developing ensembles of these types of results is not practical. Instead, we focus on evaluating the current durations for just the estuary and offshore region and the two most important model simulations: flood (Run06a) and ebb (Run07a) conditions. The approach used first involves querying the full simulation data using a Fortran script to extract the first 12 hours of model data for every grid node; we ignored data after hour 12 because the tsunami is largely over by then (see **Figure 27**). These data are subsequently processed in MathWorks MATLAB® and converted to Esri® form using a python script. For our purposes, we use the following velocity thresholds to distinguish the duration of the currents: 1.5 m/s (3 knots), 3 m/s (6 knots) and 4.5 m/s (9 knots).

Figure 34. Ensemble model results of the maximum tsunami currents generated by a (*top)* XXL1 and (*bottom)* L1 CSZ earthquake. MCR is the mouth of Columbia River.

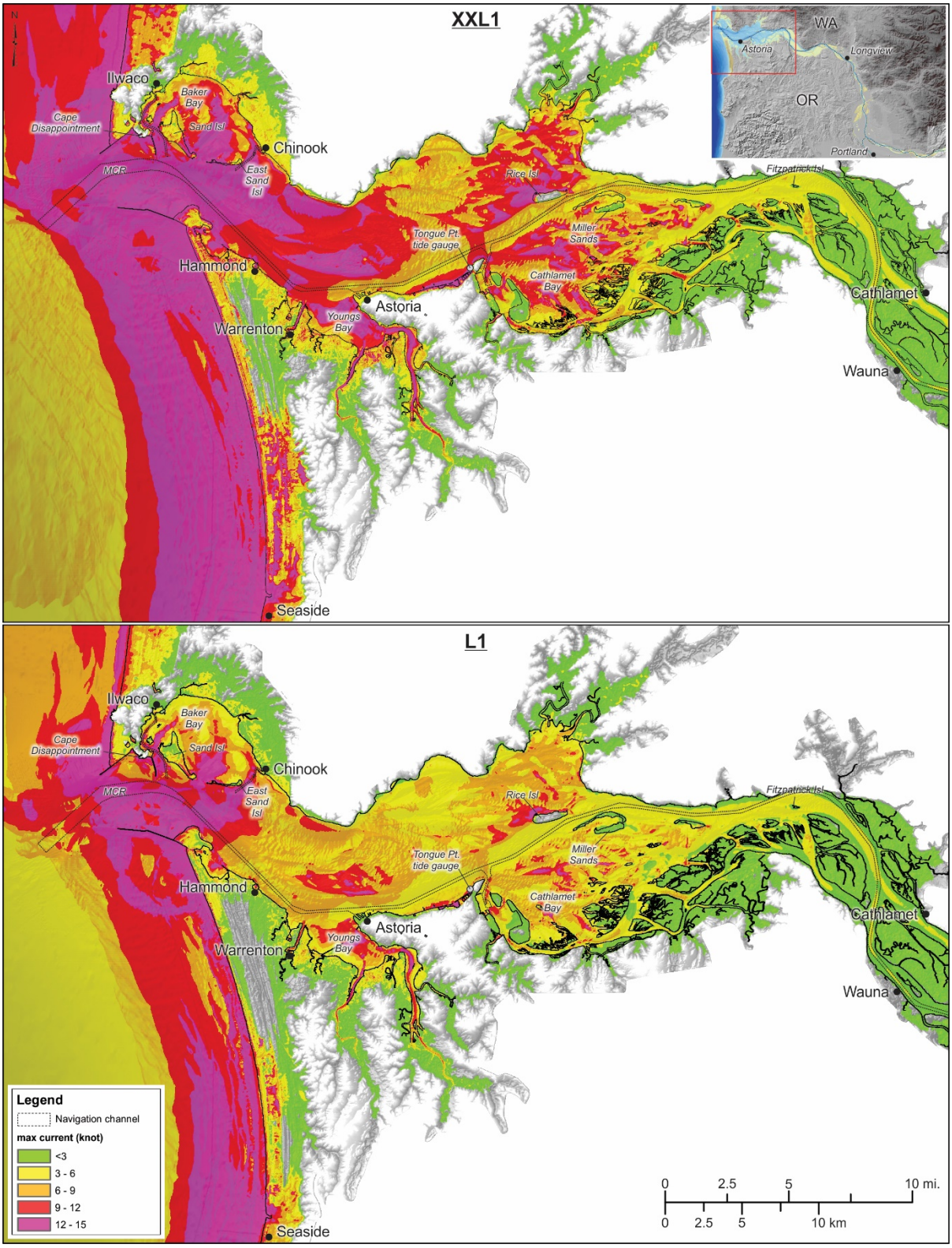

Figure 35. Time series showing the modeled currents generated for two simulations of a CSZ tsunami (XXL1) travelling along the navigation channel from the MCR to Longview. Gray shading denotes the envelope of variability in the tsunami currents from all simulations. Station 3 is at the mouth of the Columbia River, station 23 is at Tongue Point, station 38 is at Wauna, and station 46 is at Longview.

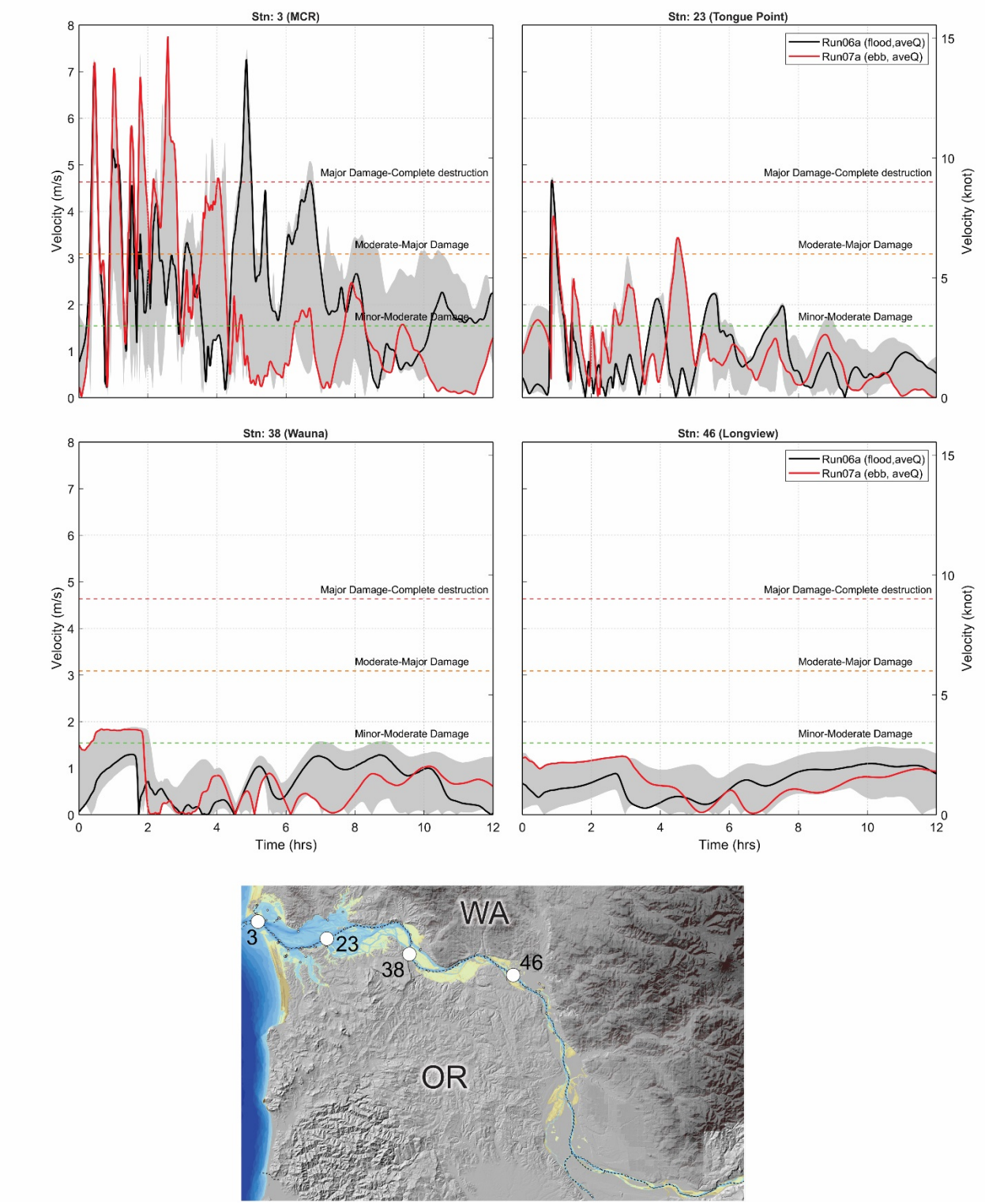

Figure 36. Time series showing the modeled currents generated for two simulations of a CSZ tsunami (L1) travelling along the navigation channel from the MCR to Longview. Gray shading denotes the envelope of variability in the tsunami currents from all simulations. Station 3 is at the mouth of the Columbia River, station 23 is at Tongue Point, station 38 is at Wauna, and station 46 is at Longview.

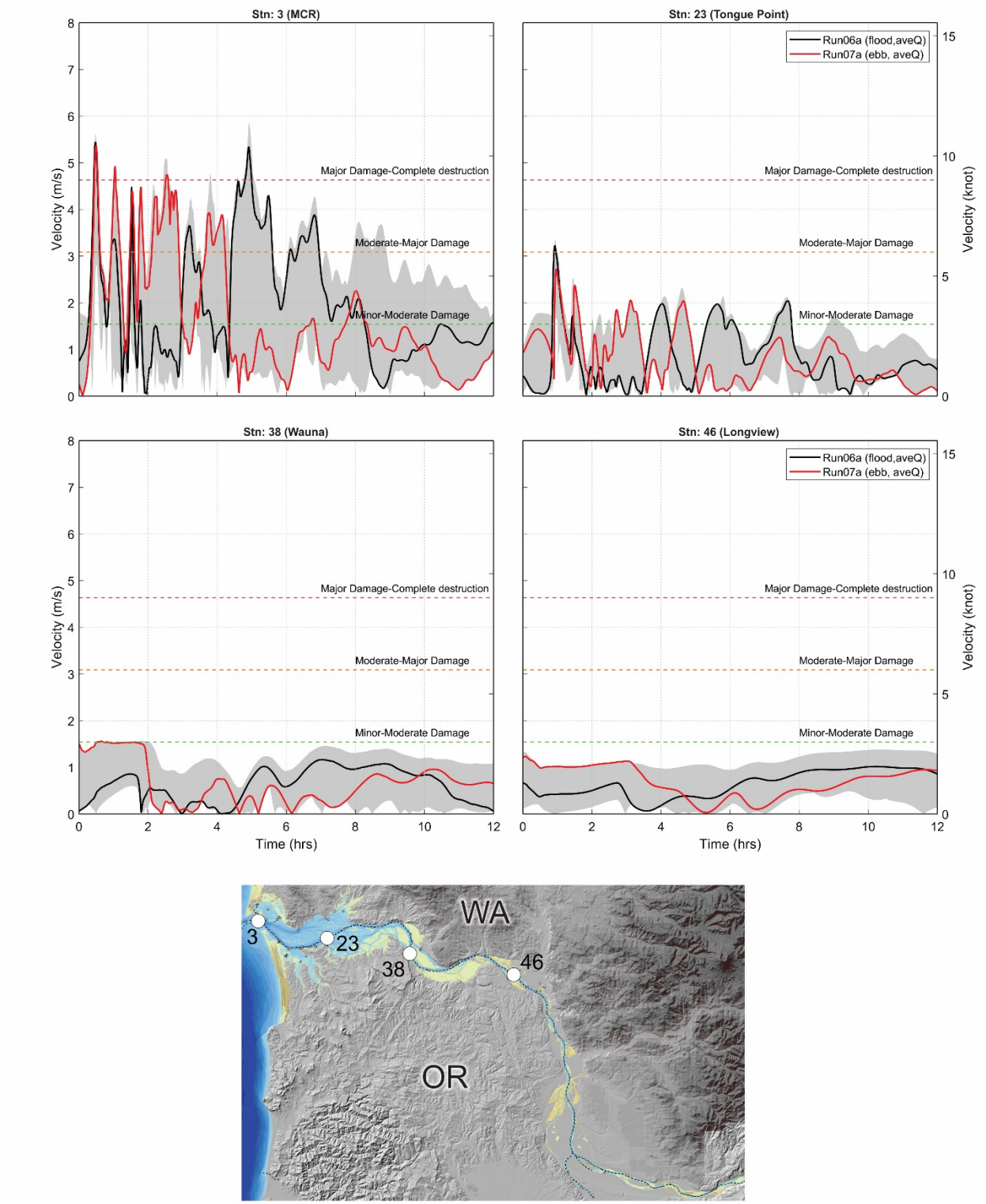

The duration of each of the current velocity bins (1.5–3 m/s [3–6 knots] and 3–4.5 m/s [6 to 9 knots]) is presented in **Figure 37**; we have chosen not to include the results for currents > 4.5 m/s (9 knots) because their effect is confined entirely to the estuary mouth. Flood conditions are shown on the left side of the figure, while ebb conditions are on the right. Not surprisingly, currents lasting up to one hour in the 1.5–3 m/s (3–6 knot) range affect the entire estuary; this pattern is repeated in **Figure 37**C for the ebb scenario. However, currents in this velocity range are expected to persist for up to 4 hours in the navigation channel west of Astoria; durations greater than 4 hours can be expected mainly on the Washington side of the channel and within the estuary mouth. Of importance, currents between 1.5 and 3 m/s (3–6 knots) can be expected to persist for 1–4 hours some 10 km (6 mi) west of the estuary mouth, making this area a potential navigation hazard. Interestingly, the patterns shown for the ebb scenario are largely the same as for flood; the main difference is that the current durations identified for ebb tend to be shorter when compared with flood. Thus, although tsunami current velocities tend to be generally stronger under ebb conditions (as noted earlier), the duration of these currents is much shorter when compared with the flood scenario. For currents in the 3–4.5 m/s (6–9 knot) range, our results again indicate that large areas of the estuary and offshore will experience such currents for up to 1 hour. Longer durations in the range of 1–3 hours are concentrated at the estuary mouth (**Figure 37**B) and tend to be a little more dispersed under the ebb scenario (**Figure 37**D).

Figure 37. Duration of XXL1 tsunami current velocities for *(left)* Run06a (flood) and *(right)* Run07a (ebb). A) Run06a, 1.5–3 m/s (3–6 knots); B) Run06a, 3–4.5 m/s (6–9 knots); C) Run07a, 1.5–3 m/s (3–6 knots); and D) Run07a, 3–4.5 m/s (6–9 knots).

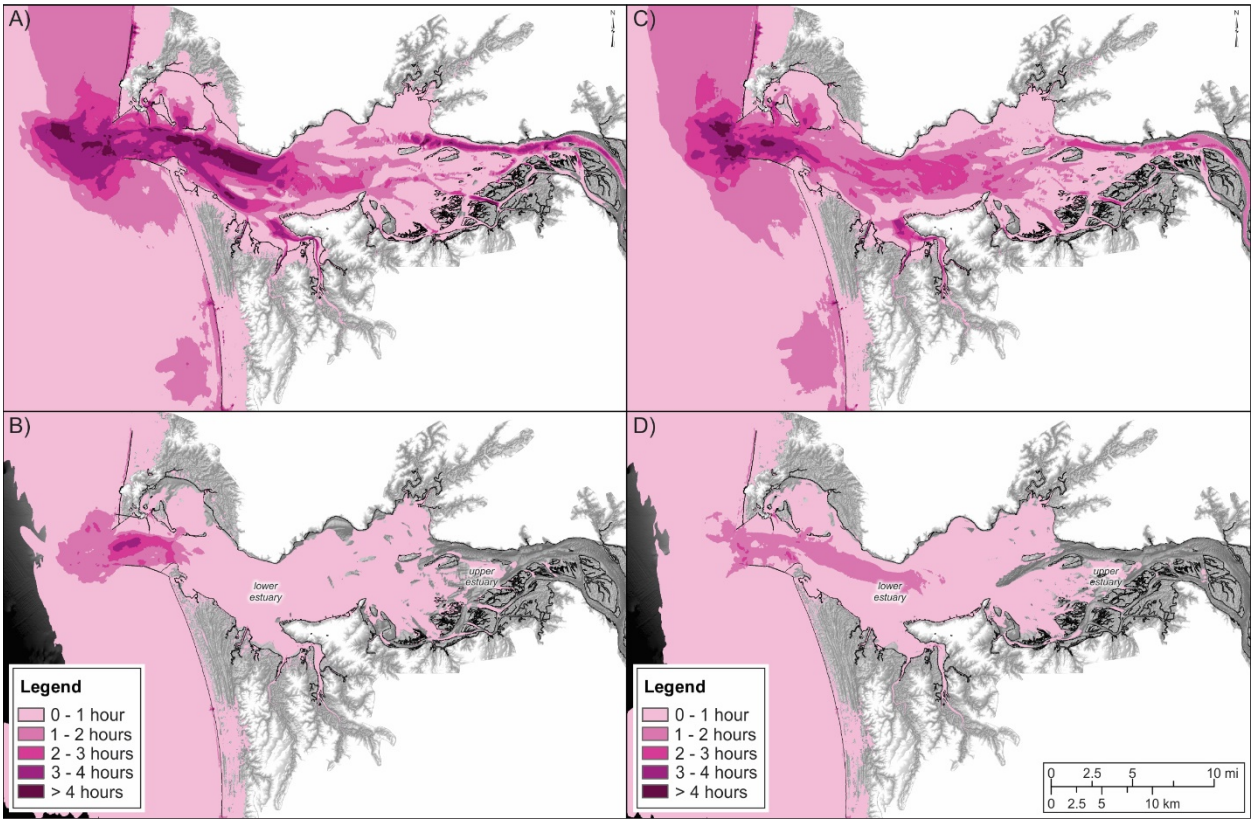

5.1.1.3 XXL1 and L1 vorticity

The occurrence of vorticity or rotation is a process that leads to the development of gyres and whirlpools. These effects can be a major factor affecting maritime operations, particularly for the ability of a vessel to maintain headway. Vorticity is defined as:

$$\text{Vorticity} = \left|\frac{dv}{dx} - \frac{du}{dy}\right| \quad (2)$$

where *dv* is the change in north velocity, *du* is the change in east velocity, *dx* is the change in distance east, and *dy* is the change in distance north. In general, values greater than 0.1 (0.01 units of 1/sec = velocity changing 1m/sec over 100-m distance) are akin to very strong shear. **Figure 38** presents the calculated vorticity generated by both the XXL1 and L1 tsunami scenarios. Not surprisingly, our modeling reveals large areas subject to strong rotation potential, with the strongest signal (>0.1/sec) evident in the nearshore ocean (within ~2.5 miles of the shoreline). Very strong rotation is also evident at the MCR, particularly adjacent to the jetties and spit tip; within Baker Bay, especially in the narrows between Cape Disappointment and Sand Island and between Sand Island and East Sand Island; within the narrow harbors of Hammond, Warrenton, Ilwaco, Chinook, and Astoria; and around Tongue Point. These same areas are also subject to strong rotation generated under the L1 scenario.

Figure 38. Ensemble model results of the maximum vorticity generated by a *(top)* XXL1 and *(bottom)* L1 CSZ tsunami. MCR is the mouth of the Columbia River.

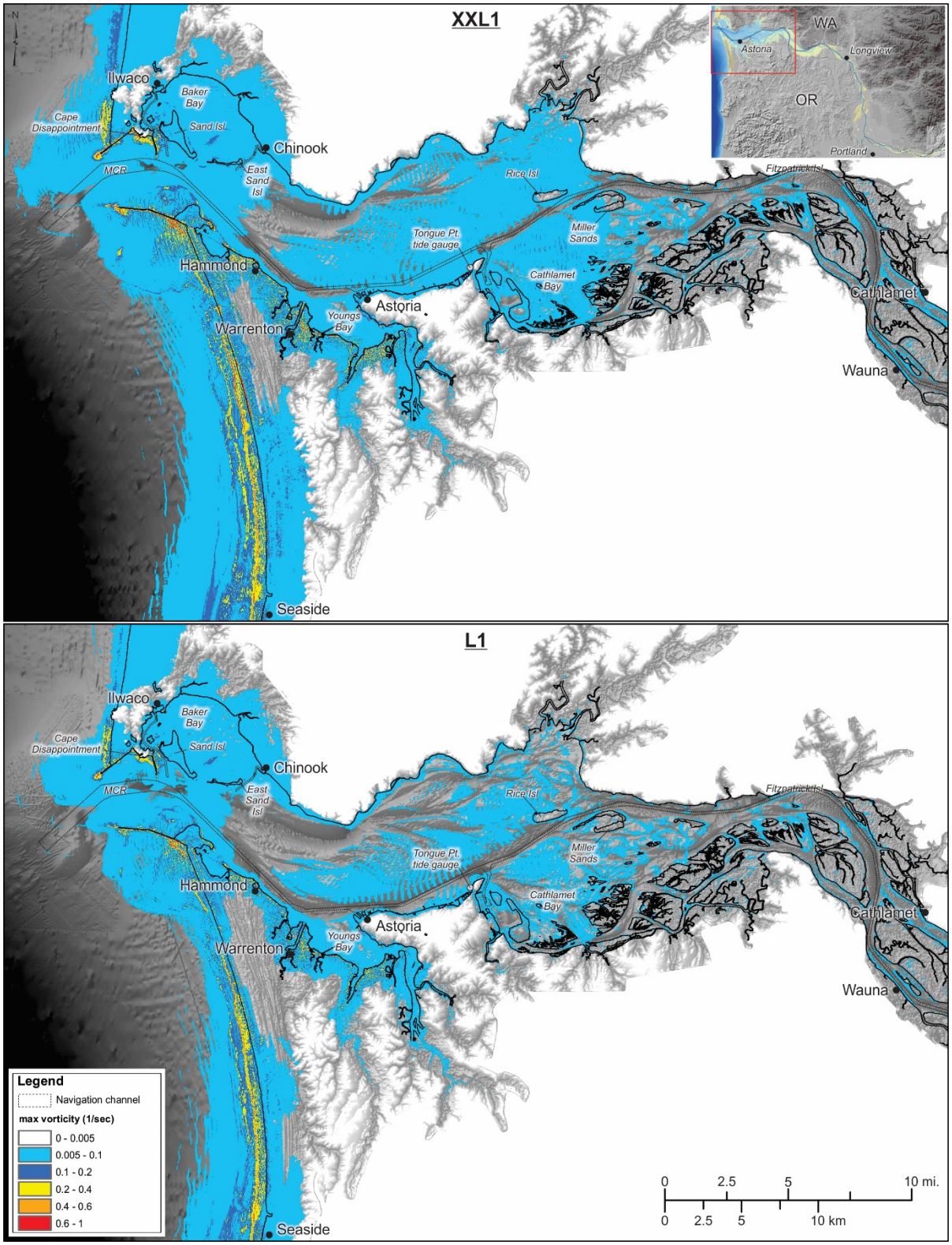

Figure 39 presents a series of current velocity vectors for selected time periods for an XXL1 event occurring at flood tide (Run06). These data are useful for visualizing the scales of gyres expected to form in the lower Columbia River estuary. The plots show the initial wave arrival at t = 26 min and the wave front arriving at Tongue Point ~18 minutes later. Of note, at t = 44 minutes one can clearly differentiate the development of a large gyre that encompasses much of Baker Bay (**Figure 39**). At t = 56 minutes, the tsunami front has reached Miller Sands. At the same time, currents are beginning to drain out of Young's Bay. Rotation is evident in the estuary north of Warrenton and Astoria. At t = 80 min, another tsunami front has entered the estuary and is located near Tongue Point. Gyres are evident at multiple locations in the estuary to the west and north of Warrenton (**Figure 39**). These continue to evolve by t = 119 minutes with multiple large gyres present throughout the estuary. Finally, at t = 231 minutes the upper estuary (west of Astoria) is showing strong seaward directed currents that are likely a function of the change in tidal regime (flood to ebb) and returning water from the tsunami waves (**Figure 39**).

Figure 39. Current vectors showing the progression of an XXL1 tsunami occurring on a flood tide and with average river flows (Run06) into the Columbia River estuary. The complete animation can be seen in the "RUN06a_animation_200m.avi" file, which accompanies this report.

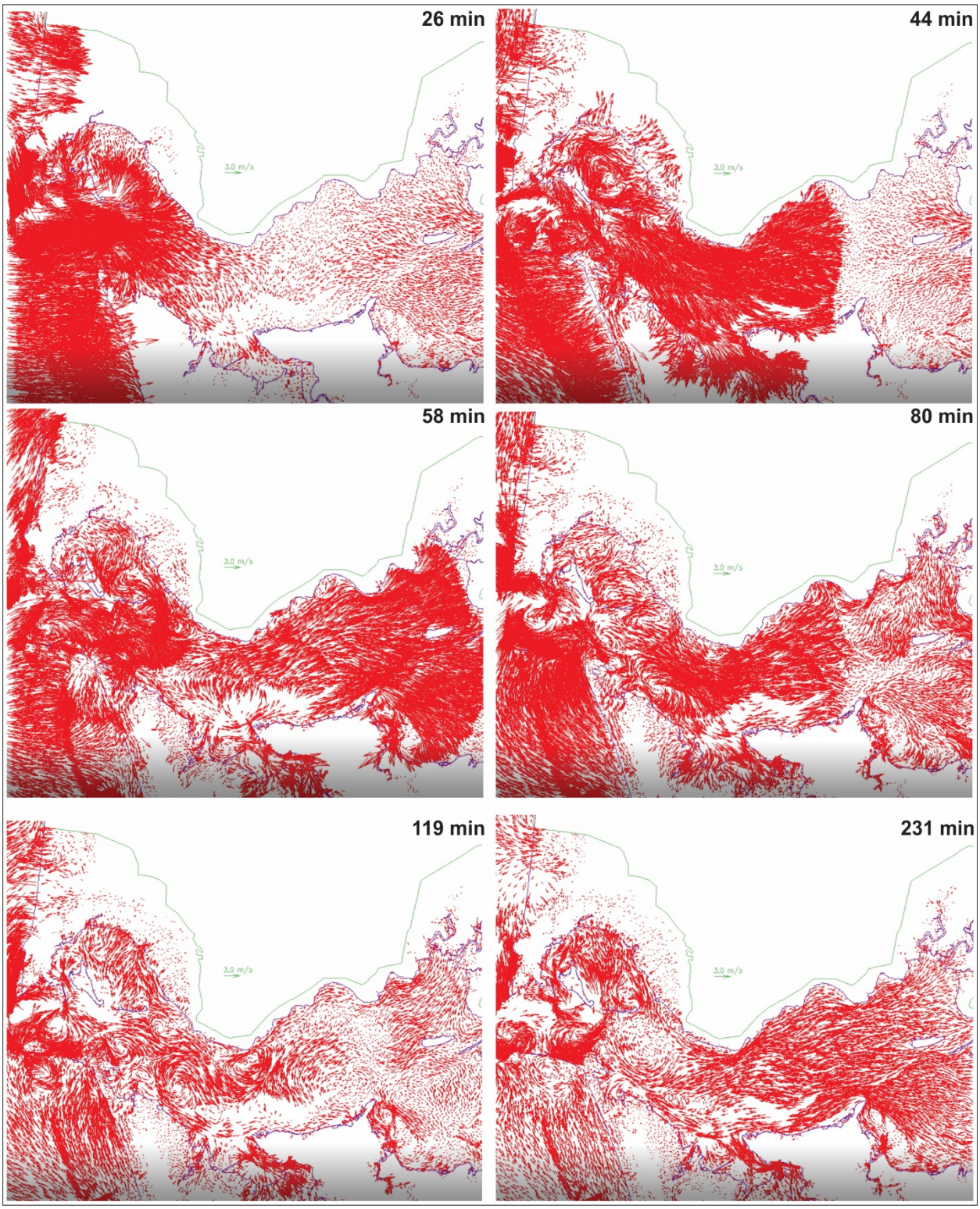

5.1.2 Distant (AKmax) tsunami ensemble results

5.1.2.1 AKMax Water Levels

Figure 40 presents the merged maximum water levels and currents for the maximum considered Eastern Aleutian Island (AKMax) distant tsunami event. As with the local scenarios, the highest tsunami water levels are observed along the open coast (warm colors), especially along the Clatsop Plains. Not surprisingly, the simulated water levels for the AKMax tsunami are considerably lower than those observed for the local scenarios (compare **Figure 40** *top* with **Figure 31**). Nevertheless, dangerous conditions are still observed at the MCR (**Figure 41**), within Baker Bay and Young's Bay, and by Tongue Point. **Figure 41** also indicates that as the tsunami travels upriver it rapidly decreases in height and, by the time it reaches Longview, contains little energy.

5.1.2.2 AKMax currents

More telling are the modeled tsunami currents, which indicate potentially dangerous currents occurring within the MCR (**Figure 40** *bottom* and **Figure 42**). Strong currents exceeding 9 knots are prevalent in the MCR navigation channel, north of Clatsop Spit, and in the narrows between Cape Disappointment and Sand Island, between Sand Island and East Sand Island, and near Chinook (**Figure 40** *bottom*). Of major concern will be the interaction of the incoming tsunami waves with opposing currents generated during an ebb tide coupled with seaward directed tsunami drainage, which will likely contribute to the amplification of wind waves occurring in the vicinity of the mouth (Allan and others, 2018).

Within the estuary, the ensemble results indicate that large parts of the estuary would be affected by currents in the 1.5–3 m/s (3–6 knot) range (**Figure 40** *bottom*). Currents of this magnitude are likely to cause moderate damage to facilities located in the ports and harbors (see **Table 3**). For ships and boats moored in the navigation channel (e.g., between Astoria and Rice Island) and in the harbors, currents of this magnitude will likely necessitate ship operators adding additional drag anchors to larger vessels. Evacuation upriver toward Fitzpatrick Island may also be feasible depending on how long it takes a ship to get underway (a conservative estimate is about 1 hour for large ships [Dan Jordan, Columbia River Bar Pilots, verbal commun., July 2018]) and the speed at which a vessel can travel.

Figure 42 presents the modeled AKMax tsunami currents for the same stations defined previously. As noted earlier, the modeled currents are strongest at the MCR (station 3) and rapidly decrease in strength as the tsunami progresses upriver (**Figure 42**). By the time the tsunami reaches Wauna (station 38), the currents fall below the 1.5 m/s (3 knot) damage index threshold. As a result, because of the combination of relatively small tsunami waves and low currents observed at Wauna, we believe that maritime operations upriver from Wauna are unlikely to be significantly impacted by a maximum considered distant tsunami.

Figure 40. Ensemble model results of the maximum tsunami (*top)* water levels and *(bottom)* currents generated by a maximum considered distant earthquake and tsunami (AKMax) occurring on the Eastern Aleutian Islands. Cartoon showing water level time history and attributes is of station 3 at the mouth of the Columbia River (MCR).

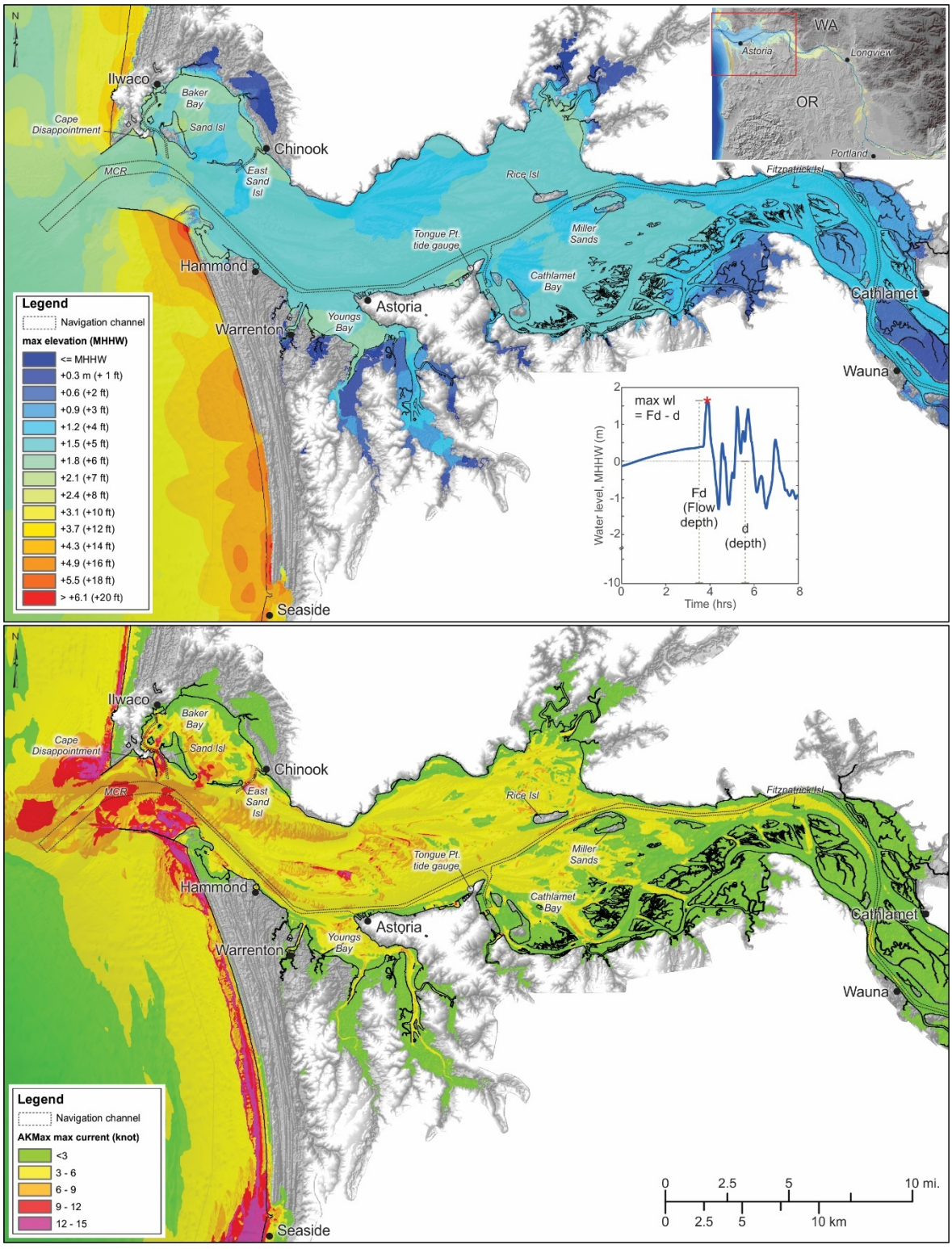

Figure 41. Time series showing the modeled water levels (flow depth–depth) for the AKMax tsunami traveling along the navigation channel from the MCR to Longview. Gray shading denotes the envelope of variability in the water levels from all simulations. Station 3 is at the mouth of the Columbia River, station 23 is at Tongue Point, station 38 is at Wauna, and station 46 is at Longview.

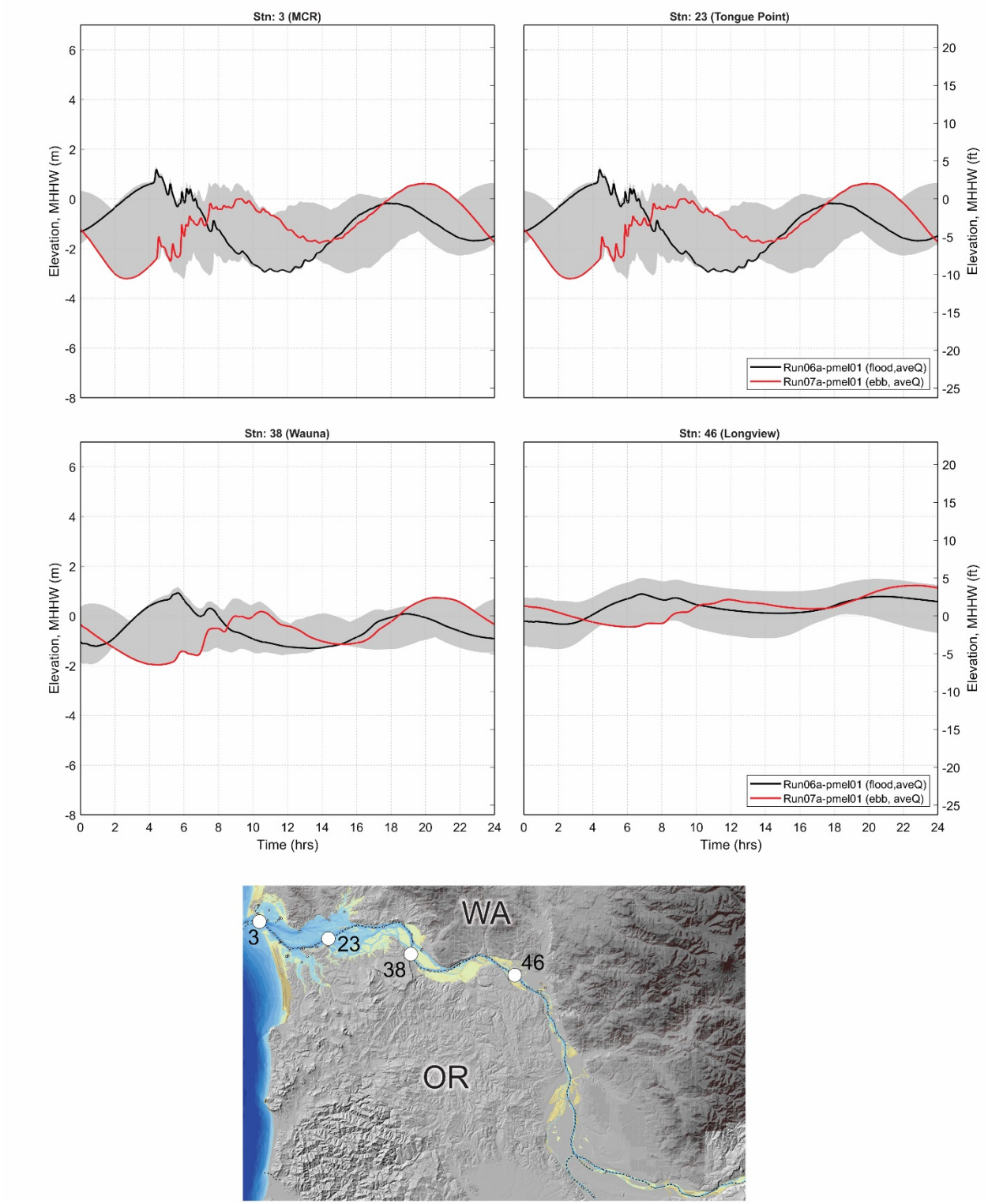

Figure 42. Time series showing the modeled currents for the AKMax tsunami traveling along the navigation channel from the MCR to Longview. Gray shading denotes the envelope of variability in the tsunami currents from all simulations. Station 3 is at the mouth of the Columbia River, station 23 is at Tongue Point, station 38 is at Wauna, and station 46 is at Longview.

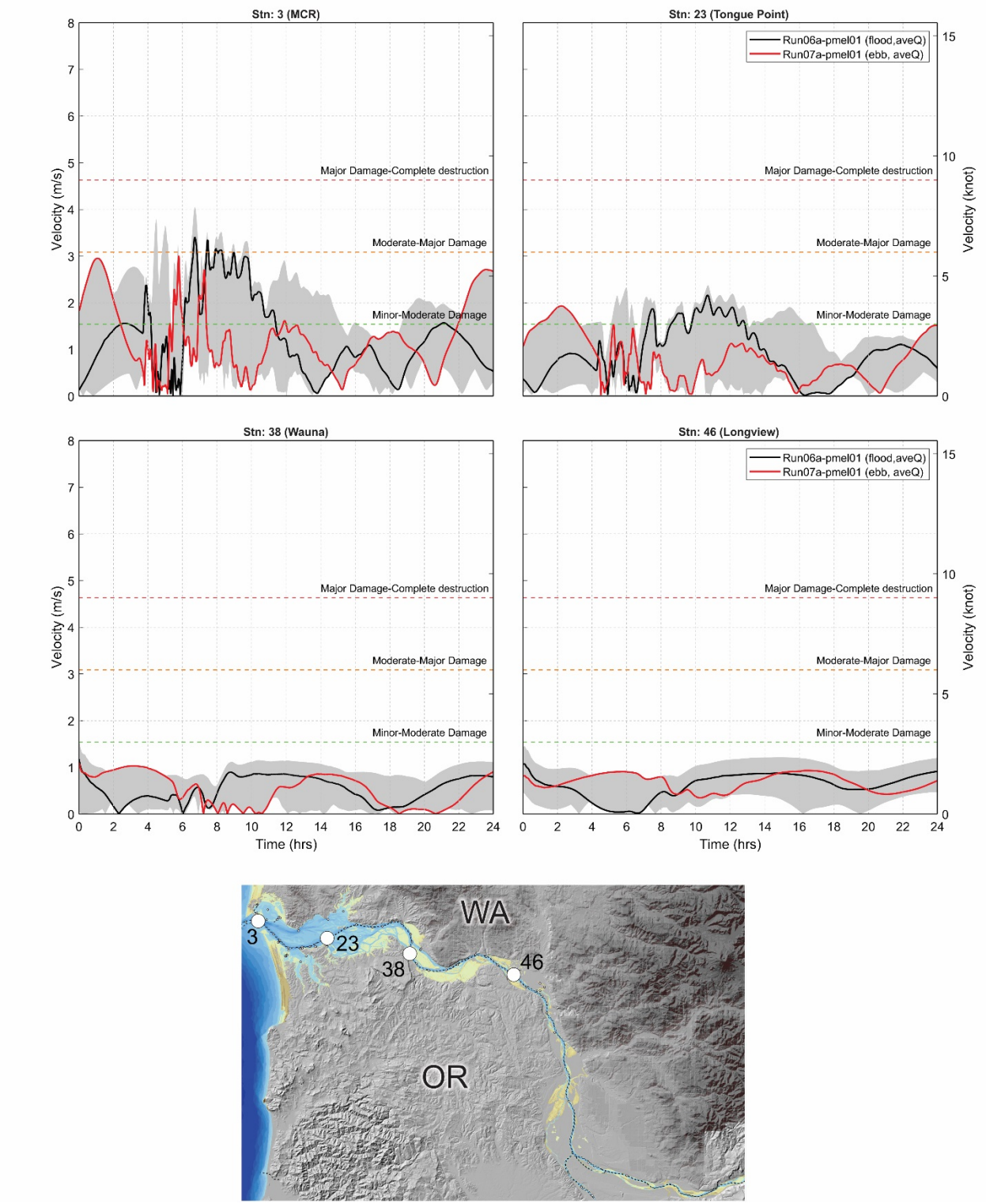

The duration in which tsunami currents are expected to exceed 1.5 m/s (3 knots) is presented in **Figure 43** for both the flood (Run06d, *left plots*) and ebb (Run07d, *right plots*) scenarios. Longer current durations again characterize the flood scenario, especially along the navigation channel where currents in the 1.5–3 m/s (3–6 knot) range are expected to last for more than 4 hours (**Figure 43**A). Conversely, under ebb conditions, the AKMax tsunami simply does not have enough energy to counter the riverine flows and the outgoing tidal currents, which cause much of the tsunami wave energy to be reflected offshore (**Figure 43**C). Thus, an Alaskan tsunami arriving on an ebb tide can be expected to be significantly muted by conditions operating in the Columbia River at the time.

At the higher velocity of 3–4.5 m/s (6–9 knots), our results indicate that stronger currents will persist for up to 3 hours within the estuary mouth in the flood scenario (**Figure 43**B), and for < 1 hour under ebb conditions (**Figure 43**D). These results suggest that different maritime planning responses may be warranted for flood and ebb conditions when dealing with a distant tsunami event.

Figure 43. Duration of AKMax tsunami current velocities for *(left)* Run06d (flood) and *(right)* Run07d (ebb). A) Run06d, 1.5–3 m/s (3–6 knots); B) Run06d, 3–4.5 m/s (6–9 knots); C) Run07d, 1.5–3 m/s (3–6 knots); and D) Run07d, 3–4.5 m/s (6–9 knots).

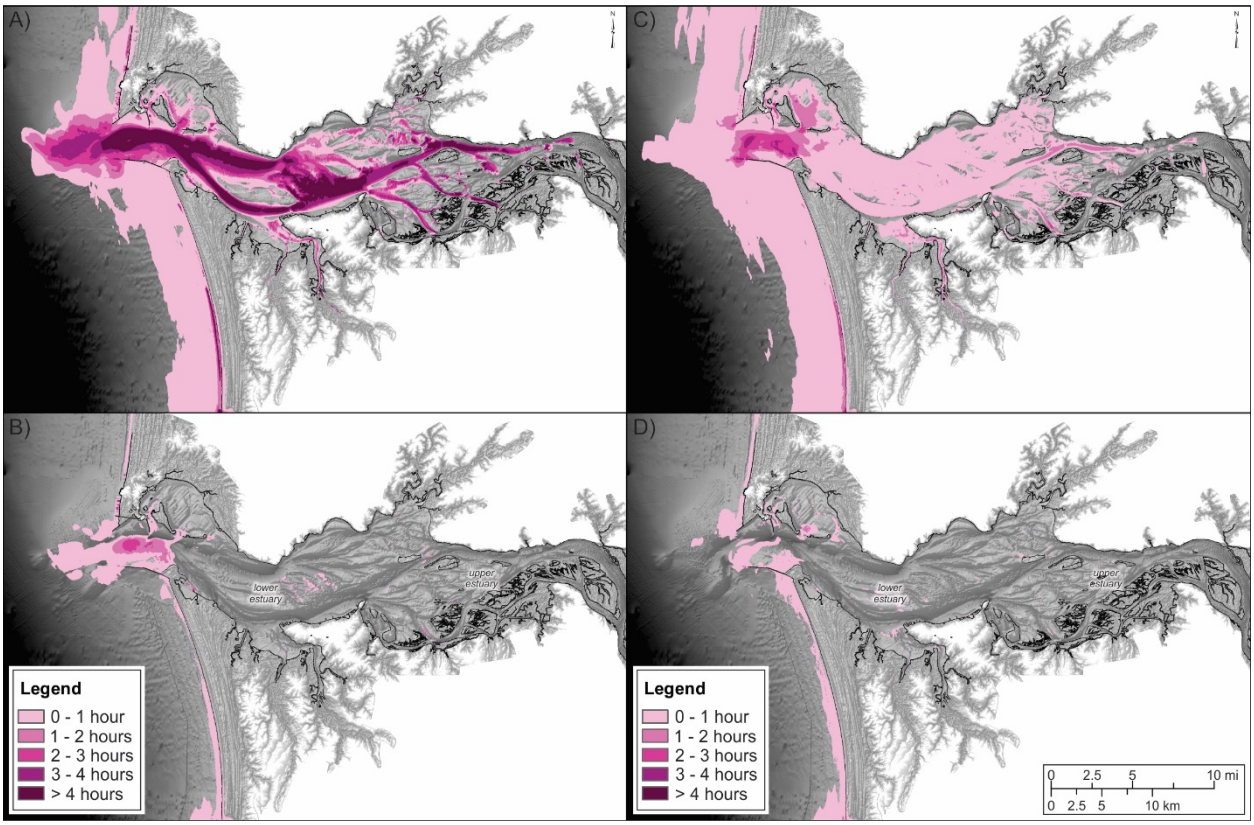

5.1.2.3 AKMax vorticity and minimum flow depth

Figure 44 (top) presents the calculated vorticity potential, while **Figure 44** (bottom) shows the water depth below the minimum trough of the tsunami. The former provides insights as to areas subject to strong rotation, while the latter is important with respect to the grounding of vessels. As with the local scenarios, areas of cool to hot colors indicate potential for rotation and the development of gyres and whirlpools (**Figure 44,** top). These areas include the entire nearshore ocean, and areas around the MCR. All major ports and harbors in the lower estuary are also affected. The issue of grounding (**Figure 44,** bottom) is largely confined to the shallower harbors, such as Warrenton, Hammond, Ilwaco, and Chinook, while effects of the passing tsunami troughs are unlikely to affect most vessels operating in the navigation channel. This is evident in **Figure 44 (**bottom) along the navigation channel, which shows water depths that are generally deeper than 39 ft (green region) for most areas in the channel. Grounding may be an issue for a few of the largest ships that are loaded with goods and moving toward the ocean along the navigation channel.

Finally, **Figure 45** presents a series of current velocity vectors for selected time periods for the AKMax simulation occurring at flood tide (Run06-pmel01). Recall, this simulation has the tsunami arriving at flood stage. The initial plot (t = 3 hours 27 min) shows the background tidal conditions prior to the arrival of the tsunami, with the tidal currents directed into lower estuary; a pronounced gyre has formed within the lee of the south jetty and Clatsop Spit. At t = 4 hours, the AKMax tsunami has entered the estuary and the current velocities have increased significantly within the navigation channel and Columbia River mouth. At this time, the tsunami wave front is located just west of Astoria, while the tsunami can be tracked travelling into Baker Bay between Cape Disappointment and Sand Island, and between Sand and East Sand Island (**Figure 45**). At 4 hours and 39 minutes, the tsunami is east of Tongue Point, traveling up the Columbia River. Strong outgoing currents can be seen receding out of Baker Bay and immediately north of Warrenton, and around the south jetty; strong southward directed currents are also evident offshore from the Clatsop Plains. These conditions persist for another 20 minutes, leading to the development of two large gyres, one immediately north of the south jetty and one at the end of the south jetty (**Figure 45**). Another tsunami front can be seen pushing onshore along the Clatsop Plains. Within the estuary, most of the flow is directed offshore. At 6 hours and 39 minutes, another tsunami wave can be seen striking the coast. The interaction of this incoming tsunami wave and the outgoing currents concentrated at the MCR will almost certainly contribute to the formation of dangerous standing waves and wave amplification due to the opposing currents.

Figure 44. Ensemble model results of the *(top)* maximum vorticity and *(bottom)* minimum water depths generated by a maximum considered distant earthquake and tsunami (AKMax) occurring on the Eastern Aleutian Islands. Cartoon showing water level time history and attributes is of station 3 at the mouth of the Columbia River (MCR).

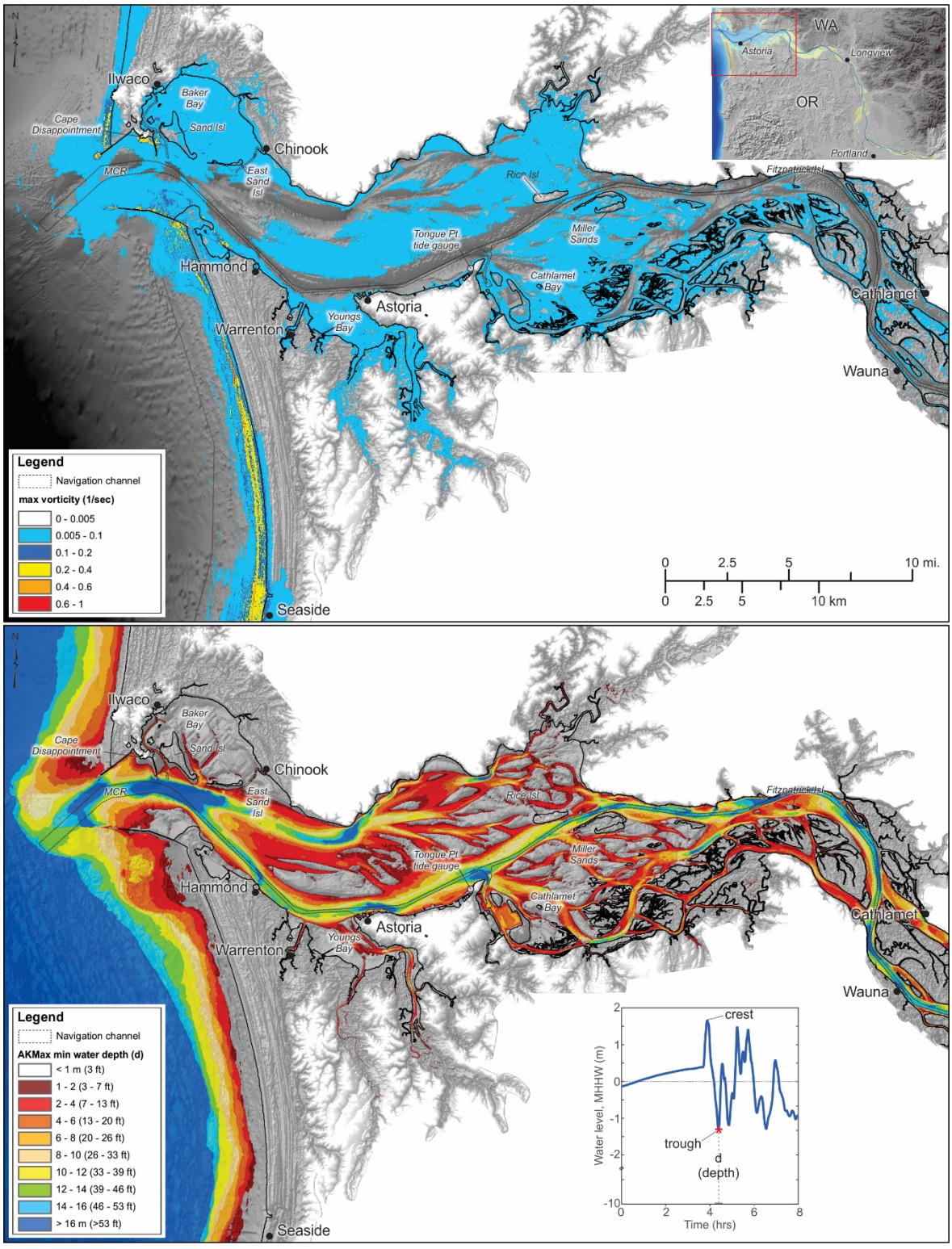

Figure 45. Current vectors showing the progression of an AKMax tsunami occurring on a flood tide and with average river flows (Run06-pmel01) into the Columbia River estuary. The complete animation can be seen in the file "RUN06d-pmel01_animation_200m.avi" that accompanies this report.

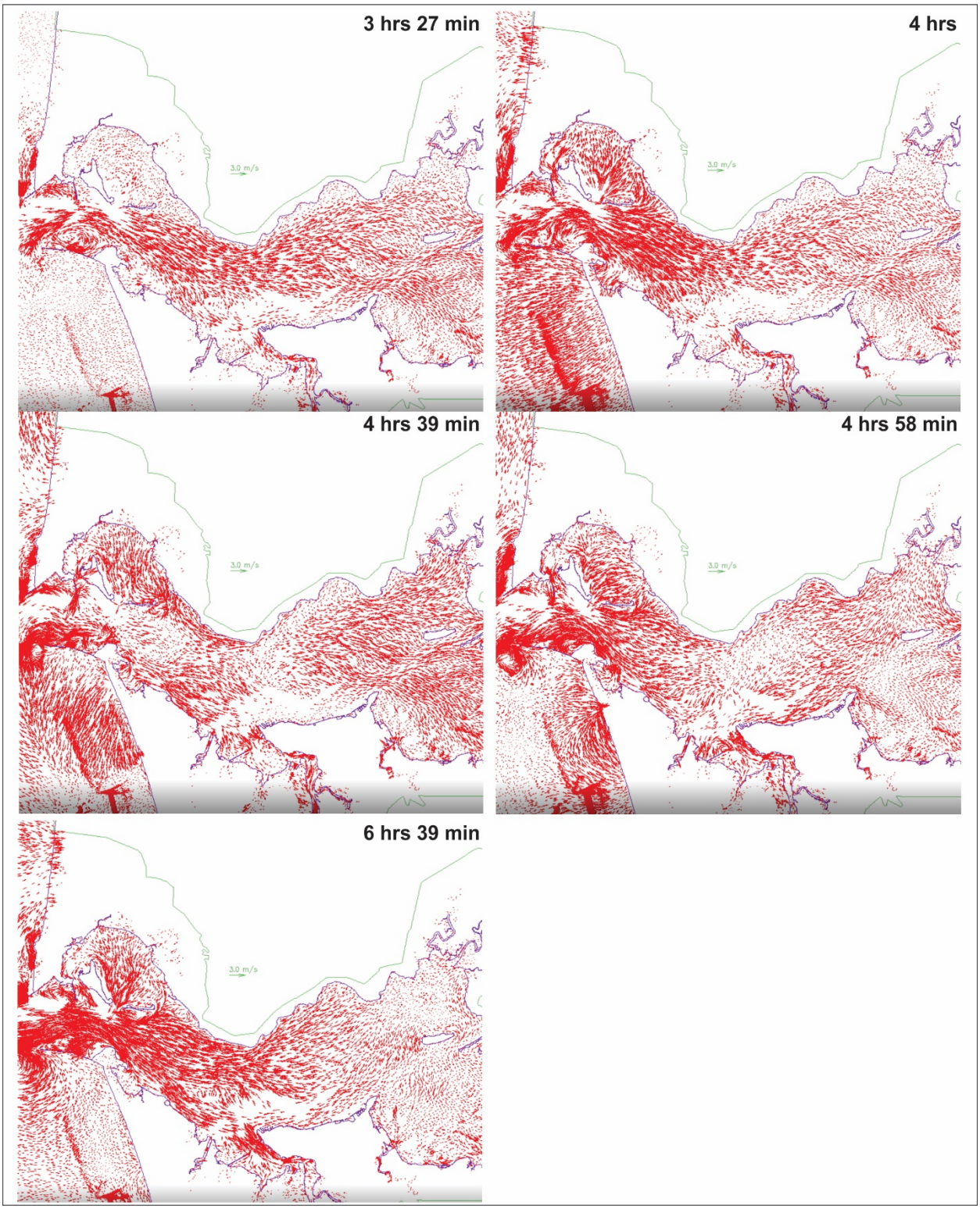

6.0 COLUMBIA RIVER MARITIME GUIDANCE

Our review of the scientific literature indicates that tsunami-generated currents pose a potential threat to the maritime community, especially within ports and harbors (Borrero and others, 2015; Lynett and others, 2014; Uslu and others, 2010). There is general agreement in the scientific literature that damage from tsunami within ports and harbors begins to occur at velocities ~1.5–2 m/s (3–4 knots). However, the same cannot be said for the effects of currents generated by a tsunami on boats operating out on the ocean. Vessel vulnerability to open ocean currents is difficult to assess because it depends not only on the strength of the currents but, importantly, on the size of the vessel and its cargo load and on prevailing antecedent conditions (wave heights and winds). An additional factor is the ability of smaller boats to cope with being in some cases tens of kilometers from the coast for potentially extended periods. All these factors have implications for where to send mariners in the event of a tsunami.

Lynett and others (2014) attempted to address the issue of offshore tsunami evacuation by comparing the maximum-simulated currents with depth for a distant tsunami affecting Crescent City, California. They noted that maximum currents of ~0.5 m/s (1 knot) are expected at a depth of 180 m (100 fathoms), while large variations in the currents exist near shore to a depth of 45 m (25 fathoms). They concluded that depths of ~55 m (30 fathoms) will generally be safe for most vessels (**Table 5**). In Japan, Suppasri and others (2015) noted that Japanese fishermen have practiced offshore evacuation (known as "oki-dashi") for generations, although prior to 2011 such a response was not recommended by the national government. This is because steering a boat toward a tsunami is considered to be dangerous and difficult, requiring expert knowledge of the offshore conditions as well as luck. Nevertheless, Japan's Fisheries Agency (2006 in Suppasri and others, 2015) indicated in its guidelines that boats should evacuate to a depth of at least 50 m (27 fathoms) in response to a tsunami warning (**Table 5**).

Since 2011, the Japanese have initiated a variety of recommendations for offshore tsunami evacuation. For example, Aomori Prefecture developed rules for offshore evacuation, such that in the case of a 5-m (16 ft) tsunami warning, the required sea depth for evacuation was 50 m (27 fathoms), which increased to 150 m (82 fathoms) for a 10-m (33 ft) tsunami warning (Suppasri and others, 2015). In the Tokushima Prefecture, a 4-m (13 ft) tsunami warning requires evacuation to 70-m (38 fathom) water depth, while evacuation to 110-m (60 fathom) water depth is recommended for a 6-m (20 ft) tsunami (**Table 5**). Although the focus there is on a locally generated tsunami, the same rules appear to apply for a distant tsunami. Most recently, Iwate Prefecture indicated that they would no longer recommend offshore maritime evacuation for a local tsunami (Dr. Anawat Suppasri, written commun., March 2018).

In the United States, considerable modeling and mapping efforts undertaken by the National Tsunami Hazard Mitigation Program (NTHMP) state programs have led to the development of maritime guidance recommendations for each state. These recommendations include a range of potential depths for maritime evacuation purposes covering both local and distant scenarios (NTHMP 2017). For Oregon, the currently recommended minimum depth is 55 m (30 fathoms) for the maximum-considered distant tsunami (DOGAMI, 2014); for the local XXL1 tsunami, the recommended depth for evacuation is 183 m (100 fathoms). For the distant event, the distances to safety range from a low of 2 km (1.2 mi) in Douglas County to as much as 16 km (10 mi) offshore from Lane County and requiring as little as 11 min to as much as 130 min to reach safety assuming a mean boat speed of 2–3 m/s (4–6 knots). In contrast, distances to safety for an XXL1 event increase significantly and range from 30 to 66 km (19–41 mi) depending on position along the Oregon coast. These distances place boaters a long way from the shore in potentially hazardous seas (Allan and others, 2018).

After evaluating the tsunami currents, their durations, and water depths, Allan and others (2018) proposed a tri-zone hazard region for both distant and local tsunamis affecting the Oregon coast. For an XXL1 event, they identified a high hazard zone (depths < 150 m [82 fathoms]) where strong, dangerous currents would predominate. Between 150 and 250 m (82–109 fathom) water depth, Allan and others defined a moderate hazard region where the simulated tsunami currents ranged from 2 to 2.6 m/s (4 to 5 knots). However, within this region the duration in which the current velocities exceed 2 m/s (4 knots) was found to be < 1 minute north of Stonewall Bank, increasing to 1.5–5.5 minutes south of the bank. Thus, it may be possible for a vessel to be moving through the moderate hazard area at the time of the event and, provided the vessel is able to maintain a westward direction and speed, the chance of survival improves. At depths > 250 m (137 fathoms), the tsunami currents fall below 2 m/s (4 knots). For the AKMax scenario, Allan and others (2018) recommended that vessels north of Stonewall Bank evacuate to depths > 45 m (25 fathoms); strong, dangerous currents can be expected at depths < 28 m (15 fathoms).

Table 4. Maritime tsunami evacuation depths previously identified.

Location	Scenario	Tsunami Height (m)	Tsunami Height (ft)	Depth (m)	Depth (ft)	Depth (fathoms)	Reference
Crescent City	distant			55	180	30	Lynett and others (2014)
Japan's Fisheries Agency	local			50	164	27	Suppasri and others (2015)
Japan, Aomori Prefecture	local	5	16	50	164	27	Suppasri and others (2015)
	local	10	33	150	492	82	
Japan, Tokushima Prefecture	local	4	13	70	230	38	Suppasri and others (2015)
	local	6	20	110	360	60	
Japan, Iwate Prefecture	local**						
Oregon, USA	distant			55	180	30	DOGAMI (2014), NTHMP (2017)
Oregon, USA	local			183	600	100	DOGAMI (2014), NTHMP (2017)
Oregon, USA	distant			45	150	25	Allan and others (2018)
Oregon, USA	local			250[#]	820	137	Allan and others (2018)
				350[##]	1150	200	

Note: **Offshore evacuation for a local tsunami is prohibited (A. Sappasri, written communication, 2018).

[#]All coastal counties except Curry County;

[##]Curry County

6.1 Maritime Guidance for a Local Tsunami

Given that initial wave arrival for a locally generated tsunami is expected to occur at the MCR in ~ 7 min, with a peak wave at 24 minutes, there is insufficient time for mariners moored in ports in the Lower Columbia River estuary or along the navigation channel downstream of Rice Island to respond to this event other than to evacuate by foot to high ground. Hence, maritime evacuation planning for a locally generated tsunami is generally limited to those vessels already operating out on the open ocean. For vessels west of the MCR, the most effective strategy is to evacuate immediately toward deeper water (ideally, Astoria Canyon) and, accordingly, toward decreasing tsunami-generated currents. However, steering a vessel toward an approaching tsunami is dangerous and difficult and should only be attempted if land-based evacuation is impossible (Allan and others, 2018). In this scenario, there will be little to no warning for operators out on the ocean. Telltale signs of an earthquake and approaching tsunami may include a background ocean roar, changes in boat motions, stronger ocean currents, and/or muddier water. Vessels located closer to shore may witness clouds of dust appearing along the coastline and in the hills, where landslides may be occurring.

As previously mentioned, Allan and others (2018) completed a comprehensive analysis of tsunami currents generated by both local and distant events for the Oregon coast, and they proposed a tri-zone hazard region for tsunami currents. Using this approach, we find that the most extreme and dangerous currents generated by a local tsunami near the MCR will occur in water depths < 90 m (50 fathoms). For currents < 2 m/s (< 4 knots), we find that this region begins at about 128-m depth (70 fathoms). However, for purposes of Columbia River maritime evacuation for a local event, ***we recommend that vessels already at sea evacuate directly toward Astoria Canyon to depths greater than 146 m (80 fathoms)*** (**Figure 46**); the offshore evacuation region is defined in **Figure 46** by the area west of the dashed yellow line and is located ~22 km (12 nautical mi) west of the Cape Disappointment lighthouse or 16.9 km (9.1 nautical mi) west northwest of buoy 46243. In these circumstances, mariners should prepare to potentially remain offshore for days due to the likelihood that navigation within the lower estuary could be dangerous if not impossible for some time. This is because of a combination of expected changes to bay hydraulics due to the likely failure and destruction of Columbia River jetties, changes in the locations of sandbanks, side channel collapse and infilling of the navigation channel, and the presence of debris throughout the estuary. More importantly, in this scenario all ports in the lower estuary are likely to be heavily damaged. As a result, vessel operators should develop plans to evacuate to potentially safe ports located to the south of Cape Mendocino on the California coast.

Figure 46. Offshore maritime evacuation zones for the Columbia River study area. Map identifies the locations of the DISTANT (orange) and LOCAL (yellow) tsunami evacuations zones offshore the coast. These zones define the region where tsunami currents fall below 4 knots. Note: bathymetric contours shown on the map are fathoms (1 fathom = 6 ft).

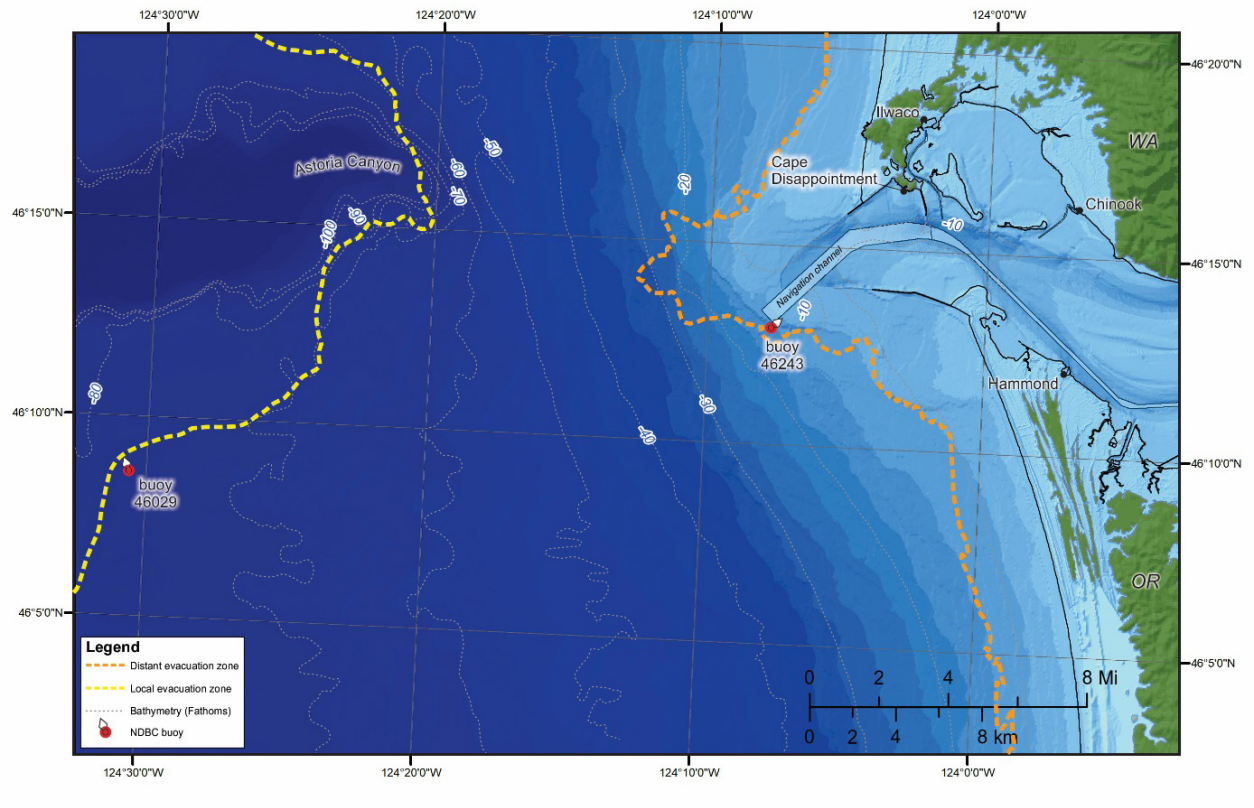

For vessels operating within the lower Columbia River estuary and west of Astoria, options are limited. Wave arrival times are presented in **Figure 25** and **Figure 26** for multiple sites along the river. Maritime operators should be aware of these arrival times and, if caught out on the estuary, attempt to evacuate to the nearest point of high ground and evacuate uphill. Depending on proximity to the MCR, this may be feasible for operators in smaller, faster boats. Upriver evacuation may also be feasible for the fastest boats.

For large ships moored in the navigation channel between Tongue Point and Rice Island, options are limited. Modeling indicates that tsunami waves caused by a local CSZ event could reach 4 m (16 ft) above the tide, with the largest wave being the first wave. Tsunami wave heights of ~ 2 m (6 ft) will persist for at least 4 hours after the initial event. Accompanying the initial peak wave will be dangerous currents that are expected to reach ~4.6 m/s (~9 knots). Strong currents in the 2 to 3.6 m/s (4–7 knot) range will persist for at least 6 hours after the event before gradually subsiding. For these ships, operators may attempt to safeguard their vessels by deploying additional drag anchors. However, in all likelihood the ships will be washed into Cathlamet Bay, where they will become grounded. Vessels located farther upriver toward Rice Island will have a greater chance of navigating as the tsunami waves and currents become more dispersed with progress upriver.

For smaller, faster boats located east of Astoria, evacuation upriver toward Fitzpatrick Island may be an option. Our modeling indicates that tsunami current velocities fall significantly upriver of river mile 39 (~Cathlamet) and are largely below the 1.5 m/s (3 knot) threshold by the time the tsunami reaches

Wauna. Hence, for every mile upriver from Fitzpatrick Island the chances of surviving the tsunami increase. For vessels upriver of Wauna, we recommend that ship operators attach additional mooring ropes to secure their boats or move vessels into the navigation channel. At the ports of Portland or Vancouver, no additional safety requirements are needed as the tsunami is barely detectable upriver of St. Helens.

6.2 Maritime Guidance for a Distant Tsunami

For the maximum-considered distant (AKMax) tsunami scenario, our modeling indicates that the tsunami begins to enter the MCR at ~ 3 hours 38 minutes after the start of earthquake shaking; for distant events occurring in Japan the tsunami will take ~9-10 hours to arrive. For the AKMax scenario, a tsunami warning will be issued by the U.S. Tsunami Warning Center[8] based out of Palmer, Alaska, as well as via channel 16 from the U.S. Coast Guard (USCG). In this scenario, maritime operators will have some time to respond. If vessels are already on the water, we advise operators to check with the USCG before taking any action. If offshore evacuation is advised by USCG, a maritime operator should consider the size of the vessel relative to the prevailing (and forecast) ocean conditions, and the vessel and operator's ability to remain offshore for a potentially extended period of time.

We recommend that vessels seaward of the MCR evacuate to depths greater than 46 m (25 fathoms), identified in **Figure 46** by the area west of the dashed orange line, which depicts where the tsunami currents are expected to fall below 4 knots. This region of lower currents is located ~9.3 (5 nautical mi) southwest of the Cape Disappointment lighthouse (near the Clatsop Spit buoy 46243). Dangerous currents (>2.6 m/s [5 knots]) are expected to occur at depths shallower than 15 fathoms in this scenario and especially within the MCR (**Figure 40** *bottom*). If conditions do not permit offshore evacuation, maritime operators should dock their vessels and evacuate on foot out of the distant tsunami evacuation zone.

For vessels operating within the lower Columbia River estuary and located west of Astoria, a variety of options are available. Offshore maritime evacuation may be feasible for some vessels operating out of the ports of Ilwaco, Chinook, Hammond, and Warrenton. For example, **Table 5** identifies the time and distance to safety for select ports in the lower Columbia River estuary. These times assume an average transit time of 6 knots and do not account for ocean or riverine conditions that could serve to slow travel times. For example, vessels operating out of Ilwaco could reach the staging area beyond the 46-m (25 fathom) line offshore the MCR in about 1 hour 31 minutes; given that time to receive a warning, mobilize, launch a boat, and get underway could take up to an hour, this leaves about 67 minutes as a buffer prior to the tsunami arriving. Offshore evacuation from Hammond and Warrenton indicate that the buffer decreases to ~ 50 minutes at Hammond, and 23 minutes at Warrenton. Vessel operators should therefore carefully weigh the time required to mobilize, transit out of the estuary towards the DISTANT staging area, as well as the offshore conditions prior to mobilizing. Farther east at Astoria and Tongue Point, we believe there is insufficient time to evacuate to the offshore staging area. For these ports, we recommend upriver evacuation.

Our modeling indicates that the worst conditions generated by the AKMax distant tsunami occurs west of Hammond, which includes the ports of Ilwaco and Chinook and much of Baker Bay. Conversely, by the time the tsunami reaches Tongue Point, the height of the tsunami waves decreases to ~1.4 m (~4.6 ft), while the expected maximum tsunami currents are mostly below the 3-knot threshold, with some discrete peaks reaching 4 knots (**Figure 41** and **Figure 42**). Thus, for ships moored between Tongue Point and

[8] https://www.tsunami.gov/

Rice Island, we recommend that the vessel operators deploy additional drag anchors to further safeguard their vessels. Evacuation upriver is probably not warranted for these larger vessels. No additional measures are required for vessels operating upstream of Fitzpatrick Island.

Table 5. Maritime evacuation times to nearest offshore[A] (where currents fall below 4 knots) and upriver[B] staging destinations for a *DISTANT* tsunami. Evacuation times assume an average vessel speed of 6 knots.

Location	Distance to Offshore Safety[A] (km / NM)	Time to Safety (min)	Distance to Upriver Safety[B] (km / NM)	Time to Safety (min)
Ilwaco, WA	17 / 9.2	1 hour 31 min	47 / 25.4	4 hours 14 min
Chinook, WA	18 / 9.7	1 hour 37 min	41 / 22	3 hours 41 min
Hammond, OR	20 / 10.8	1 hour 48 min	33 / 17.8	2 hours 58 min
Warrenton, OR	25 / 13.5	2 hours 15 min	31 / 16.7	2 hours 47 min
Astoria, OR	26 / 14	2 hours 22 min	25 / 13.5	2 hours 15 min
Tongue Point, OR	36 / 22.4	3 hours 14 min	16 / 8.6	1 hour 26 min

km = kilometers. NM = nautical miles.

7.0 CONCLUSIONS

Over the past 160 years, 29 distant (far-field) earthquake events have produced transoceanic tsunamis that struck the Oregon coast (Lander and others, 1993; NGDC, 2017). The majority of these have resulted in negligible effects in ports and harbors located on the Oregon coast. Of these, the largest event was the 1964 Alaska tsunami, which generated water levels that ranged from ~2.5–3.7 m (8–12 ft) (Schatz and others, 1964; Zhang and others, 2011) with higher wave heights at the open coast. In the Columbia River, the Alaska 1964 event produced estimated runup levels that reached 1.74 m (5.7 ft) near Cape Disappointment and 1.4 m (4.6 ft) at Ilwaco. The most recent tsunami is the March 11, 2011, event that resulted in significant damage to several ports and harbors (e.g., Depoe Bay, Coos Bay, and at Brookings), as well as to recreational and commercial vessels attempting to escape the tsunami (Allan and others, 2018). Accordingly, even modest distant tsunamis like the one in 2011 pose a significant risk within the ports and harbors of Oregon, as well as to the safety of commercial and recreational mariners that operate offshore the coast.

To address the issue of maritime tsunami preparation and safety on the northern Oregon coast, this study has evaluated an entirely new suite of tsunami modeling results completed for both distant and local Cascadia tsunamis for the lower Columbia River estuary and river. The goal of this effort has been to examine the interaction of tsunamis with dynamic tides, different riverine flow regimes, and friction in order to provide an improved understanding of tsunami effects offshore the mouth of the Columbia River, within the estuary, and upriver toward the ports of Longview, Vancouver, and Portland. These data are necessary for developing improved maritime guidance for this region. Modeling involved some 35 simulations based around two distant earthquake scenarios: the 1964 Anchorage, Alaska (AK64) event and a maximum considered eastern Aleutian Island (AKMax) earthquake, and two local CSZ scenarios: Large1 (L1) and Extra-extra-large1 (XXL1).

Although the Alaska event was used to quality control our modeling, results from this event also provide an excellent reference for the effects of the most extreme distant event to strike the northern Oregon coast in the past 160 years; as a result, the Alaska event remains an important benchmark when developing maritime guidance. Thus, for the 1964 scenario (coinciding with a spring flood tide) the modeled maximum tsunami water levels reach 1–2 m (3–7 ft) along the open coast (**Figure 9**), while the water levels at the MCR, in Baker Bay, Warrenton, and Astoria ranged from 0.6 to 1.2 m (2 to 4 ft) high. Upriver from Astoria, the tsunami waves rapidly decrease in height, becoming negligible east of Tongue Point. Moderately strong currents of ~ 1.5–3 m/s (3–6 knots) are concentrated within the MCR (**Figure 10**), particularly the navigation channel, before dropping below the 1.5 m/s (3 knot) threshold; damage to ports and harbors tends to occur above this threshold.

For the AKMax scenario, our analyses indicate that the initial wave arrival at the MCR occurs ~3 hours 38 minutes after the start of the earthquake (**Figure 28**). The tsunami takes an additional 19 minutes to travel up into Baker Bay, where it eventually inundates the lower areas of Ilwaco; the AKMax tsunami takes 27 minutes to reach Warrenton, 39 minutes to reach Tongue Point, and arrives ~91 minutes later at Wauna (**Figure 28**); total time to Wauna is 5 hours 9 minutes. The tsunami is detectable as far upstream as St. Helens, although the amount of energy in the tsunami is effectively negligible at this stage, such that the event can largely be ignored upriver of Longview.

The simulations demonstrated significant along-coast and in-water variability in maximum tsunami water levels and currents (**Figure 40**), a function of localized bathymetric effects, as well as interactions with tidal and riverine hydraulics. From a maritime standpoint, the most dangerous conditions will be observed at the MCR, within Baker and Young's Bay, and at Tongue Point (**Figure 40**). Strong currents

exceeding 9 knots will dominate the in estuary west of Chinook and Hammond, and out to some 5 miles seaward of the MCR (**Figure 40**, *bottom*). ***For vessels seaward of the MCR, we recommend evacuation to depths greater than 46 m (25 fathoms/150 ft) (*****Figure 46*****). In this scenario, dangerous currents (> 2.6 m/s [5 knots]) are expected to occur at depths shallower than 27 m (15 fathoms/90 ft)***.

For vessels operating within the lower Columbia River estuary west of Astoria, several options are available to maritime operators in the event of a distant tsunami. Offshore maritime evacuation may be feasible for some vessels operating out of the ports of Ilwaco, Chinook, Hammond, and Warrenton (**Table 5**). Conversely, vessels east of Warrenton may choose to evacuate upriver; seaward evacuation for vessels upriver of Warrenton is not advised because those vessels might be transiting the mouth at the time when a tsunami arrives. Operators of large ships moored between Tongue Point and Rice Island could deploy additional drag anchors to further safeguard their vessels; evacuation upriver is probably not warranted for these ships. No additional measures are required for vessels operating upstream of Fitzpatrick Island.

In a real distant tsunami event, local officials will have time to work with the National Oceanic and Atmospheric Administration, U.S. Coast Guard, and Oregon Emergency Management to provide guidance tailored to the size of the expected tsunami. Mariners should follow that guidance, if possible.

A locally generated CSZ event will reach the MCR in as little as 7 minutes (**Figure 25**), and will take an additional 18 minutes to travel up into Baker Bay, where it inundates Ilwaco; the XXL1 local tsunami takes 31 minutes to reach Warrenton, 46 minutes to reach Tongue Point, and arrives ~99 minutes later at Wauna. An XXL1 CSZ tsunami is detectable as far up stream as the confluence of the Columbia and Willamette Rivers, arriving 4 hours and 40 minutes after the start of earthquake shaking (**Figure 27**). However, the tsunami contains little energy upriver of St. Helens and can be effectively ignored. Accordingly, ***a maximum-considered XXL1 local tsunami will not impact the ports of Portland or Vancouver and no additional measures will be needed to safeguard vessels at these locations***, aside from having to deal with the earthquake shaking.

We find that for the modeled XXL1 and the smaller L1 event, water levels and tsunami currents along the open coast and offshore the MCR will be disastrous. Maximum water levels exceeding 18 m (60 ft) will be observed at Seaside, decreasing to 10–12 m (~33 to 40 ft) along the Clatsop Plains; water levels in the MCR will range from 6 to 12 m (20 to 40 ft) (MHHW) at the mouth, decreasing to ~ 5 m (16 ft) by Sand Island (**Figure 31** and **Figure 32**). Extreme currents exceeding 6.1 m/s (12 knots) will be observed across much of the lower estuary west of Astoria (**Figure 34** and **Figure 39**). These currents will be enhanced during ebb tide conditions (**Figure 17**), which could contribute toward localized amplification of tsunami waves at the MCR. Damage to ports and harbors in this scenario will probably be devastating for all ports in the lower estuary.

Because the tsunamis arrive at the MCR in ~ 7 minutes, there is insufficient time for mariners moored in the various ports in the Lower Columbia River estuary or along the navigation channel downstream of Rice Island to respond to this event other than to evacuate by foot to high ground. Thus, maritime evacuation planning for a locally generated tsunami is largely limited to those vessels operating out on the open ocean. For these vessels, the most effective strategy is to immediately evacuate toward deeper water and, accordingly, toward decreasing tsunami-generated currents. ***We recommend that vessels evacuate directly toward Astoria Canyon to depths greater than 146 m (80 fathoms)*** **(Figure 46)*****.*** Under these circumstances, mariners should prepare to remain offshore for potentially days as the MCR is unlikely to be navigable. Hence, mariners should develop plans to evacuate to potentially safe ports located to the north within Puget Sound.

For vessels caught in the estuary west of Astoria, options are limited. Given the range of wave arrival times, it may be feasible for operators of smaller, faster boats to evacuate to the nearest point of high

ground and evacuate uphill. Upriver evacuation toward Fitzpatrick Island may also be possible, especially for operators of smaller, faster boats located east of Astoria. Our modeling indicates that tsunami current velocities fall significantly upriver of RM 39 (~Cathlamet) and are largely below the 1.5 m/s (3 knot) threshold by the time the tsunami reaches Wauna (**Figure 34** and **Figure 35**). Hence, for every mile upriver from Fitzpatrick Island chance of surviving the tsunami increases. For vessels upriver of Wauna, we recommend that ship operators attach additional mooring ropes to secure their vessels or move vessels into the navigation channel. At the ports of Portland or Vancouver, no additional safety requirements are needed as the tsunami is barely detectable upriver of St. Helens.

Simulations undertaken as part of this study using dynamic tides and varying river flows have yielded some useful insights, when compared with static models undertaken at MHHW and with no flows. These include:

- The predicted maximum velocities exhibit more local extrema along the coast and within the lower estuary, especially near the mouth where the interaction is found to be strongest due to powerful currents and shoaling of tsunami waves (**Figure 17** to **Figure 19**);
- The conventional wisdom is that tsunamis arriving with a flood spring tide are usually more damaging. This is generally true in the deep channel around Tongue Point. However, the situation becomes very complex in the shallow waters of the upper estuary, where tsunamis arriving at ebb and flood slack were found to be considerably energetic (**Figure 19** and **Figure 18**);
- Our analyses indicate that tsunamis arriving at flood slack produced little difference in the current velocities relative to the flood stage, yet conditions during the flood stage resulted in the greatest upriver penetration of the tsunami, with strong currents in the shallows east of Tongue Point and as far upstream as Wauna (**Figure 18**);
- The violent collision between tidal and tsunami currents at the MCR makes the ebb scenarios especially dangerous for ships of all sizes (**Figure 19**). Our modeling confirms that tsunami arrival during an ebb phase produces considerably stronger currents when compared with the flood scenario (**Figure 20** and **Figure 21**);
- Model results that included varying the river discharge indicate generally little difference in the current velocities associated with low, average, or high flow scenarios in the Columbia River;
- For the low flow scenario, the model simulations indicate that the largest differences in the tsunami current are confined to offshore the MCR and along the open coast, where slightly stronger tsunami currents predominate (**Figure 22**). This is probably because the river is not as efficient at counteracting the incoming tsunamis. Furthermore, the model results indicate that the tsunami water levels are ~ −0.25 m (−0.8 ft) lower compared with average flow conditions (**Figure 24**, *top*);
- Conditions generated under the high flow scenario indicate even stronger currents at the mouth (**Figure 23**). Not surprisingly, with progress upriver we see the emergence of strong currents upriver of Rice Island, which are associated with effects from the higher river flows. Under the high flow situation, we find that its contribution to the maximum water levels is ~0.2 m (0.7 ft) within the lower Columbia River estuary (**Figure 24**, *top*);
- Changes caused by varying river flows on the modeled tsunami currents were found to be negligible in the lower estuary (< ±0.2 m/s [< ±0.4 knots]) (**Figure 24**, *bottom*); and
- The above observations apply to both distant and local tsunamis.

Model results presented as part of this study have provided an improved understanding of both distant and local tsunami impacts in the lower Columbia River. These data may be integrated into guidance information that can be used by the maritime community.

8.0 ACKNOWLEDGMENTS

This project was funded under award # NA16NWS4670037 by the National Oceanic and Atmospheric Administration (NOAA) through the National Tsunami Hazard Mitigation Program. We thank Corina Forson and Daniel Eungard from the Washington Geological Survey, Randy Clark from the U.S. Coast Guard, Dr. George Priest (retired, formerly Oregon Department of Geology and Mineral Industries), Rick Wilson from the California Geological Survey, and Ian Madin from the Oregon Department of Geology and Mineral Industries for their insightful report reviews and comments. We also thank Mr. Dan Jordan of the Columbia River Bar Pilots for comments on the guidance document. Simulations used in this paper were conducted using the following computational facilities: (1) SciClone at the College of William and Mary which was provided with assistance from the National Science Foundation, the Virginia Port Authority, Virginia's Commonwealth Technology Research Fund, and the Office of Naval Research; (2) the Extreme Science and Engineering Discovery Environment (XSEDE; grant TG-OCE130032), which is supported by National Science Foundation grant number OCI-1053575; and (3) NASA's Pleiades.

9.0 REFERENCES

Allan, J.C., Komar, P.D., Ruggiero, P., and Witter, R.C., 2012, The March 2011 Tōhoku tsunami and its impacts along the U.S. West Coast: Journal of Coastal Research, v. 28, no. 5, p. 1142–1153. https://doi.org/10.2112/JCOASTRES-D-11-00115.1

Allan, J.C., Priest, G.R., Zhang, Y.J., and Gabel, L.L., 2018, Maritime tsunami evacuation guidelines for the Pacific Northwest coast of Oregon: Natural Hazards, v. 94, no. 1, p. 21–52. https://doi.org/10.1007/s11069-018-3372-2

Atwater, B.F., and others, 1995, Summary of coastal geologic evidence for past great earthquakes at the Cascadia subduction zone: Earthquake Spectra, v. 11, no. 1, p. 1–18. https://doi.org/10.1193/1.1585800

Atwater, B.F., Satoko, M.-R., Satake, K., Yoshinobu, T., Kazue, U., and Yamaguchi, D.K., 2005, The orphan tsunami of 1700—Japanese clues to a parent earthquake in North America: U.S. Geological Survey Professional Paper 1707, 144 p. https://doi.org/10.3133/pp1707

Borrero, J.C., Lynett, P.J., and Kalligeris, N., 2015, Tsunami currents in ports: Philosophical Transactions of the Royal Society A, v. 373, no. 2053, p. 20140372. https://doi.org/10.1098/rsta.2014.0372

Bricker, J.D., Gibson, S., Takagi, H., and Imamura, F., 2015, On the need for larger Manning's roughness coefficients in depth-integrated tsunami inundation models: Coastal Engineering Journal, v. 57, no. 02, p. 1550005. https://doi.org/10.1142/S0578563415500059

Bunya, S., and others, 2010, A high-resolution coupled riverine flow, tide, wind, wind wave, and storm surge model for southern Louisiana and Mississippi. Part I: Model development and validation: Monthly Weather Review, v. 138, no. 2, p. 345–377. https://doi.org/10.1175/2009MWR2906.1

Burla, M., Baptista, A.M., Zhang, Y., and Frolov, S., 2010, Seasonal and interannual variability of the Columbia River plume: a perspective enabled by multiyear simulation databases: Journal of Geophysical Research: Oceans, v. 115, no. C2. https://doi.org/10.1029/2008JC004964

Flores, L., Mojica, J., Fletcher, A., Casey, P., Christin, Z., Armistead, C., and Batker, D., 2017, The value of natural capital in the Columbia River Basin: A comprehensive analysis: Tacoma, Wash., Earth Economics, 154 p. http://www.columbiana.org/PDFs/CRBV-FINAL-DIGITAL.pdf

Goldfinger, C., Nelson, C.H., and Johnson, J.G., 2003, Holocene earthquake records from the Cascadia Subduction Zone and Northern San Andreas fault based on precise dating of offshore turbidites: Annual Review of Earth and Planetary Sciences, v. 31, p. 555–577. https://doi.org/10.1146/annurev.earth.31.100901.141246

Goldfinger, C., and others, 2012, Turbidite event history: methods and implications for Holocene paleoseismicity of the Cascadia subduction zone: U.S. Geological Survey Professional Paper 1661-F, 170 p. https://pubs.usgs.gov/pp/pp1661f/

Goldfinger, C., Galer, S., Beeson, J., Hamilton, T., Black, B., Romsos, C., Patton, J., Nelson, C.H., Hausmann, R., and Morey, A., 2017, The importance of site selection, sediment supply, and hydrodynamics: A case study of submarine paleoseismology on the northern Cascadia margin, Washington USA: Marine Geology, v. 384, p. 4–16, 17, 25–46. https://doi.org/10.1016/j.margeo.2016.06.008

González, F., Geist, E.L., Jaffe, B., Kânoğlu, U., Mofjeld, H., Synolakis, C., Titov, V.V., Arcas, D., Bellomo, D., and Carlton, D., 2009, Probabilistic tsunami hazard assessment at Seaside, Oregon, for near-and far-field seismic sources: Journal of Geophysical Research: Oceans, v. 114, no. C11. https://doi.org/10.1029/2008JC005132

Gregor, N.J., Silva, W.J., Wong, I.G., and Youngs, R.R., 2002, Ground-motion attenuation relationships for Cascadia subduction zone megathrust earthquakes based on a stochastic finite-fault model: Bulletin of the Seismological Society of America, v. 92, no. 5, p. 1923–1932. https://doi.org/10.1785/0120000260

Homer, C.G., Dewitz, J.A., Yang, L., Jin, S., Danielson, P., Xian, G., Coulston, J., Herold, N.D., Wickham, J.D., and Megown, K., 2015, Completion of the 2011 National Land Cover Database for the conterminous United States—representing a decade of land cover change information: Photogrammetric Engineering and Remote Sensing, v. 81, no. 5, p. 345–354.

Hyndman, R.D., and Wang, K., 1995, The rupture zone of Cascadia great earthquakes from current deformation and the thermal regime: Journal of Geophysical Research, v. 100, no. B11, p. 22,133–22,154. https://doi.org/10.1029/95JB01970

Jay, D.A., Leffler, K., Diefenderfer, H.L., and Borde, A.B., 2015, Tidal-fluvial and estuarine processes in the lower Columbia River: I. Along-channel water level variations, Pacific Ocean to Bonneville Dam: Estuaries and Coasts, v. 38, no. 2, p. 415–433. https://doi.org/10.1007/s12237-014-9819-0

Jay, D.A., Borde, A.B., and Diefenderfer, H.L., 2016, Tidal-fluvial and estuarine processes in the Lower Columbia River: II. Water level models, floodplain wetland inundation, and system zones: Estuaries and Coasts, v. 39, no. 5, p. 1299–1324. https://doi.org/10.1007/s12237-016-0082-4

Johnson, J., Satake, K., Holdahl, S.R., and Sauber, J., 1996, The 1964 Prince William Sound earthquake: joint inversion of tsunami and geodetic data: Journal of Geophysical Research, v. 101, no. B1, p. 523–532. https://doi.org/10.1029/95JB02806

Kelsey, H.M., Nelson, A.R., Hemphill-Haley, E., and Witter, R.C., 2005, Tsunami history of an Oregon coastal lake reveals a 4600 yr record of great earthquakes on the Cascadia subduction zone: Geological Society of America Bulletin, v. 117, no. 7/8, p. 1009–1032. https://doi.org/10.1130/B25452.1

Kukulka, T., and Jay, D.A., 2003, Impacts of Columbia River discharge on salmonid habitat: 1. A nonstationary fluvial tide model: Journal of Geophysical Research: Oceans, v. 108, no. C9. https://doi.org/10.1029/2002JC001382

Lander, J.F., Lockridge, P.A., and Kozuch, M.J., 1993, Tsunamis affecting the west coast of the United States, 1806–1992: National Oceanic and Atmospheric Administration, National Geophysical Data Center key to geophysical Records Documentation (KGRD) No. 29, 242 p. ftp://ftp.ngdc.noaa.gov/hazards/publications/Kgrd-29.pdf

Lynett, P.J., Borrero, J., Son, S., Wilson, R., and Miller, K., 2014, Assessment of the tsunami-induced current hazard: Geophysical Research Letters, v. 41, no. 6, p. 2048–2055. https://doi.org/10.1002/2013GL058680

Lynett, P.J., and others, 2017, Inter-model analysis of tsunami-induced coastal currents: Ocean Modelling, v. 114, p. 14–32. https://doi.org/10.1016/j.ocemod.2017.04.003

Madin, I.P., and Burns, W.J., 2013, Ground motion, ground deformation, tsunami inundation, coseismic subsidence, and damage potential maps for the 2012 Oregon Resilience Plan for Cascadia Subduction Zone Earthquakes: Oregon Department of Geology and Mineral Industries Open-File Report O-13-06. https://www.oregongeology.org/pubs/ofr/p-O-13-06.htm

McCaffrey, R., Qamar, A., King, R.W., Wells, R.W., Khazaradze, G., Williams, C., Stevens, C., Vollick, J.J., and Zwick, P.C., 2007, Fault locking, block rotation and crustal deformation in the Pacific Northwest: Geophys. J. Int., v. 169, p. 1315–1340.

McCrory, P.A., Blair, J.L., Oppenheimer, D.H., and Walter, S.R., 2004, Depth to the Juan de Fuca slab beneath the Cascadia subduction margin—a 3-D model for sorting earthquakes: U.S. Geological Survey Data Series DS-91. https://pubs.usgs.gov/ds/91

Mitchell, C.E.., Vincent, P., Weldon, R.J., II, and Richards, M.A., 1994, Present-day vertical deformation of the Cascadia margin, Pacific Northwest, United States: Journal of Geophysical Research: Solid Earth, v. 99, no. B6, p. 12,257–12,277. https://doi.org/10.1029/94JB00279

Mori, N., and Takahashi, T., 2012, Nationwide post event survey and analysis of the 2011 Tohoku earthquake tsunami: Coastal Engineering Journal, v. 54, no. 1, p. 1250001-1–27. https://doi.org/10.1142/S0578563412500015

Mori, N., Takahashi, T., Yasuda, T., and Yanagisawa, H., 2011, Survey of 2011 Tohoku earthquake tsunami inundation and run-up: Geophysical Research Letters, v. 38, no. 7. https://doi.org/10.1029/2011GL049210

National Geophysical Data Center/World Data Service (NGDC), 2017, NCEI/WDS Global Historical Tsunami Database. NOAA National Centers for Environmental Information. https://doi.org/10.7289/v5pn93h7 [accessed June 2017]

Nelson, A.R., Kelsey, H.M., and Witter, R.C., 2006, Great earthquakes of variable magnitude at the Cascadia subduction zone: Quaternary Research, v. 65, no. 3, p. 354–365. https://doi.org/10.1016/j.yqres.2006.02.009

NTHMP, 2017, Guidance for safe minimum offshore depth for vessel movement for tsunamis. National Tsunami Hazard Mitigation Program. https://nws.weather.gov/nthmp/documents/GuidanceforSafeMinimumOffshoreDepthforVesselMovement.pdf. Accessed July 10, 2017.

Oregon Department of Geology and Mineral Industries (DOGAMI), 2014, Tsunami! What Oregon boat owners need to know. http://www.oregongeology.org/pubs/tsubrochures/TsunamiBrochureMaritime.pdf, 2 p. Accessed August 5, 2017.

Priest, G.R., Goldfinger, C., Wang, K., Witter, R.C., Zhang, Y., and Baptista, A.M., 2009, Tsunami hazard assessment of the northern Oregon coast: A multi-deterministic approach tested at Cannon Beach, Clatsop County, Oregon: Oregon Department of Geology and Mineral Industries Special Paper 41. https://www.oregongeology.org/pubs/sp/SP-41.zip

Priest, G.R., Goldfinger, C., Wang, K., Witter, R.C., Zhang, Y., and Baptista, A.M., 2010, Confidence levels for tsunami-inundation limits in northern Oregon inferred from a 10,000-year history of great earthquakes at the Cascadia subduction zone: Natural Hazards, v. 54, no. 1, p. 27–73. https://doi.org/10.1007/s11069-009-9453-5

Priest, G.R., Witter, R.C., Zhang, Y.J.., Wang, K., Goldfinger, C., Stimely, L.L., English, J.T., Pickner, S.G., Hughes, K.L.B., Willie, T.E., and Smith, R.L., 2013, Tsunami inundation scenarios for Oregon: Oregon Department of Geology and Mineral Industries Open-File Report O-13-19. https://www.oregongeology.org/pubs/ofr/p-O-13-19.htm

Satake, K., Wang, K., and Atwater, B.F., 2003, Fault slip and seismic moment of the 1700 Cascadia earthquake inferred from Japanese tsunami descriptions: Journal of Geophysical Research, v. 108, no. B11. https://doi.org/10.1029/2003JB002521

Schatz, C.E., Curl, H., and Burt, W.V., 1964, Tsunamis on the Oregon coast: Ore Bin, v. 26, no. 12, p. 231–232. https://www.oregongeology.org/pubs/og/OBv26n12.pdf

Stewart, M., 2006, Developing Tsunami Ready Communities [tutorial]: Tsunami, 100th Anniversary Earthquake Conference Commemorating the 1906 San Francisco Earthquake, San Francisco, April 18-22, 2006: Earthquake Engineering Research Institute, 8th EERI Conference, 25 p. http://www.1906eqconf.org/tutorials/DevTsunamiReadyComm_Stewart3.pdf

Suppasri, A., Shuto, N., Imamura, F., Koshimura, S., Mas, E., and Yalciner, A.C., 2013, Lessons learned from the 2011 Great East Japan tsunami: performance of tsunami countermeasures, coastal buildings, and tsunami evacuation in Japan: Pure and Applied Geophysics, v. 170, no. 6–8, p. 993–1018. https://doi.org/10.1007/s00024-012-0511-7

Suppasri, A., Nguyen, D., Abe, Y., Yasuda, M., Fukutani, Y., Imamura, F., and Shuto, N., 2015, Offshore evacuation of fishing boats—Lessons from the 2011 great east Japan tsunami and its future challenge: Tsunami Engineering Technical Report, 32, p. 33-45.

Torrence, C., and Compo, G.P., 1998, A practical guide to wavelet analysis: Bulletin of the American Meteorological society, v. 79, no. 1, p. 61–78. https://doi.org/10.1175/1520-0477(1998)079<0061:APGTWA>2.0.CO;2

Tsunami Pilot Study Working Group (TPSWG), 2006, Seaside, Oregon tsunami pilot study—modernization of FEMA flood hazard maps: Seattle, Wash., U.S. National Oceanic and Atmospheric Administration, Office of Oceanic and Atmospheric Research, Pacific Marine Environmental Laboratory, NOAA OAR special report (Contribution No. 2975), 94 p., 7 appendices. https://www.pmel.noaa.gov/pubs/PDF/tsun2975/tsun2975.pdf

U.S. Army Corps of Engineers (USACE), 2008, HEC-RAS River Analysis System, Hydraulic Reference Manual, v. 4.0, March 2008: Davis, Calif., USACE Hydraulic Engineering Center, Computer Program Documentation CPD-69.

U.S. Army Corps of Engineers (USACE), 2010, Lower Columbia River digital terrain model development: prepared by David Smith and Associates, Portland, Oreg., CC Patterson and Associates, Ashland, Oreg., and David Evans and Associates, Inc., Vancouver, Wash., Contract No. W9127N-09-D-0009, Task Order No. 0005, 8 p.

Wilson, B.W., and Tørum, A., 1972, Runup heights of the major tsunami on North American coasts, *in* National Research Council, ed., The great Alaska earthquake of 1964: Washington, D.C., National Academy of Sciences, Oceanography and Coastal Engineering, NAS Publication 1605, p. 158–180.

Wilson, R.I., Admire, A.R., Borrero, J.C., Dengler, L.A., Legg, M.R., Lynett, P., McCrink, T.P., Miller, K.M., Ritchie, A., Sterling, K., and Whitmore, P.M., 2013, Observations and impacts from the 2010 Chilean and 2011 Japanese tsunamis in California (USA): Pure and Applied Geophysics, v. 170, no. 6–8, p. 1127–1147. https://doi.org/10.1007/s00024-012-0527-z

Whitmore, P., and others, 2008, NOAA/West Coast and Alaska Tsunami Warning Center Pacific Ocean response criteria: Science of Tsunami Hazards, v. 27, no. 2, 1–21. http://tsunamisociety.org/272Whitmore.pdf

Wiśniewski, B., and Wolski, T., 2012, The safety of the shipping and ports in the aspect of the tsunami events: Maritime University of Szczecin Scientific Journals [Zeszyty Naukowe/Akademia Morska w Szczecinie], v. 30, no. 102, p. 150–157.

Witter, R.C., 2008, Prehistoric Cascadia tsunami inundation and runup at Cannon Beach, Clatsop County, Oregon: Oregon Department of Geology and Mineral Industries Open-File Report O-08-12, 36 p plus 3 appendices. https://www.oregongeology.org/pubs/ofr/O-08-12.zip

Witter, R.C., Kelsey, H.M., and Hemphill-Haley, E., 2003, Great Cascadia earthquakes and tsunamis of the past 6700 years, Coquille River estuary, southern coastal Oregon: Geological Society of America Bulletin, v. 115, no. 10, p. 1289–1306. https://doi.org/10.1130/B25189.1

Witter, R.C., Zhang, Y., Goldfinger, C., Priest, G.R., and Wang, K., 2010, Validating numerical tsunami simulations in southern Oregon using late Holocene records of great Cascadia earthquakes and tsunamis [abs.], Seismological Society of America 2010 Annual Meeting, Portland, Oreg.: Seismological Research Letters. v. 81, no. 2, p. 290. https://doi.org/10.1785/gssrl.81.2.284

Witter, R.C., Zhang, Y., Wang, K., Priest, G.R., Goldfinger, C., Stimely, L.L., English, J.T., and Ferro, P.A., 2011, Simulating tsunami inundation at Bandon, Coos County, Oregon, using hypothetical Cascadia and Alaska earthquake scenarios: Oregon Department of Geology and Mineral Industries Special Paper 43, 57 p. https://www.oregongeology.org/pubs/sp/p-SP-43.htm

Witter, R.C., Zhang, Y., Wang, K., Goldfinger, C., Priest, G.R., and Allan, J.C., 2012, Coseismic slip on the southern Cascadia megathrust implied by tsunami deposits in an Oregon lake and earthquake-triggered marine turbidites: Journal of Geophysical Research; Solid Earth, v. 117, no. B10. https://doi.org/10.1029/2012JB009404

Witter, R., Zhang, Y.J., Wang, K., Priest, G.R., Goldfinger, C., Stimely, L.L., English, J.T., and Ferro, P.A., 2013, Simulated tsunami inundation for a range of Cascadia megathrust earthquake scenarios at Bandon, Oregon, USA: Geosphere, v. 9, no. 6, p. 1783–1803. https://doi.org/10.1130/GES00899.1

Uslu, B., Eble, M., Titov, V.V., and Bernard, E.N., 2010, Distant tsunami threats to the ports of Los Angeles and Long Beach, California; Tsunami Hazard Assessment Special Series, v. 2: National Oceanic and Atmospheric Administration, Office of Oceanic and Atmospheric Research (OAR) Special Report, 100 p. https://nctr.pmel.noaa.gov/hazard_assessment_reports/02_LA_LB_CA_3532_web.pdf

Yeh, H., Tolkova, E., Jay, D., Talke, S., and Fritz, H., 2012, Tsunami hydrodynamics in the Columbia River: Journal of Disaster Research, v. 7, no. 5, p. 604–608. doi: 10.20965/jdr.2012.p0604

Zhang, Y.J., and Baptista, A.M., 2008, SELFE: A semi-implicit Eulerian-Lagrangian finite-element model for cross-scale ocean circulation: Ocean Modelling, v. 21, no. 3-4, p. 71–96. https://doi.org/10.1016/j.ocemod.2007.11.005

Zhang, Y.J., Witter, R.C., and Priest, G.R., 2011, Tsunami–tide interaction in 1964 Prince William Sound tsunami: Ocean Modelling, v. 40, p. 246–259. https://doi.org/10.1016/j.ocemod.2011.09.005

Zhang, Y.J., Stanev, E.V., and Grashorn, S., 2016a, Seamless cross-scale modelling with SCHISM: Ocean Modelling, v. 102, p. 64–81. https://doi.org/10.1016/j.ocemod.2016.05.002

Zhang, Y.J., Priest, G.R., Allan, J.C., and Gabel, L., 2016b, Benchmarking an unstructured-grid model for tsunami current modeling: Pure and Applied Geophysics, v. 173, no. 12, p. 4075–4087. https://doi.org/10.1007/s00024-016-1328-6